REVIEW

ADVANCED
FUNCTIONAL
MATERIALS
www.afm-journal.d

Check for
updates

Magnetic Actuation Methods in Bio/Soft Robotics

*Nafiseh Ebrahimi, Chenghao Bi, David J. Cappelleri, Gastone Ciuti,
Andrew T. Conn, Damien Faivre, Neda Habibi, Alexander Hošovský, Veronica Iacovacci,
Islam S. M. Khalil, Veronika Magdanz, Sarthak Misra, Chytra Pawashe,
Rasoul Rashidifar, Paul Eduardo David Soto-Rodriguez, Zoltan Fekete, and Amir Jafari**

In recent years, magnetism has gained an enormous amount of interest among researchers for actuating different sizes and types of bio/soft robots, which can be via an electromagnetic-coil system, or a system of moving permanent magnets. Different actuation strategies are used in robots with magnetic actuation having a number of advantages in possible realization of microscale robots such as bioinspired microrobots, tetherless microrobots, cellular microrobots, or even normal size soft robots such as electromagnetic soft robots and medical robots. This review provides a summary of recent research in magnetically actuated bio/soft robots, discussing fabrication processes and actuation methods together with relevant applications in biomedical area and discusses future prospects of this way of actuation for possible improvements in performance of different types of bio/soft robots.

1. Introduction

Traditional robots are fast and precise systems, based on rigid-body mechanisms that enabled them to accurately control the motion and to apply torques and forces on joints and tips, respectively. Since medical robots become smaller and penetrate deeper into the body of patients through its natural pathways, incorporating stiff components and rigid mechanical couplings to the outside environment in the robot's design have become infeasible. Hence, it has caused the exploration of new techniques for removing the mechanical coupling and emerging the concept of wireless force generation and

N. Ebrahimi, Prof. A. Jafari
Advanced Robotic Manipulators (ARM) Lab
Department of Mechanical Engineering
University of Texas at San Antonio UTSA
One Circle, San Antonio, TX 78249, USA
E-mail: amir.jafari@utsa.edu

C. Bi, Prof. D. J. Cappelleri
School of Mechanical Engineering
Purdue University
585 Purdue Mall, West Lafayette, IN 47907, USA

Prof. G. Ciuti, Dr. V. Iacovacci
BioRobotics Institute and the Department of Excellence in Robotics
& AI Santa'Anna School of Advanced Studies
Piazza Martiri della Libertà, 33, Pisa, PI 56127, Italy

Dr. A. T. Conn
Department of Mechanical Engineering
University of Bristol
Bristol BS8 1TR, UK

Dr. D. Faivre, P. E. D. Soto-Rodriguez
Aix Marseille University
CEA, CNRS, BIAM, Saint Paul-Lez-Durance, Marseille 13108, France

Prof. N. Habibi
Northwest Vista College
3535 N Ellison Dr., San Antonio, TX 78251, USA

Dr. A. Hošovský
Technical University of Košice
Faculty of Manufacturing Technologies with Seat in Prešov
Bayerova 1, Presov 08001, Slovakia

Prof. I. S. M. Khalil
Assistant Professor with Biomechanical Engineering
Faculty of Engineering Technology
University of Twente
Five, Drienerlolaan, Enschede, NB 7522, The Netherlands

Dr. V. Magdanz
Chair of Applied Zoology
Faculty of Biology
Zellescher Weg 20b, 01069 Dresden, Germany

Dr. V. Magdanz
IBEC
Carrer de Baldiri Reixac, 10, 12, Barcelona 08028, Spain

Prof. S. Misra
Biomechanical Engineering
Faculty of Engineering Technology
University of Twente
Drienerlolaan Five, Enschede, NB 7522, The Netherlands

Dr. C. Pawashe
Technology Computer Aided Design Group
Logic Technology Development
Intel Corporation
Portland, OR 97124, USA

R. Rashidifar
Center for Advanced Manufacturing and Lean Systems
Department of Mechanical Engineering
University of Texas at San Antonio UTSA
One Circle, San Antonio, TX 78249, USA

Dr. Z. Fekete
Faculty of Information Technology and Bionics
Pázmány Péter Catholic University, Budapest
Práter u. 50/A, Budapest 1083, Hungary

**ADVANCED
SCIENCE NEWS**

www.advancedsciencenews.com

**ADVANCED
FUNCTIONAL
MATERIALS**

www.afm-journal.de

transmission. Since magnetic actuators are able to be driven wirelessly by a magnetic field, exploiting the concept of magnetism to generate force and torque for the new generation of medical robotics has been considered and proven itself as a promising technique. It is capable of providing both needed power and precise control of the robotic device specially in miniaturized applications.[1,2] Magnetism already has found its special place and has proven to be an effective and impactful method in many engineering applications.[3–16]

In the current state-of-the-art, microrobots are more accurately described as the sub-millimeter sized wireless end-effector of a larger scale system, which externally provides energy and control inputs. The use of magnetism has gained popularity for controlling such microrobots, which can be via an electromagnetic-coil system, or a system of moving permanent magnets.[17] Other actuation mechanisms have also been studied, such as electrostatic, and thermal approaches.[18,19] Magnetic actuation mechanisms offer advantages such as 1) creating relatively strong torques and forces at microscale, which can be used for 2D and 3D motion and orientation control, 2) the microrobots themselves can be relatively simple objects, which are robust to handling, and 3) in some implementations, the working environment does not need to be specialized. In an ideal interpretation, an untethered microrobot can be imagined as a self-contained device, with all dimensions under 1 mm, capable of mobility, sensing and reacting to the environment, and communicating to the outside world. Such a device would require an onboard power source, actuation system, sensory systems, and communication modules. Certainly, there exist centimeter-scale robots that meet these criteria, but in the realm of the micrometer-scale, there currently does not exist sufficient miniaturization of components to have a fully self-contained microrobot.

Magnetically actuated robots are being developed for minimally invasive diagnosis and surgical intervention in many regions of body including abdomen, heart, brain, eye, ear, and vascular system. These include diagnostic imaging, implants, drug delivery and biopsy. The magnetically actuated devices are being used for aforementioned purposes works based on different locomotion strategies like swimming or bacteria propelled microrobots, catheters, capsule endoscopes, and robotics. They also vary in size ranging from submillimeter to tens of centimeters. These devices are functioning based on the same physical principles although the design and implementation seems different and each device has its unique challenges.[1,20]

In this new approach of magnetic actuation the system could be built using permanent magnet or electromagnetic systems. Both represent sufficient capability of driving and propulsion of miniature robotic devices like helical swimming microrobots, steering catheters and continuum manipulators, launching pumps of implanted artificial heart, and navigating the capsule endoscopes inside the human body.[1,21] These magnetic instruments have the ability to reduce the invasiveness of medical interventions and diagnoses, as they can get rearranged inside the abdominal area without the necessity of dedicated port during the procedure. In such instruments on-board actuators can be implemented to accomplish a controlled and replicable motion at the interface with the body.[22] Moreover, magnetic resonance imaging (M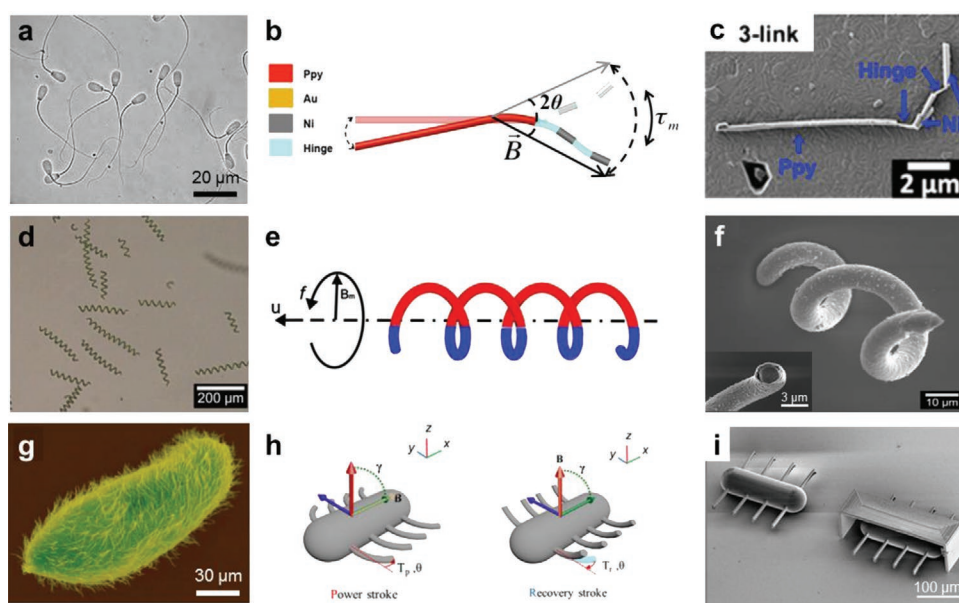RI) scanners also have been used to provide robot tracking and control of the devices inserted into the body for navigation along the vascular system or needle biopsy and tissue ablation. There are some common challenges for such kind of magnetic actuation systems especially applicable in medical devices like generating appropriate force and torques, precise localization and navigation of the device, minimization of the magnetic actuation device footprint, and optimization of the operational workspace.[23]

Due to the significance of the magnetic actuation method in soft/bio robots applicable in medical diagnostic and surgical interventions, we reviewed the latest advances happened in recent years to provide a comprehensive resource for future researchers interested in this field. In the following sections, a broad variety of magnetically actuated bio/soft robotic devices will be reviewed. This includes bio-inspired microrobots, tetherless microrobots, cellular microrobots, and even normal size soft robots such as electromagnetic soft robots and medical robots. Finally, a discussion on current limitations and possible future improvements of the above-mentioned bio/soft robots is presented.

2. Bioinspired Magnetic Microrobots

The discovery of the propelling motion of microorganisms relying on flagella and cilium dates back to the 19th century. Much later in 1973, Berg proved that *E. coli* bacteria use molecular motors to rotate their helical flagella.[24] To change position in fluids, such microscale organisms need a special strategy as low Reynolds number (typically between 10^{-2} and 10^{-5}) in their environment makes reciprocal motion ineffective. Instead, they achieve propulsion by propagating traveling waves along their flagella. To mimic this concept widely exploited in nature, a number of synthetic microrobots have been proposed that mostly rely on planar, helical, and cilia based microstructures. Due to the fundamentally different flow regime at very low Reynolds numbers, these bio-inspired magnetic microrobots require design and control strategies which are unique to milli- and mesoscale magnetic robots. In this section, microrobots inspired by planar, helical, and cilia based microstructures will be described and examples from the literature are shown in **Figure 1**.

Planar locomotion can be triggered by a flexible flagellum, which requires only a 1D structure. Mimicking the beating of spermatozoa flagellum, planar waveform can be generated. Artificial planar propellers are composed of flexible sheets attached to magnetic head and actuated using oscillating magnetic field. Early prototypes of planar microswimmers were demonstrated by Dreyfus et al. in 2005, when a flexible tail made of self-assembled magnetic beads was used to evoke drag forces.[25] Their method was further improved to connect the beads with DNA strands, and demonstrated the drag of a red blood cell.[26] Later, developments in the technical implementation of this configuration paved the way to optimize the efficiency of propulsion. Magnetically driven locomotion of flexible Au/Ag/Ni nanowires, with a gold "head" and nickel "tail," linked by a partially dissolved and weakened silver bridge was presented by Gao.[27] Rigid magnetic Ni head with flexible silver tail was produced by template directed electrodeposition.[28]

**ADVANCED
SCIENCE NEWS**

www.advancedsciencenews.com

**ADVANCED
FUNCTIONAL
MATERIALS**

www.afm-journal.de

Figure 1. a) Microscopic view of mature spermatozoa, b) Schematic of a planar nanoswimmer comprising *n* elastic eukaryote-like polypyrrole tail and rigid magnetic nickel links connected by flexible polymer bilayer hinges.[30] Undulatory motion is produced by magnetic field oscillation. c) SEM view of the 3-link nanoswimmer.[30] d) Microscopic view of Spirulina bacteria. e) Schematic on the propulsion of helical microrobots. f) Biotemplated helical microswimmer. Inset picture shows cross-section of the helix before dissolving Spirulina bacteria as the biotemplate.[62] g) Colored SEM micrograph of a paramecium. h) Schematic on the two-stroke locomotion of a ciliary microrobot. i) Ciliary microswimmers fabricated by the combination of two-photon polymerization and subsequent metal deposition.[52] b,c) Reproduced with permission.[30] Copyright 2015, American Chemical Society. f) Reproduced with permission.[62] Copyright 2018, Cell Press. g–i) Reproduced with permission.[52] Copyright 2016, American Association for the Advancement of Science (AAAS).

Bending of its flexible tail was achieved by precession of the magnetic field around the direction of movement. Optimizing the magnetization profile, Diller et al. proposed dispersed ferromagnetic powder in an elastomer matrix, and showed propagation of bending waves generated by external rotating magnetic field.[29] Jang et al. demonstrated a robot comprising an elastic eukaryote-like polypyrrole tail and rigid magnetic Ni links connected by flexible polymer bilayer hinges. Their pioneering work showed that planar undulation in nanowire-based chains propelled by planar-oscillating magnetic field is possible.[30] A combination of multistep electrodeposition and selective etching has been used to produce undulating slender micropropellers with multiple magnetic links.[31] Such distributed magnetization in the structure allows the propagation of bending waves along the flagellum, circumventing the limitation of typical one-sided, synchronous bending of artificial flagella.

Helix-like flagella of several bacteria (like *E. coli*) are used as molecular motors to propel these microorganisms. Artificial helical microrobots use rotating magnetic fields for propulsion, without the need for an on-board rotary motor. Conceptually, they consist of a rigid helical tail attached to a soft ferromagnetic head, eventually diametrically magnetized. The swimmer is rotated around its helical axis, while the direction of locomotion is perpendicular to the plane of rotation. These structures can be propelled forward or backward by simply changing the direction of rotation of the magnetic field.

To produce helical structures for magnetic locomotion, several microfabrication methods have been proposed in the last decade. The so-called self-scrolling method in the pioneering work of Bell and colleagues was demonstrated to control the internal stress of thin film multilayered ribbons ending in a square shaped, deposited Ni head.[32,33] Glancing angle deposition (GLAD) was first proposed by Ghosh et al.[34] They grow helical pillars on spherical seeds during rotation of a tilted stage in an evaporation chamber, while cobalt layer deposited and permanently magnetized perpendicular to the helical axis was performed afterward. Template assisted electrodeposition processes have been utilized to produce helical magnetic microstructures. Khalil et al. have utilized electrospinning with a polymer solution (polystyrene in dimethyl formamide) and iron-oxide nanoparticles to create a robotic sperm that can swim faster than microswimmers that rely on planar wave propulsion.[35] with the ability to dynamically switch between planar and helical flagellar propulsion to replicate the unique ability of sperm cells to vary swimming patterns in this way.[36] El Alaoui-Faris et al. subsequently investigated how the drive signal that generates nonplanar flagellar wave propulsion in microrobots could be optimized using a numerical technique and demonstrated significantly faster swimming compared to the conventional sinusoidal wave form.[37]

Li et al. has demonstrated how Pd nanospring as templates can be used to synthetize helical microstructures after Ni deposition and selective Pd dissolution.[38] 3D printed micromolds have also been applied for template-assisted electrodeposition in the work of Alcantara et al., where helical Fe-based microswimmers were proposed to reduce cytotoxicity of the metallic parts.[39] Soft lithography and micromolding processes were utilized by Ye et al. to demonstrate that multiple flagella on one microrobot can generate a higher propulsive force and therefore faster swimming.[40] GLAD and template assisted deposition allows the formation of structure of sub-micrometer scale, while earlier

**ADVANCED
SCIENCE NEWS**

www.advancedsciencenews.com

**ADVANCED
FUNCTIONAL
MATERIALS**

www.afm-journal.de

approaches ended in structures 10^{-6} or 10^{-7} m in length. This is especially important as microscale propellers are able to swim in Newtonian fluids, however, apart from urine and CSF, biological fluids are non-Newtonian and only nanoscale robots having a filament diameter below 70 nm range can move.[41] Template-based synthesis has been improved by using biological organs as replica. First, Schuerle et al. used diacetylenic phospholipids as a template, and coated with a multialloy magnetic coating.[42] Later, Yan exploited the helical structure of *Spirulina platensis*, and deposited magnetite precursors on its surface, which was followed by annealing treatment and reduction processing to create porous hollow magnetic microhelices.[43] Ali et al. repolymerized flagella that were mechanically sheared from *Salmonella typhimurium* and coated them with magnetic nanoparticles to create steerable microrobots capable of changing their helical form in response to environmental stimuli.[44]

To transport micro-objects, or particles, the helical body as a stand-alone structure needed further improvements. The rapid development of two-photon polymerization enabled to extend the basic helix with microholders to facilitate the stable manipulation of cargos. One of the early demonstration of such 3D machinery was reported by Tottori et al., who achieved the transportation of polysterene beads with a helical micromachine.[45] The magnetic property of these polymer structures can be established with either evaporation after the laser writing process or simply adding magnetic microparticles to the photosensitive constituting material of the 3D patterned objects.[34,46] Further advantage of the 2P polymerization was demonstrated by Barbot and co-authors, whose so-called roll-to-swim microrobot showed 3D navigation in a fluid medium combining three type of motions (rolling, swimming, spin-top) in a controlled fashion.[47]

Cilia are short, hair-like nanostructures covering the cell body. A well-known unicellular organism to mimic is Paramecium, which uses cilia to propel its body in the surrounding medium. Unlike the undulatory motion of flagella, cilia exhibit flexural motion with a characteristic power stroke to drive fluid flow and a flexible recovery stroke.[48] Cilia beat in an asynchronous motion that forms a metachronal wave.[49] Artificial magnetic cilia, in contrast to its natural counterpart, moves simultaneously to achieve locomotion. Artificial cilia have been developed by forming magnetoelastic microstructures made from polydimethylsiloxane (PDMS)-ferromagnetic particle composites, which can be integrated on the surface of lab-on-chip devices to pump and mix fluids.[50,51] Due to the synchronous beating of these hair-like appendages exposed to the global magnetic field, fluid propulsion is unsteady, therefore ciliary motion of microrobots is still limited. Besides theoretical difficulties, the first ciliary microrobot cruising with stroke motion was proposed in 2016. Kim et al. designed a lithographically defined ellipsoidal body with cilia on its sides.[52] Cilium of the two-photon polymerized structure was deposited with Ni. The power stroke and recovery stroke was programmed through a magnetic field of gradually changing direction. Numerical simulations of magnetic microcilia have shown that different control strategies can generate the asymmetric motion of cilia, such as exploiting the buckling of a permanently magnetic film and using elastic coupling between a pair of magnetic bodies within a rotating magnetic field.[53,54]

Demonstrations of early in vitro applications of bioinspired magnetic microrobots are promising. Medina-Sanchez et al. have shown the controlled transport of sperm cells with reduced motility aided by a synthetic microhelix propelled with rotating magnetic field.[55] Functionalization of these microswimmers have also open up new perspectives in molecular delivery. The controlled release of drugs was achieved by ABF functionalized with liposomes.[56] The advances in two-photon polymerization fostered further improvements in cargo delivery. A scaffold-like 3D helical microrobot was presented for 3D culturing and delivery of stem cells in vitro.[57] Hollow microhelices with improved kinetic properties were proposed by Xin et al. to targeted delivery of nanoparticles and stem cells.[58] Their special fabrication approach also relied on 2PP by helical scanning using femtosecond vortex beams produced by spatial light modulation. Yan et al. used a dip-coating process with *S. platensi* in a Fe_3O_4 suspension so that the inherent properties of the microalgae could be exploited for fluorescence imaging during in vivo experiments.[59]

More recently, efforts to facilitate the practical, in vivo use of magnetic microrobots have been made by several groups. Soft helical microswimmers composed of nontoxic photocrosslinkable hydrogel gelatin methacryloyl (GelMA) rendered with magnetic nanoparticles is reported by Wang and co-authors.[60] Their exemplary approach to use only biodegradable materials will be definitely a basic feature of future microrobots for biomedical purposes. The Nelson group presented the first in vivo demonstration of fluorescent tracking of magnetically actuated ABF (functionalized with NIR probes) in the peritoneal cavity of mouse.[61] Such advancement in the development of microswimmers are definitely necessary to move toward real medical applications.

3. Untethered Magnetic Microrobots

The fact that small objects can be controlled via external magnetic fields has led to developments of untethered magnetic microrobots. In this section, we review current advances in grasping and manipulation of tetherless microrobots and then discuss how with an external magnetic field, microrobots can be operated in 2D surfaces and 3D environments. Finally, this section presents recent advancements in tumbling and rolling microrobots via an external magnetic field.

### 3.1. Tetherless Microgrippers and Magnetic Micromanipulation

Manipulation and assembly of micro-objects has potential unique applications in many areas including biomedicine, chemistry, nanotechnology and biology. These applications have experienced several significant advances through manipulator-based and tetherless micromanipulation.[63,64] Manipulator-based micromanipulation relies on the miniaturization of microelectromechanical systems (MEMS). At this scale, surface, adhesion, and drag forces have significant influence on the interactions between the micro-objects which makes precise positioning at prescribed locations challenging using manipulator-based techniques. In the case of tetherless

micromanipulation, microrobots are used to exert forces via mechanical contact or fluidic trapping without direct contact or use utilize fluid boundary layers to produce contact-free motion. In this technique, the geometric scaling has been enabled through magnetic,[65,66] acoustic,[67] light,[68] and chemical,[69,70] stimuli to transmit power wirelessly. Hence, they can overcome the disadvantages of manipulator-based techniques.

Randhawa et al. have demonstrated pick and place tasks using chemomechanically triggered microgrippers.[71] Their design consists of a trilayer hinge joint capable of opening and closing by residual stresses, and the ability to manipulate tubes and bead has been demonstrated. Since these microgrippers could be opened and closed by chemicals, their material and range of applications are limited. Leong et al. have developed thermobiochemically actuated microgrippers suitable under biological conditions.[72] These microgrippers are remotely actuated by a temperature trigger and picking up beads off substrates and removal of cells from tissue samples have been demonstrated. Fusco et al. have also used a similar approach and presented a microrobotic platform that works by increasing the temperature to allow for controlled encapsulation and release of micro-objects.[73] Diller and Sitti have demonstrated 3D microassembly and parallel operation by multiple microgrippers (force- and torque-based microgrippers) using uniform field and field gradient to achieve programmable magnetic actuation.[74] Zhang et al. have also presented autonomous 3D micrograsping and cargo delivery.[75] Microassembly of micro-objects to microstructures have also been demonstrated using cluster of paramagnetic microparticles under the influence of controlled magnetic field gradients by Khalil et al.[76] In the previous techniques, the microgrippers exert manipulative forces via direct contact with the micro-objects, and adhesive forces are likely to prevent their release at prescribed positions.

This problem could be partially overcome if an external stimulus can influence the interaction between the microrobot and the micro-object. Consider, for example, the soft microrobot illustrated in **Figure 2**. It consists of a magnetic head and an ultra-thin flexible tail.[77] The microrobot undergoes travelling-wave propulsion under the influence of uniform magnetic field along the desired direction of motion with a sinusoidally varying orthogonal component, leading to controlled swim toward the micro-objects (microbeads). At $t = 83$ s, the soft microrobot achieves contact manipulation of the micro-object toward the prescribed position (red mark). Once positioned at the target position, the microrobot has to swim away from the manipulation site. Therefore, the external stimulus, in this case we have magnetic actuation, has to enable the microrobot to break free from the micro-object using relatively high actuation frequencies. Figure 2 shows that the microrobot ($t = 506$ s) swims away from the manipulation site after a successful release of the micro-object. However, the adhesive forces between the microrobot and the micro-object result in stickiness, which can be avoided in all times in the case of noncontact manipulation.

Noncontact micromanipulation techniques are more suitable when direct contact results in contamination to biological samples or stickiness, and provide alternative approach for micrograsping. These techniques include electrophoresis,[78] optical trapping,[79] fluidic trapping,[80] acoustic manipulation,[81] vibration,[82,83] and magnetic manipulation.[84] Most of
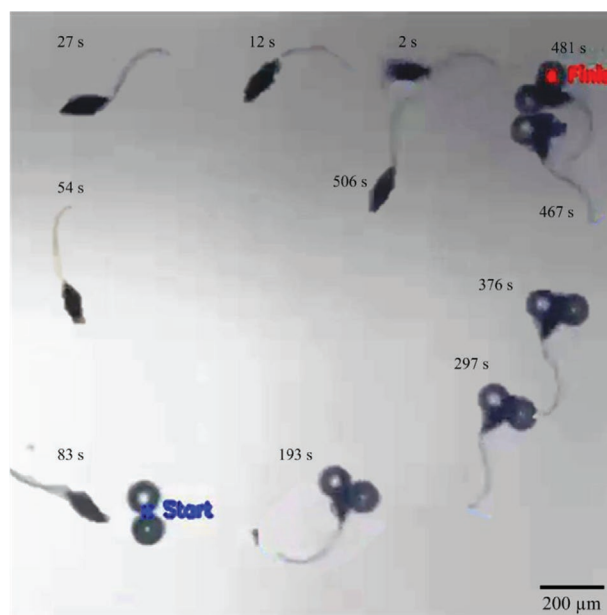
Figure 2. A soft microrobot translates two nonmagnetic polystyrene microbeads by direct contact toward a reference position (red mark). At $t = 2$ s, the microrobot swims toward the microbeads (blue mark) using uniform magnetic field along the desired direction of motion with sinusoidally varying orthogonal components.[77] Images obtained during 506 s and superimposed.

these systems have limited workspace with the exception of magnetic manipulation. Floyed et al. have presented a contact-free micromanipulation method based on fluidic trapping using microrobots.[85,86] These microrobots are utilized to create local flow to push microspheres, and two methods of noncontact manipulation based on front and side pushing have been presented. In this method, stick-slip motion of the magnetic microrobots under the influence of magnetic fields are used to create the fluid flow. This approach depends on a nearby surface to achieve the stick-slip motion. Peyer et al. have also shown fluidic trapping using artificial bacterial flagella under the influence of rotating magnetic fields.[87] The rotation of these helical microrobots create rotational fluid flow and manipulate microbeads without contact. Petit et al. have also demonstrated selective trapping and micromanipulation of micro-objects using a tangential flow-field induced by a rotating nanowire.[88] They have demonstrated sequential pick-and-place micromanipulation of polystyrene microspheres with a microvortex created by the rotating nanowire. This method has been also implemented to manipulate (fluidic trapping and transportation) individual *E. coli* bacterium with the controlled microvortex near a solid boundary. This technique overcomes the limitation associated with optical tweezers, magnetic tweezers, dielectrophoresis which cannot be used for the manipulation of many biological samples.

Ye et al. have also used the locally induced rotational fluid flows to achieve noncontact micromanipulation.[90] This method relies on the velocity field which decay in space nearly as $1/r^2$, where r is the distance between the rotating microrobot and the micro-object, as shown in **Figure 3**. Ye et al. have utilized groups of untethered magnetic microrobots
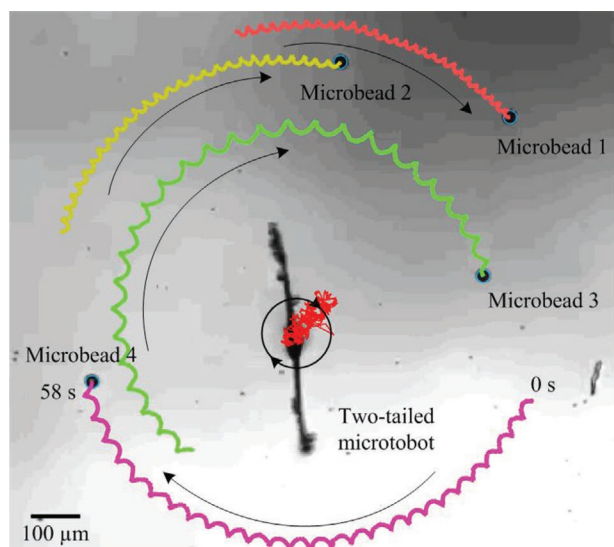
Figure 3. A two-tailed soft microrobot rotates under the influence of a rotating magnetic field. The induced flow-field enables nonmagnetic polystyrene microbeads to orbit the soft microrobot along sprocket-like trajectories at different angular velocities. The noncontact manipulation has significant importance in the manipulation of biological samples.[89] Images obtained during 58 s and superimposed. The red line indicates the trajectory of the center of rotation of the two-tailed microrobot, and the black arrows indicate the direction of rotation.

that can have reconfigurable configurations to create virtual fluidic channels. The microrobots can be arranged in any desirable configuration to create the desired flow-field in the channel. Noncontact pushing and pulling of nonmagnetic micro-objects have also been achieved by microrobots under the influence of controlled magnetic field gradient,[91] and scaled bilateral tele-manipulation enabled the operator to sense the interaction forces between the microrobot and the micro-objects.[89] Rolling microrobots have also been used by Tung et al. to manipulate micro-objects.[92] Flow-fields are created by transversely magnetized rolling microrobots and micromanipulation is achieved through the transmitted forces to the manipulated micro-objects. The capability of soft microrobots to swim controllably toward the manipulation site to achieve noncontact manipulation, and swim away after manipulation has been demonstrated by Khalil et al.[93] In this approach, two tailed soft microrobots achieve a combination of flagellar swim and rotations to move toward micro-objects and create controlled flow-field, respectively. This induced flow-field enables the micro-objects to orbit the soft microrobot (without contact) and translate to prescribed positions in open- and closed-loop. They have shown that the additional soft tail increases the angular velocity of the orbiting microbeads and results in a sprocket-like trajectory, as shown in Figure 3. They have also shown that the unique geometry of the soft microrobot enables bidirectional motion. This feature has a significance importance to swim away from the manipulation site without affecting the positioning accuracy of the micro-object at the prescribed position. Soft microrobots with travelling-wave propulsion have a wave-pattern that can be scale with the actuation frequency. At relatively low actuation frequencies, the overall amplitude of the pattern is relatively high, which is a desirable feature during noncontact manipulation and fluidic trapping.[94] This amplitude decreases at relatively high actuation frequencies and creates lower flow-field in the background fluid, which is desirable to move away from the manipulation site. In addition, soft microrobots have the advantage that they do not require a nearby surface for locomotion. Rigid microrobots are dependent on stick-slip motion or rolling, thereby limiting the manipulation site to regions near to a solid boundary. In contrast to rigid microrobots, soft microrobots (or microrobots based on travelling-wave propulsion) can achieve noncontact and contact manipulation everywhere in the fluid. Consider, for example, artificial bacterial flagella,[87] which have rigid helical structure and can swim without in 3D space and does not depend on a nearby solid boundary. These microrobots can achieve fluidic trapping and transportation of micro-objects and biological samples. However, they achieve fluidic trapping through rigid body rotation and it is likely that the positioning accuracy is decreased when the microrobot swim away from the manipulation site. In contrast, soft microrobots have wave-pattern that scales with the actuation frequencies. Therefore, they can achieve 3D contact and noncontact manipulation without affecting the positioning accuracy between several tasks. These desirable features, combined to their simplicity in design and manufacturing, less density, and high level of biodegradability,[95] provide soft microrobots with relative importance in manipulation of micro-object and significant importance in manipulation of biological samples.[88]
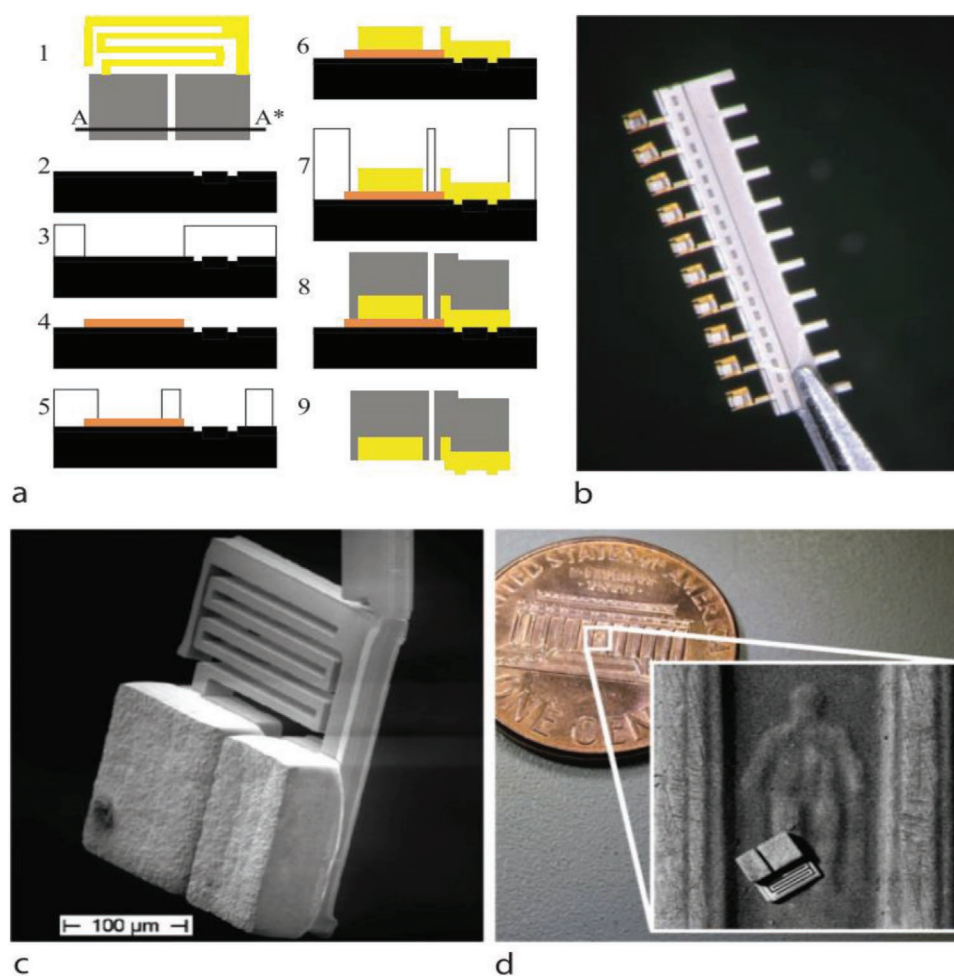
3.2. Microrobots Operating on 2D Surfaces

A simple way to move a magnetic object on a surface using an external magnetic field is to apply a magnetic field gradient, which results in a force applied on that magnet. This force is proportional to the volume of the magnet. When the magnet is at the microscale, i.e., a magnetic microrobot, area-based forces dominate volume-dependent effects. A microrobot can experience high surface friction due to interfacial adhesion, which can dominate the effect of magnetic forces, effectively making the microrobot "sticky" with the surface. Applying a sufficiently strong magnetic field gradient can result in a large enough force to overcome this friction. However, this can lead to high accelerations, and thus an uncontrollable microrobot, especially in gaseous environments with low damping. Instead, oscillatory actuation methods have been employed in the literature to control magnetic microrobot motion, which overcomes the friction effects in a controllable fashion.

Three submillimeter magnetic-based microrobots will be discussed, which employ unique actuation methods using oscillatory external inputs: the MagMite, the Mag-μBot, and the MagPier.[96–98]

3.2.1. MagMites

The MagMite is a magnetic microrobot whose motion is derived from wireless resonant magnetic actuation.[96] Constructed using microfabrication techniques, it consists of

ADVANCED
SCIENCE NEWS

www.advancedsciencenews.com

ADVANCED
FUNCTIONAL
MATERIALS

www.afm-journal.de

Figure 4. a) Microfabrication process steps to fabricate MagMite, b) a strip of released MagMite microrobots, c) scanning electron micrograph of a MagMite, and d) a MagMite on a US penny. Adapted with permission.[96] Copyright 2009, IEEE.
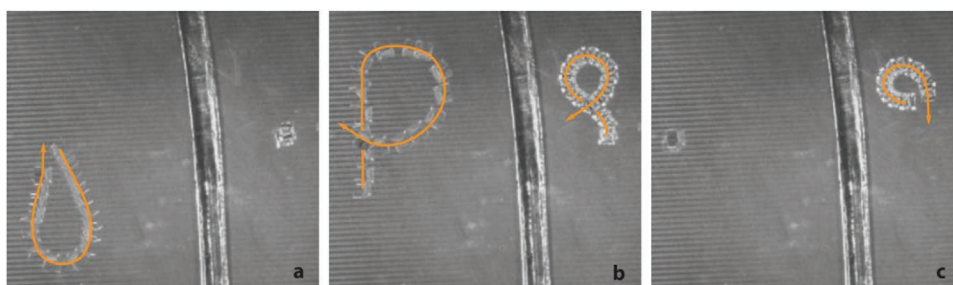
a gold frame, a spring element, and two nickel soft magnetic bodies. One of these bodies is mobile and is attached to the spring element. The other body is stationary, and rests on the MagMite's frame. The overall dimensions of the MagMite are below 300 µm. **Figure 4** shows the MagMite and its fabrication process.

The MagMite achieves mobility by momentum transfer from its mobile magnetic body impacting the stationary magnetic body, which vibrates from the forces induced by oscillating external magnetic field gradients. These gradients are generated by a pair of Helmholtz coils, and the frequency of the field is specified to achieve mechanical resonance in the MagMite's mass-spring system. For a MagMite with symmetric magnetic bodies, this process would nominally result in a MagMite that vibrates in place. To achieve forward motion, a rectification signal is applied through the means of a downward force generated by electrostatic fields on a specialized surface, which allows the MagMite's friction with the surface be controlled. The rectifying signal is applied at the same frequency as the magnetic field, shifted 180° out of phase. The result is that for one half of the oscillation cycle, there is no MagMite motion due to high friction, but in the other half, there is an increment

in motion due to low friction. With driving frequencies in the kHz range, continuous motion can be achieved. Orientation and turning is achieved by magnetic torques arising from the external magnetic fields.

The MagMite can achieve velocities of over 12.5 mm s^{-1}, and can move forward and backward depending on the phase of the magnetic and electrostatic signals. Using a MagMite with asymmetric magnetic bodies, mobility can be achieved without the electrostatic clamping signal, although with a loss of efficiency and control. However, this allows the microrobot to operate on nonspecialized surfaces, such as glass, bare silicon, or flat nonmagnetic metals. In addition, the MagMite can operate in fluid environments, where motion is observed to be smoother due to the added damping of the environment.

Controlling multiple MagMites poses a challenge, because the driving magnetic fields are approximately uniform throughout the workspace. To select an individual MagMite, each is designed with different resonant frequencies. Through the application of time-division multiplexed signals, each individual MagMite can be independently controlled by taking turns moving. **Figure 5** shows an example of two MagMites independently moving on a surface.

**ADVANCED
SCIENCE NEWS**

www.advancedsciencenews.com

**ADVANCED
FUNCTIONAL
MATERIALS**

www.afm-journal.de

Figure 5. Two MagMites independently operating on the same surface, with motion paths illustrated. MagMites are separated by a polymer wall. Adapted with permission.[101] Copyright 2011, SAGE.

In an effort to reduce the fabrication complexity of the Mag-Mite, the PolyMite was developed, based on similar operation principles as the MagMite.[99] The PolyMite is built using SU8 polymer, with electrodeposited CoNi alloy to form the resonant magnetic bodies, shown in **Figure 6**a.

3.2.2. Mag-μBots

The Mag-μBot is a magnetic microrobot that achieves mobility by a stick-slip rocking motion mechanism.[97] The microrobot itself is a simple permanent or soft magnet, fabricated to have sub-millimeter dimensions. It can be fabricated using laser micromachining, or by using a polymer-based casting process, which allows it to be formed into arbitrary shapes.[86] Being constructed out of bulk metallic material without delicate parts, the Mag-μBot is robust to handling.

External magnetic fields of 1–10 mT generated by five or six coils produce the necessary signal to locomote the Mag-μBot. Magnetic fields induce torques, which are relatively strong at this scale, and provide orientation as well as induce a rocking motion in the Mag-μBot. This rocking motion has a rotation axis parallel to the surface, which allows the Mag-μBot to intermittently break static friction, especially if the rocking motion is rapid in one half cycle of oscillation (a sawtooth waveform is typical). Combined with a magnetic field gradient to apply force, the Mag-μBot achieves controlled motion upward of 10 mm s^{-1}, as it sticks and slips across the surface. It can operate on arbitrary surfaces, such as glass or silicon, and can also operate on rough surface such on the surface of a coin (Figure 6b). The Mag-μBot can operate in air and liquid environments, which

has been observed to significantly affect motion characteristics; the added damping of a viscous liquid, such as silicone oil, leads to smoother and more controlled motion.

Control of multiple Mag-μBots has been demonstrated with two different approaches, with the constraint of having an approximately uniform driving magnetic fields throughout the workspace. In the first approach, a specialized surface provides an electrostatic anchoring signal, which can freeze Mag-μBots spatially.[97] This allows multiple Mag-μBots to move independently of each other by taking turns. This electrostatic surface also has been used to assemble and disassemble multiple microrobotic modules (here called Mag-μMods), demonstrating the ability to create reconfigurable microscale constructs, which are also mobile using the same stick-slip mechanism as the Mag-μBot (see **Figure 7**A for the assembly, motion, and disassembly of eight Mag-μMods).[100]

The second approach to controlling multiple Mag-μBots obviates the need for a specialized surface. This approach relies on heterogenous microrobots, which can have varying dimensions and/or different internal magnetizations.[101] By varying the frequency and amplitude of the applied magnetic field, different sets of Mag-μBots would react with motion. With an appropriate sequence of driving signals, these Mag-μBots can be independently positioned. Figure 7B demonstrates this approach, where three Mag-μBots were controlled on a nonspecialized surface.

3.2.3. MagPieR

MagPieR is a hybrid microrobot whose motion is based on magnetic and piezoelectric principles.[98] Its body consists of
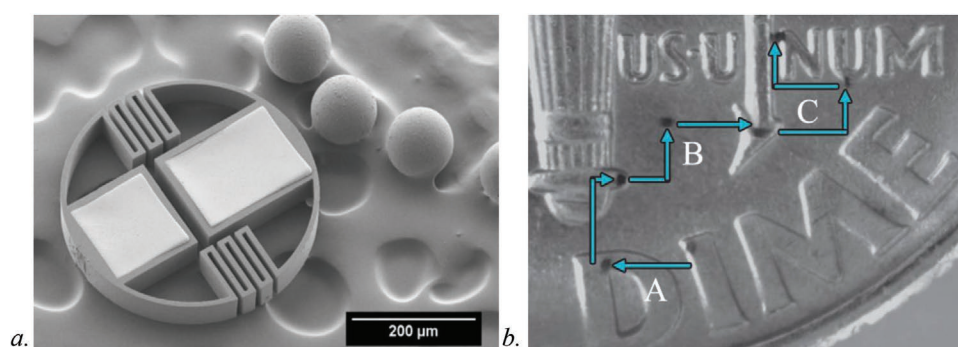
Figure 6. a) Scanning electron micrograph of a PolyMite, with three polystyrene beads adjacent. b) Frames from a video of a NdFeB Mag-μBot traversing on a US dime, which can move over smooth and bumped regions of the dime. Adapted with permission.[100] Copyright 2011, SAGE.

**ADVANCED
SCIENCE NEWS**
www.advancedsciencenews.com

**ADVANCED
FUNCTIONAL
MATERIALS**
www.afm-journal.de
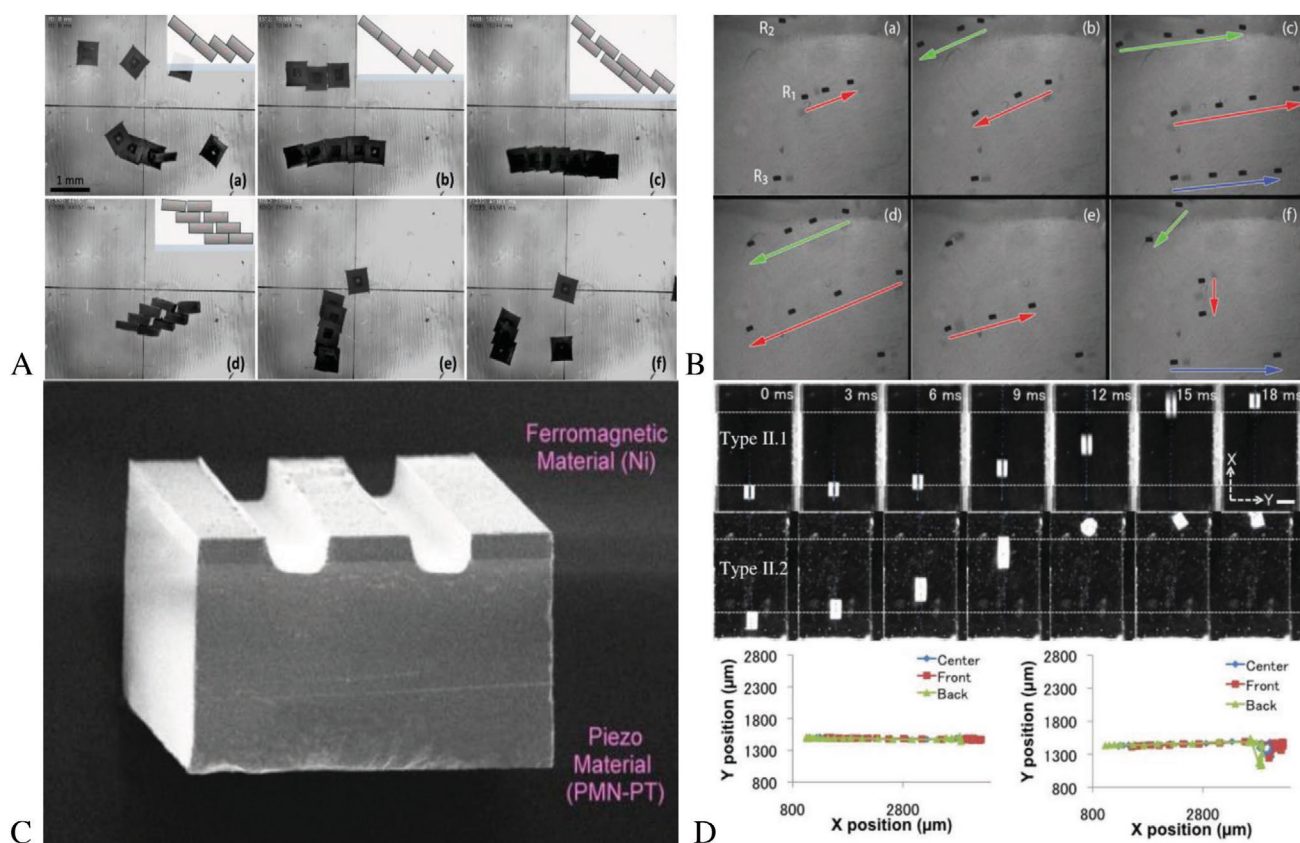
Figure 7. A) Eight Mag-μMods demonstrating assembly, disassembly, and mobility on an electrostatic surface. a–d) Assembly and mobility of individual Mag-μMods; inset shows schematic side-view. e,f) Disassembly and reconfigurability of the Mag-μMods. B) Frames from a video of three heterogeneous Mag-μBots, R1, R2, and R3, operating on a nonspecialized glass surface, demonstrating independent positioning. Arrows indicate motion of each individual Mag-μBot in sequence shown. C) Scanning electron micrograph of a MagPieR microrobot, consisting of a piezoelectric material and a ferromagnetic material. Trenches shown are 50 μm wide. D) Frames from a video of a MagPieR traversing a surface, and trajectory plots for two different types of MagPieR. Adapted with permission.[100] Copyright 2011, SAGE.

a piezoelectric material, with a magnetic nickel layer on top, shown in Figure 7C, and is fabricated to be under 400 μm in all dimensions. This microrobot is specifically designed to achieve high velocities, upward of 600 mm s^{-1}.

The MagPieR achieves mobility by a combination of external magnetic and electrostatic driving fields. Magnetic field gradients of magnitude ≈5 mT mm^{-1} apply a force on the MagPieR, however this is insufficient to induce motion due to the high friction with the surface. To break the friction, an electric-field waveform is applied across the MagPieR to induce piezoelectric strain in the piezoelectric material. This is achieved by the specialized environment that the MagPieR must reside in, which is effectively inside the dielectric of a capacitor. Impulse waveforms of 300 V and 100 Hz has been shown to break the MagPieR's friction with the surface, allowing the magnetic field gradients to propel the microrobot in the desired direction (see Figure 7D).

3.3. Microrobots Operating in 3D in a Fluid by Gradient Pulling

A magnetic microrobot in a fluid medium can levitate and move in 3D by the application of external magnetic field gradients, which act to pull the microrobot in desired directions.

These microrobots typically operate in a liquid environment, where viscous damping forces act to slow down the motion of the microrobot (as compared to a gaseous environment), making it controllable. Two systems are discussed in this section, the OctoMag and the system developed by Diller et al. for multiple microrobot control.[65,102] In other sections, magnetic fields and torques can be used to propel microrobots in liquids, with actuation mechanisms inspired from nature.

For example, the OctoMag is an electromagnetic system intended to control microrobots for human surgical procedures in liquid environments, such in intraocular therapy and diagnosis.[65] A set of eight electromagnetic coils is designed to surround a human head. These coils provide energy inputs to operate a levitating magnetic microrobot with 5-DOF control in a relatively large 25 mm diameter workspace, shown in **Figure 8**.

The microrobot itself can be comprised of a permanent or soft-magnetic material. One type of microrobot is comprised of Ni or CoNi and is built into an oval shape (inset in Figure 8, schematically shown in **Figure 9**), with maximum dimensions varying from 500 to 2000 μm. Another microrobot useful for biopsy is a pair of NdFeB permanent magnet cubes (800 μm cube edge) with a 1.2 mm hypodermic needle attached (**Figure 10**d).

**ADVANCED
SCIENCE NEWS**

www.advancedsciencenews.com

**ADVANCED
FUNCTIONAL
MATERIALS**

www.afm-journal.de

Figure 8. Experimental apparatus of the Octomag system, showing eight electromagnetic coils surrounding a workspace. Inset shows an optical image of an oval-shaped magnetic microrobot in the workspace. Adapted with permission.[85] Copyright 2009, IEEE.

Magnetic field gradients are applied to create force, which accelerates the microrobots. A constant magnetic field of 15 mT is applied to orient the microrobot. To resolve the problem of ferromagnetic systems being inherently unstable (Earnshaw's theorem), an active closed-loop visual feedback system is implemented to create stable microrobot position control. The Octomag system can both control position and orientation of the microrobot throughout the workspace using this visual feedback system, and servo the microrobot through arbitrary trajectories (**Figure 11**).

In addition to motion, the OctoMag can perform surgical tasks. The microrobot in Figure 10 is used to operate on a chicken embryo, where it successfully punctures large blood vessels for biopsy purposes.

Controlling multiple 3D microrobots in fluids is also another recent approach. Diller et al. investigate methods to control multiple 3D microrobots independently, which are levitating in a fluid environment.[102] Eight electromagnetic coils are utilized to provide magnetic fields of up to 8.3 mT, and gradients of up to 0.34 T m^{-1}, which orient and apply forces to magnetic microrobots in the workspace. The setup of this system allows for full 6-DOF control of the microrobot, allowing for any microrobot position and orientation to be achieved in the workspace. Microrobots are fabricated to
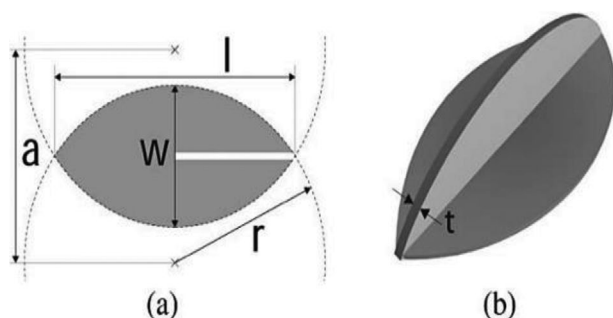
Figure 9. a,b) Schematic of an oval-shaped Ni or CoNi microrobot. Adapted with permission.[86] Copyright 2012, IEEE.
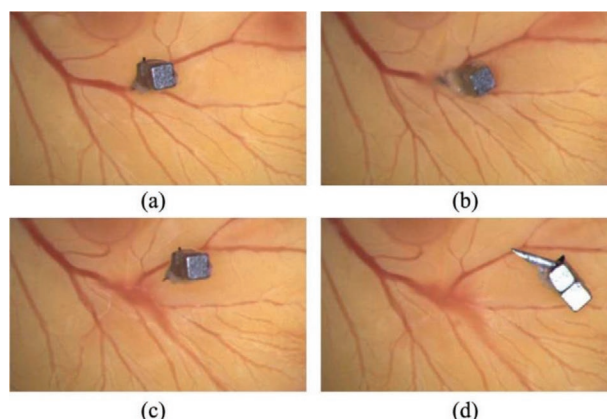
Figure 10. a) The Octomag system controlling a NdFeB microrobot with a hypodermic needle tip on a chicken embryo. In b), the microrobot punctures the embryo, c) retracts, and d) microrobot lays on the embryo. Adapted with permission.[65] Copyright 2010, IEEE.

be 400–4000 µm in size, can consist of a permanent or soft magnetic material, and can have polymer additions, such as "wings" (**Figure 12**). An air cavity can be integrated to create buoyant microrobots.
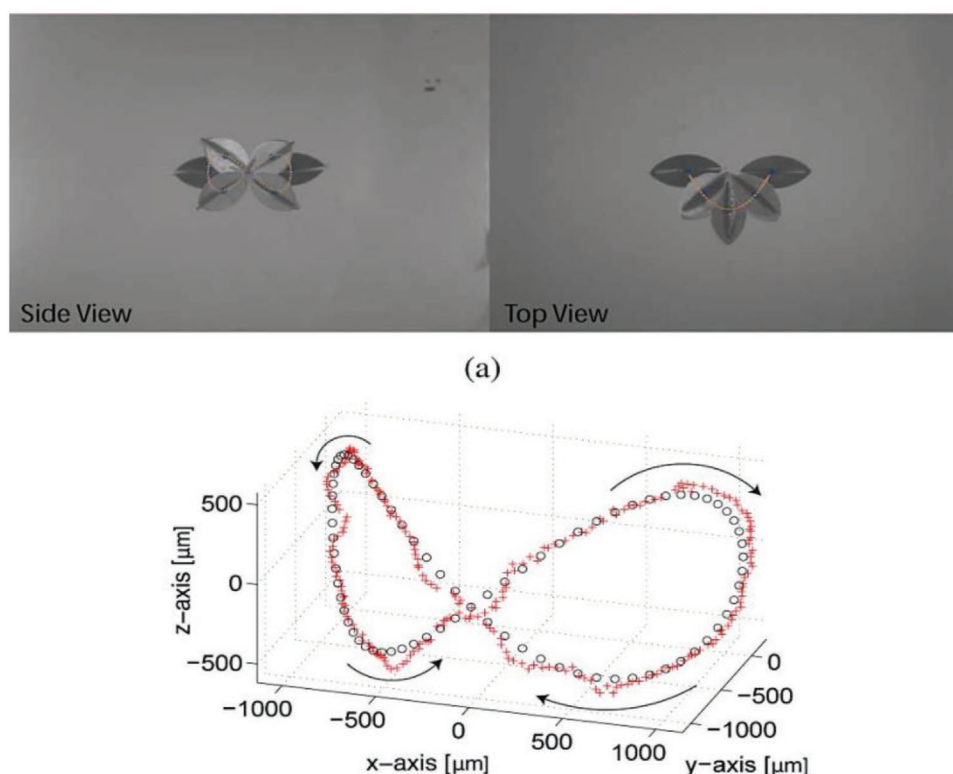
To enable the selection of individual microrobots in the presence of approximately uniform magnetic fields inside the workspace, heterogenous microrobots are utilized, with different geometries and properties. Under an externally applied magnetic field, which is used to orient or rotate a microrobot, microrobots with differing magnetizations or geometries with varying fluid drag coefficients will rotate in the fluid at different angular rates; this incurs a phase lag in motion. Thus, during these rotation events, heterogenous microrobots can instantaneously have different orientations. When a magnetic field gradient is applied, which causes acceleration, microrobots with different instantaneous orientations will accelerate toward different headings.

Using a two-camera vision feedback system, combined with a feedback controller that comprehends the microrobot's phase lag due to fluid interactions, two microrobots were independently and simultaneously positioned in 3D, while following a path (see **Figure 13**). The ability to move three microrobots in different directions was also demonstrated, see **Figure 14**.

3.4. Tumbling and Rolling Magnetic Microrobots

Tumbling and rolling magnetic microrobots locomote by rotating over solid surfaces under an applied magnetic torque. At the microscale, the inertia produced from rotational motion alone is not sufficient to produce net displacement in low Reynolds number fluid environments. A solid surface is necessary to create dissimilar boundary conditions between different ends of the untethered microrobot, allowing for forward propulsion.

Compared to direct pulling using magnetic field gradients, tumbling and rotating locomotion has several advantages. At smaller scales, magnetic torque demonstrates higher efficiency than magnetic force under the same external magnetic field.[103] Magnetic force scales with the volume of magnetic material (i.e., L^3) while the equivalent force from magnetic

ADVANCED
SCIENCE NEWS

www.advancedsciencenews.com

ADVANCED
FUNCTIONAL
MATERIALS

www.afm-journal.de

Figure 11. An oval microrobot being served by the Octomag system in a figure-eight trajectory in the workspace. Adapted with permission.[106] Copyright 2010, IOP.

torque scales with L^2.[104] As a result, rotation induced through magnetic torque is generally preferred at the microscale over force-based pulling. Additionally, rolling friction is less than sliding friction at all size scales. The stiction resisting pulling locomotion over solid surfaces is much higher than the stiction resisting tumbling and rolling locomotion. This behavior reduces the actuation effort required for the latter method and also avoids the sudden acceleration that occurs when large stiction forces are broken, eliminating the need for additional damping effects. Finally, tumbling and rolling magnetic microrobots are capable of traversing over 3D surfaces with inclines, valleys, and other complex surface features in dry conditions while gradient-pulled magnetic microrobots are limited to operation within fluid environments. These qualities make tumbling and rolling magnetic microrobots well-posed for applications with low-strength magnetic fields over unpredictable, complex terrains.
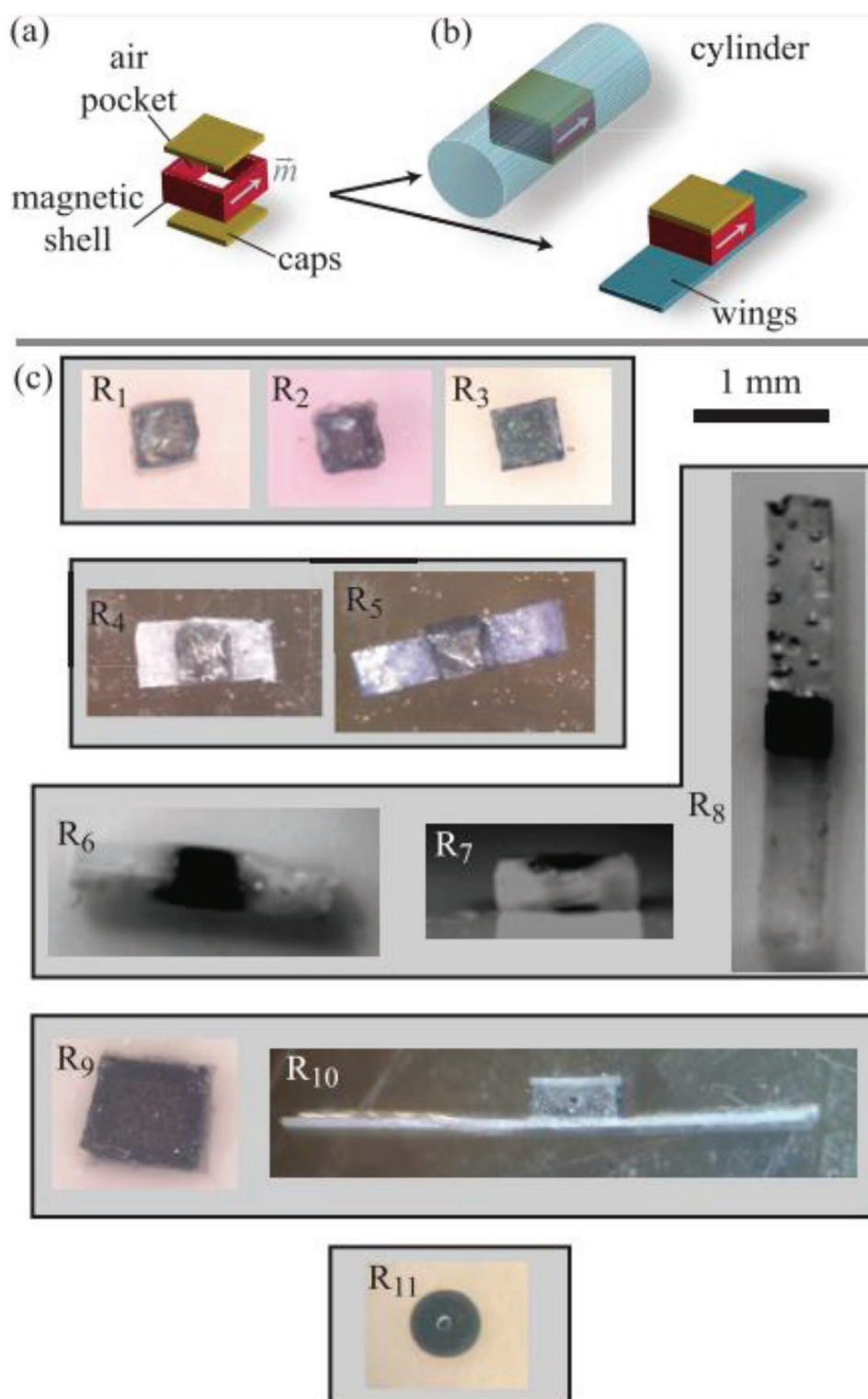
Despite differences in definition, the terms "tumbling" and "rolling" are sometimes used interchangeably in microrobot literature, both indicating a combination of rotational and translational motion. In general, rolling refers to the rotating motion of a spherical, ovoid, or cylindrical object spinning about an axis that stays fixed relative to the object's body. Tumbling refers to the cyclical rotation produced from repeatedly falling end-over-end, typically associated with rod-like objects with noncircular cross-sections. In this case, the rotational axis will shift relative to the object's body during the motion cycle. Tumbling can also refer to gaits where an unstable state, similar to falling motion of an inverted pendulum, occurs during the motion cycle.[105] For magnetic microrobots, similar actuation methods are used

for both tumbling and rolling locomotion, with robot geometry and the location/orientation of the axis of rotation being the primary differences.

Tumbling and rolling microrobots are typically actuated by the projection of a rotating magnetic field on the robot, though other forms of field modulation can be used as well. Electromagnetic coils are often used as the field source due to their lack of moving parts and ability to create spatially uniform fields, but rotating permanent magnets can also be used. These magnets are more straightforward to implement, require no electrical power to maintain the field, and are well suited for sustaining large magnetic fields. However, the magnetic field of a permanent magnet cannot be turned off like an electromagnetic coil and field manipulation is only possible through physical movement of the magnet. This limitation can lead to stray field gradients that pull on the microrobot as the permanent magnet is rotating, causing undesirable sliding motion.

Rolling locomotion using a rotating permanent magnet was demonstrated by Jiang et al. using a spherical magnetic microrobot.[106] The microrobot consisted of a 440 µm diameter UV adhesive ball encapsulating a 30 µm diameter iron wire. Cohesive forces produced the spherical geometry after UV adhesive was dripped directly onto a suspended iron wire. The resulting microrobot was shown to be capable of moving in air, water, and silicone oil over flat and bumpy surfaces at speeds of up to 13.2 mm s^{-1}. It could also be manipulated to move on predefined 2D trajectories.

Individual magnetic wires without encapsulating material are also capable of tumbling locomotion within liquid environments near solid surfaces. Rather than direct surface

**ADVANCED
SCIENCE NEWS**
www.advancedsciencenews.com

**ADVANCED
FUNCTIONAL
MATERIALS**
www.afm-journal.de

Figure 12. a,b) Schematics of a microrobot agent with an air pocket for buoyancy, and wings for increased fluid drag coefficient. c) Optical micrographs of various species of microrobots. Adapted with permission.[102] Copyright 2013, SAGE.

contact, hydrodynamic interactions occur between the wires and nearby walls when the wires are rotated. These interactions result in dissimilar boundary conditions between the two ends of the wire, yielding nonreciprocal motion and allowing for forward propulsion in low Reynolds number environments. Zhang et al. showed Ni nanowires ranging from 10 to 30 μm in length tumbling over flat surfaces and climbing vertical microchannel walls.[107] The wires could penetrate a 6 μm polystyrene

**ADVANCED
SCIENCE NEWS**

www.advancedsciencenews.com

**ADVANCED
FUNCTIONAL
MATERIALS**

www.afm-journal.de
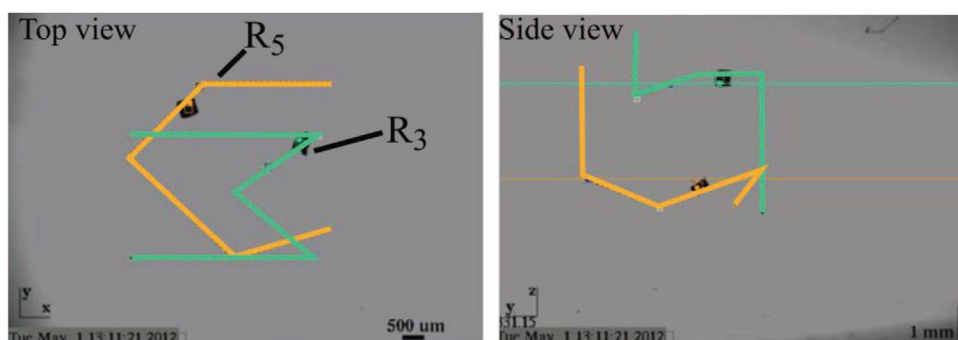
Figure 13. Two microrobots being independently positioned in 3D, following a path. Adapted with permission.[97] Copyright 2009, SAGE.

microbead onto one end and transport it to a target location in a controlled manner. Compared to direct pushing methods using catalytic nanowire motors, the tumbling nanowires experienced significantly less drag resistance from the cargo due to its noncontact nature with the underlying substrate.[108,109] Various step-out field rotational frequencies were observed for different lengths of wire, where the available magnetic torque was insufficient for counteracting fluid drag and keeping the wire's rotation synchronized with the rotating magnetic field. This limitation could be circumvented by increasing the field strength of the applied external field.

Mair et al. loaded alginate capsules with aligned ferromagnetic nanorods to create a microrobotic platform (MANiACs) for delivering biomedical payloads (**Figure 15**a).[110] The high magnetization of the fixed dipole nanorods allowed the capsules to be rotated with small magnetic fields using relatively low loading volume fractions. The capsules demonstrated guided tumbling locomotion on glass surfaces, biological tissue surfaces (rat intestine), and inclined surfaces (up to 15°) over centimeter-scale distances. As a group, they were able to manipulate other exterior objects, pushing a T-shaped microstructure four times their individual size across a flat surface in liquid. When loaded with a model small molecule in a controlled release study, the alginate capsules exhibited combined tumbling translation and payload release over a 1 h period. Pausing the tumbling locomotion led to increased molecular concentrations at given locations and allowed for location-specific payload delivery.

Self-assembling colloidal rotors can tumble along surfaces in the presence of a rotating magnetic field (Figure 15b).[111] Superparamagnetic beads were observed to assemble together
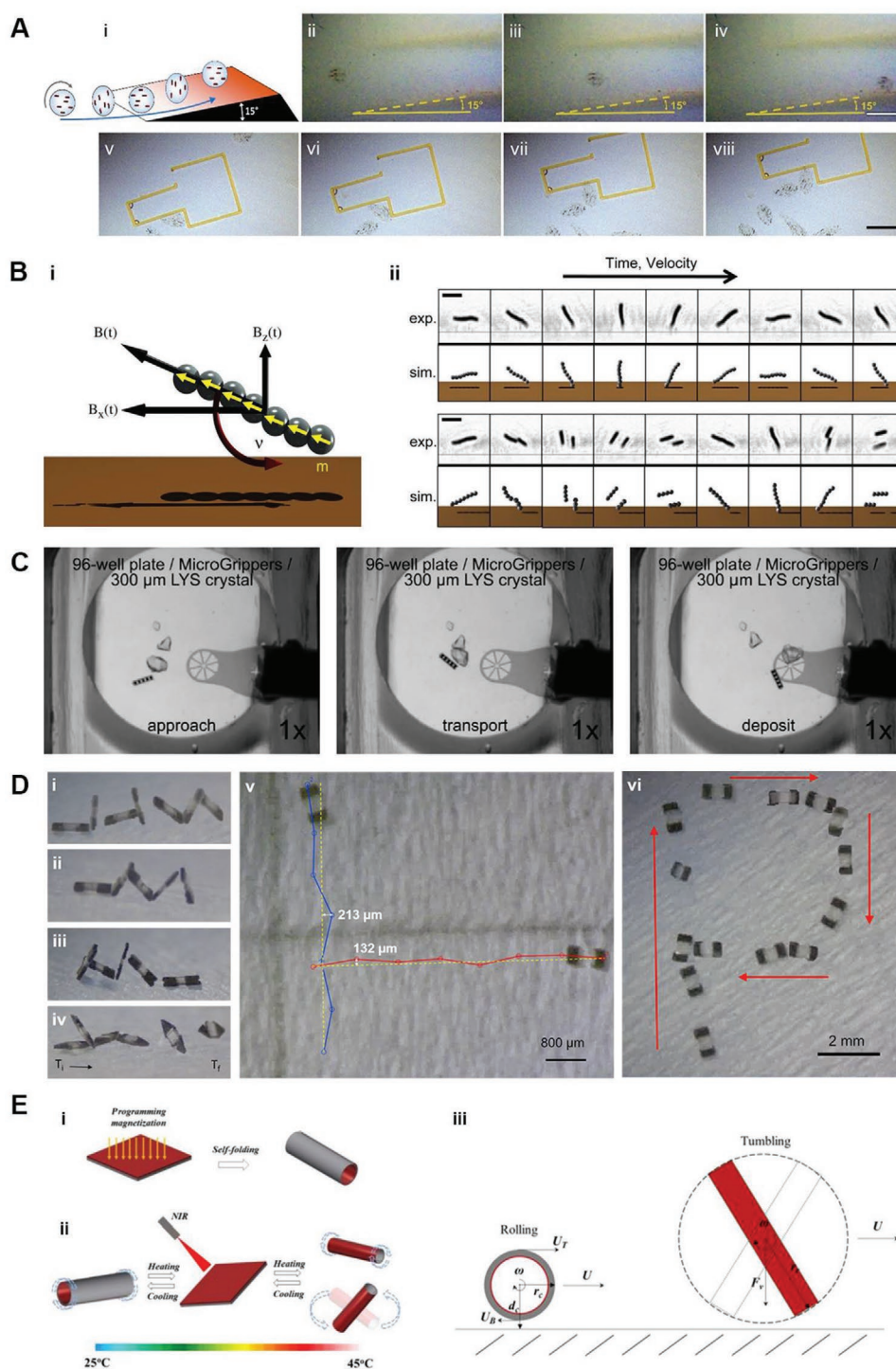
in chains when an external field was applied. The chains of beads behaved like elongated magnetic magnets and were held together solely with magnetic forces, allowing for their reversible assembly and disassembly. The length of the chains could be dynamically adjusted through the disassembly and assembly process to cater it toward a specific application or movement speed. As field rotational frequencies increased, fluid-induced drag forces overcame the cohesive forces between the beads and chain breakup occurred, resulting in reduced translational velocity. A simulation model was developed to accurately predict when the critical chain breakup frequency would occur. When collected in large numbers, groups of superparamagnetic bead chains were able to support and precisely move vesicles several times larger than the length of an individual chain.

A variety of additional geometries and substances have been demonstrated to tumble in liquid environments as well, including iron-containing multiwalled carbon nanotubes, red blood cells with attached magnetic particles, and DNA-linked anisotropic doublets of paramagnetic colloidal particles.[112,113] In liquid environments, instabilities during the tumbling gait are dampened by fluid drag and buoyancy forces. Many rod-like microrobots with geometry not optimized for tumbling locomotion can tumble under the presence of a rotating magnetic field. For example, helical magnetic microswimmers were observed to tumble after hippocampal neural stem cells were cultured on their surface.[57] When the cells were removed, the microswimmers rotated about their long axis as intended in a corkscrew motion.

Untethered magnetic micromanipulators rotating in viscous fluid induce local rotational fluid flows that can move micro-objects in the flow region without direct contact with the
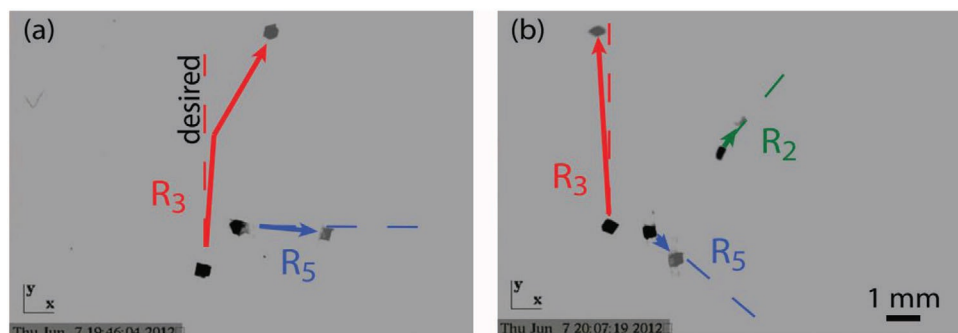
Figure 14. a) Two microrobots moving along perpendicular headings and b) three microrobots moving with different headings, in 3D. Adapted with permission.[97] Copyright 2009, SAGE.

**ADVANCED
SCIENCE NEWS**

www.advancedsciencenews.com

**ADVANCED
FUNCTIONAL
MATERIALS**

www.afm-journal.de

Figure 15. Tumbling and rolling magnetic microrobots. A) Rotating magnetic alginate capsules (MANiACs) are able to climb inclines and push photoresist structures several times their individual size. i) Schematic depicting MANiACs rotation and incline climbing. ii–iv) An alginate capsule climbing a 15° incline. Scale bar is 1 mm. v–viii) MANiACs are tumbling next to the corner of a hollow photoresist structure, resulting in successful manipulation by pushing the structure on a smooth glass surface. Reproduced with permission.[107] Copyright 2019, MDPI AG. B) Self-assembled colloidal rotors exhibit tumbling motion near solid surfaces under a rotating magnetic field. i) The geometry of an individual rotor. Each chain is composed of superparamagnetic beads that move according to the dynamics of the magnetic field B that induces a magnetic moment m on each bead. ii) Rotation along the x–z plane at a frequency v. Top: The aggregate moves along the surface in both experiment (frames taken 16 ms apart in a 5 Hz rotating field, scale bar is 5 μm) and simulation upon confinement at the surface. Bottom: When the field rotation is raised to 7 Hz, the rotors fragment periodically. Reproduced with permission.[11] Copyright 2010, National Academy of Sciences. C) Microscopic view of RodBot crystal manipulation with a fluidic vortex.

ADVANCED
SCIENCE NEWS
www.advancedsciencenews.com

ADVANCED
FUNCTIONAL
MATERIALS
www.afm-journal.de

manipulator.[90] A transversely magnetized rolling magnetic microrobot (RodBot) exploited this behavior to perform noncontact manipulation and transportation of micro-objects in liquids (Figure 15c).[92,114] The microrobot, a 50 × 60 × 300 μm polymeric block with internal cobalt-nickel posts, rolls continuously about its long axis to generate a fluid vortex above it while simultaneously translating forward. The vortex attracts and traps micro-objects without direct contact, offering coarse motion control of delicate, tiny objects ranging from a few microns to several hundred microns in size. Forces from the vortex range from a few nano-Newtons to tens of nano-Newtons and are spread over the surface of the object. Rising fluid flow generated in front of the microrobot from the rolling motion helps with trapping objects within the vortex. Using real-time visual tracking of the microrobot and surrounding obstacles, a holistic system was developed to automate the motion of the microrobot for protein crystal harvesting.[115–117] The microrobot was also capable of directly pushing 200 × 350 μm SU-8 micro-objects into a densely packed formation within a narrow channel.

While tumbling magnetic microrobots are typically actuated with a rotating magnetic field, Wuming et al. developed a tumbling microrobot actuated using an alternating magnetic field.[118,119] Here, a composite magnetic structure of a dumbbell shape was designed. The two "bell" ends of the structure each consisted of permanent magnets polarized in opposite directions, and a nonmagnetic bridge piece connected the ends. An electromagnetic coil system alternating between horizontal and vertical magnetic fields cycled the microrobot through different orientations, using forward momentum to produce a tumbling motion. The opposing magnetic polarities on each of the microrobot's ends ensured the resulting tumbling rotation maintained consistent directionality. Steering was achieved by changing the orientation of the projected magnetic field in the horizontal plane. The microrobot was able to move in dry and fluid environments on various 3D surfaces, including a tissue sample in saline, and capable of directly pushing SU-8 micro-objects using field gradients in liquid environments.

Tumbling locomotion using rotating magnetic fields exhibits similar performance over arbitrary surfaces in dry air conditions. Hou et al. demonstrated a rectangular stainless steel microrobot tumbling over an acrylic plate and over the surface of a coin.[120] The microrobots were shown to generate large forces relative to their size, capable of lifting small pieces of paper ≈7.8 mg in mass. Bi et al. further characterized tumbling motion using rectangular, polymeric NdFeb microrobots (μTUM), which showed improved magnetic response and configurable magnetic polarization (Figure 15d).[121] Photolithography using an SU-8/NdFeB microparticle slurry allowed for arbitrary 2D geometries on the magnetic ends of the microrobot. Various end geometries, including a triangular point and spiked corners, were tested and shown to be ineffectual for improving microscale mobility. Maximum incline climbing angles were measured to be 45° and 60° in dry air and liquid environments, respectively. The tumbling microrobot was also able to traverse over complex, patterned surfaces with protruding features and trenches smaller than the robot's body length. To better predict the impact of different design and environmental parameters, a novel simulation model was developed—capable of simulating the intermittent and non-point contact that occurs during tumbling locomotion.[122] The microrobot was able to locomote in vivo, inside a murine colon, while being observed through visual occlusions using ultrasound imaging, and could be functionalized with a drug payload coating.[123]

Soft magnetic materials can lead to microrobots capable of reconfiguration between tumbling and rolling locomotion. Huang et al. developed shape shifting soft microrobots made from self-folding hydrogel bilayer structures that morphed in response to temperature changes (Figure 13e).[124] On-demand modulation of individual microrobot mobility was demonstrated by morphing their shape using selective near infrared light (NIR) exposure. The magnetized hydrogel bilayer starts off as a planar sheet, folding into a tube shape when temperature decreases below a critical threshold (≈40 °C). When temperature increases above this threshold, the sheet refolds in the opposite direction around the perpendicular axis. Between the two shape configurations, the orientation of the folded tube changes with respect to the polarity of embedded magnetic particles and the microrobot can alternate between tumbling and rolling locomotion. Using NIR lasers, the tube radius and configuration of individual microrobots could be selectively controlled within a group. Tuning the tube radius directly affects the translation velocity of the microrobot, leading to differential motion control within a global magnetic field. Hu et al. also demonstrated microrobots capable of transiting between rolling and tumbling locomotion, among a variety of other locomotive modes.[125] These magnetoelastic microrobots used interactions between their nonuniform magnetization profiles and changes in the magnetic strength/orientation of the external field to curl and undulate into various shapes and gaits.

4. Magnetic Biohybrid Cellular Micro-Biorobots

Downscaling macroscopic actuation mechanisms to create microscale motion is often not feasible due to the limitation in fabrication methods and the difference of physical phenomena governed by low Reynolds number hydrodynamics

---

The RodBot lifts, transports, and deposits a lysozyme crystal toward an extraction-tool without physical contact. The RodBot and the crystal both have a maximum extent of 300 μm and are submerged in a 20%PEG3350 solution. Reproduced with permission.[114] Copyright 2015, IEEE. D) Motion lapse images of NdFeB tumbling microrobots (μTUM). Sideview tumbling gaits of i) rounded rectangular, ii) asymmetric rounded rectangular, iii) rounded protruding corner, and iv) triangular end geometry variations. v) μTUM tumbling trajectories (blue/red) relative to an ideal 5 mm long straight-line trajectory (yellow); the maximum trajectory drift for each is reported. vi) Rectangular μTUM traversing in a P-shaped trajectory using open-loop control. Reproduced with permission.[121] Copyright 2018, MDPI AG. E) Diagrams of shape shifting microrobots generated from magnetized hydrogel bilayer structures. i) Programmable magnetization and folding of hydrogel bilayers to generate magnetically controllable microrobots. ii) Shape switching concept for soft microrobots by increasing temperature using near infrared light exposure. iii) Free body diagram of the microrobot rolling and tumbling on a surface. Reproduced with permission.[124] Copyright 2016, IEEE.

**ADVANCED
SCIENCE NEWS**

www.advancedsciencenews.com

**ADVANCED
FUNCTIONAL
MATERIALS**

www.afm-journal.de

on the microscale. Biological systems have evolved over millions of years to move and function in an optimized way on the microscale. Thus, during the last decade, biohybrid systems have become attractive approaches to develop magnetic microrobots for several reasons. Evidently, for targeting biomedical applications, biocompatible microrobots are required which can propel, function, and be controlled under physiological conditions. For this reason, biohybrids are promising options. Further, cells are known to respond to their environment by many sensing and taxis mechanisms, as mentioned above for magnetotactic bacteria. As described in a previous review, the biological components can serve as various functional units, namely as templates, loading units or propulsion units.[126] Nanotechnology has allowed the integration of biological components as templates to create novel magnetically controlled biohybrid systems. Plant-derived structures have served as a basis to fabricate drug carriers that are magnetically actuated or guided.[127–131] Further, flexible magnetic microswimmers were created on the basis of bovine sperm cells, covered with magnetic nanoparticles.[132,133]

Regarding the magnetic control, we can distinguish between directional control and actuating control. If the biohybrid microrobots display self-propulsion by other means (as in the case of motile cells such as sperm cells or bacteria), only weak, constant magnetic fields are needed to introduce magnetic directional guidance. In contrast, when the magnetic fields serve as driving source, different configurations of magnetic fields have been employed. Here, planar oscillations or 3D rotating magnetic fields with various cone angles are applied.

In this section, we will summarize the advances of magnetic microrobots based on the integration of spermatozoa or bacteria.

4.1. Sperm-Based Biohybrid Microrobots

Spermatozoa were incorporated as propulsion sources or as templates for flexible magnetic swimmers, as illustrated in the following two sections. Spermatozoa are male gametes which swim to the egg cell with the help of their powerful flagellum. Their motility is based on the orchestrated action of molecular dynein motors, which bend and release the microtubule all along their axoneme. This leads to a bending wave motion of the tail, while the head is passively moved forward. Thanks to the strong propulsion force of sperm, they have been applied as power sources of hybrid microrobots. Lately, due to the intrinsic flexibility of the sperm cells, they have also been utilized as templates for magnetic microrobots.

4.1.1. Sperm-Driven Microrobots

Ferromagnetic microtubes offer a method for the capture and remote control of motile cells. By the use of strain engineering, 50 µm long rolled up nanomembranes were tuned in size to fit single bovine sperm cells.[134] The 60 µm long sperm cells randomly entered the rolled up microtubes, became mechanically trapped and started pushing the

microtubes forward. The rolled up nanomembranes contained a nanometer-thin iron layer, which enabled the magnetic remote directional control of the sperm-driven microrobots by small magnetic fields of just a few milliTesla.[135] In comparison to free sperm, the sperm-driven microtubes displayed a velocity reduced by around 80% due to the physical confinement of the cell, which restricts the flagella bending motion. In order to improve the performance of such hybrid microrobots, shorter rolled up microtubes (20 µm long) were fabricated and used for the coupling with the sperm cells.[136] This maintained a higher velocity of the biohybrid robots, but the coupling success was lower due to sperm cells being able to escape through the short microtubes more frequently. Next, surface functionalization methods were applied to bring sperm-binding proteins onto the inner surface of the microtubes for increased sperm binding.[136] This achieved a higher coupling success rate between the sperm cells and microtubes. Sperm cell release was implemented by incorporating a thermoresponsive polymer into the Ti/Fe microtubes. This enabled the opening and thereby releasing of the cells by a small temperature increase while also offering magnetic directional control.[137] In another approach, 3D printed polymeric microstructures were coated with an iron and titanium layer and used for capturing drug-loaded bovine sperm.[138] While the sperm cell was the propulsion source, weak magnetic fields were used for directional guidance to cancer spheroids demonstrating the suitability of the system for drug delivery applications. The 3D printed microstructure contained a four-armed front structure which offered a mechanical cell release mechanism. Recently, gelatin-based microcartridges were employed for sperm manipulation.[139] The magnetic nanoparticle-containing microstructures were fabricated by template-based polymerization of gelatin inside the pores of a polycarbonate membrane. The resulting microcartridges captured single sperm cells, which propel the structures under directional guidance of weak magnetic fields. These microcartridges were loaded with heparin, a sperm-activating agent that induced capacitation, a crucial sperm maturation step prior to fertilization. These gelatin structures also showed a controlled biomolecule release upon pH change, biodegradation under physiological conditions and a reactive oxygen scavenging effect. The latter is an important protection against reactive oxygen species, one of the main causes of sperm damage during in vitro handling. A study of motion of spermbots in bovine oviduct fluid demonstrated their ability to penetrate highly viscous fluids and how sperm adapt their beat pattern to the cargo load and surrounding media.[140] In an approach to deliver anticoagulants by spermbots, stream-like caps where used to capture bovine sperm cells and equipped with heparin-loaded liposomes.[141] These spermbots were introduced into a microfluidic flow chamber filled with diluted blood. It was demonstrated that the spermbots can swim against flow similar to the human blood stream and therefore hold potential in the drug delivery in the blood stream.

These gelatin structures also showed a controlled biomolecule release upon pH change and a reactive oxygen scavenging effect. The latter is an important protection against reactive oxygen species, one of the main causes of sperm damage during in vitro handling.

4.1.2. Sperm-Carrying Microrobots

Nonmotile sperm cells can be motorized by capturing them in tailored microhelices and applying rotating magnetic fields for their forward propulsion.[142] The microhelices were fabricated from photoresist by 3D nanolithography and subsequently coated with nickel. This enables a precise rotational magnetic actuation as well as forward and backward screw-like motion allowing the pick-up and release of the nonmotile sperm cells. This approach is especially promising for the delivery of nonmotile, but viable sperm to the oocyte. This method has prospects in assisted reproduction to treat certain types of asthenospermia (low or no sperm motility).

4.1.3. Sperm-Templated Microrobots

The flagellum of spermatozoa has an intrinsic flexibility with a bending stiffness that varies along the length of the tail. This has inspired researchers to use immotile sperm cells as templates for the facile fabrication of flexible magnetic microswimmers. The fabrication is based on the electrostatically driven self-assembly of magnetic micro- or nanoparticles and the sperm's surface. This resulted in different amount and localization of magnetic particles on the sperm's membrane. First, planar, undulating magnetic fields were applied with the use of four electromagnetic coils.[132] This resulted only in small forward velocity. In addition, the flexibility of the sperm template could not be maintained in an optimal way, because 1 µm microparticles impaired the flexibility of the sperm tail. In a next study, smaller, elongated 100 nm iron oxide particles were used for the self-assembly with the sperm. This maintained the flexibility of the sperm tail in an improved fashion.[143] The application of a 3D rotating magnetic field resulted in flexible bending motion of the magnetic sperm-templated swimmer. The applied frequency and cone angles can be used to control their forward motion and overall performance. When comparing the swimming mechanisms of the magnetically actuated sperm versus the motile sperm, the resulting waveforms differ from each other.[133] The magnetically actuated sperm are characterized by lower linearity, higher asymmetry and lower forward progression than their motile counterparts. The thrust force calculated by resistive force theory is higher in the case of the motile cells compared to the magnetically actuated sperm. This leads us to the conclusion that there is still much to learn from the biological motion mechanisms of spermatozoa. The study of such systems is useful for improving the design of flexible biohybrid microrobots.

4.2. Bacteria-Driven Biohybrid Microrobots

Similar to sperm cells, motile bacteria have been integrated as propulsive forces of hybrid microrobots. Bacterial motility types is diverse,[144–146] but for biohybrid propulsion, mostly flagellated bacteria have been employed. Prokaryotic flagella have a rotor on its base, anchored in the membrane of the bacteria. The propulsive force is generated by a molecular motor complex converting a proton gradient into the rotational motion of the bacterial flagellum that spins around a central axis. Bacteria display various taxis abilities which inspired microrobotics researchers to employ them as guidance and control mechanisms. Taxis mechanisms of bacteria include response to gradients of substrates, oxygen, pH, temperature, light or magnetic and electric fields. For the control of microrobots, thus far, chemotaxis,[147–150] aerotaxis,[151] magnetotaxis,[151–153] and pH-taxis[154] have been explored. A unique role play magnetotactic bacteria which display reorientation within magnetic fields due to their intrinsic magnetic moment created by their magnetosomes (see Section 4.3). Another nice feature of using bacteria as components of microrobots is the ability to genetically modify them easily to obtain certain desired properties.

In most bacteria-driven microsystems, the motile cells were attached to the artificial components by functionalizing the particle's surface to achieve receptor-based covalent coupling to the cell. *E. coli* was applied as driving source of bacteriabots by attaching them to polyelectrolyte multilayer microparticles.[155] Another attachment route is charge-based interaction, e.g., binding positively charged micro-objects to gram-negative bacteria.[156]

The guidance mechanisms of bacteria-driven microbots are vast, but here we restrict the scope to cases that apply magnetic guidance. Analog to the sperm-driven microtubes, bacteria were captured inside magnetic microtubes.[157] Here, the magnetic microtubes were fabricated by electrodeposition onto a polycarbonate membrane, resulting in polypyrrole microtubes containing nickel nanoparticles and polydopamine. In a planar setup of electromagnetic coils, *E. coli* bacteria were transporting the microtubes and guided directionally by weak magnetic fields. Further, Janus-type bacteriabots were fabricated by attaching *E. coli* to the iron caps of polystyrene particles. While the bacteria propelled the drug-loaded particles, weak magnetic fields could be used to reorient the bacteriabots.[158] Multiple bacteria were attached to superparamagnetic microbeads to decrease the stochasticity of motion and thereby enhance the magnetic steering controllability.[159]

Other types of microorganisms such as algae have also been employed as propulsion sources of magnetic microrobots. *Chlamydomonas reinhardtii* propels attached micro-objects with two flagella.[160] Microalgae such as *S. platensis* have been utilized as templates for magnetic helical swimmers.[129,43]

All here described types of cellular biohybrid microrobots display promise for translation into clinical scenarios, such as minimally invasive therapies for cancer treatment, biopsy and cell manipulation.[146]

4.3. Magnetotactic Bacteria

Magnetotactic bacteria (MTB) are aquatic microorganisms that are capable of biomineralizing nanometric magnetic particles (iron oxide or iron sulfide) supposedly to navigate along the earth's magnetic field lines.[161] These magnetic particles are protected by a biocompatible membrane and the whole, combined structure of particle and membrane, are commonly known as magnetosomes.[162,163] The size and shapes of the magnetite nanoparticles are genetically controlled and possess a single magnetic domain. Inside the bacteria, these

**ADVANCED
SCIENCE NEWS**
www.advancedsciencenews.com

**ADVANCED
FUNCTIONAL
MATERIALS**
www.afm-journal.de

Table 1. Shape, size, motility, magnetosome and magnetoaerotactic properties of several magnetotactic bacteria strains.

Magnetotactic bacteria strain	Cell shape	Size [μm]	Average speed[a] [μm s⁻¹]	Magnetosome ⟨crystal length⟩ [nm]	Magnetosome shape	Flagella	Magnetoaerotactic behavior	Ref.
Magnetococcus marinus (MC-1)	Cocci	1–2	119 ± 13.6	30–110	Elongated octahedral	2 × 7	Dipolar	[165,155]
Magnetospirillum gryphiswaldense (MSR-1)	Spirillum	3–4	23.3 ± 2.9	33	Cuboctahedral	2	Axial or mix of axial and dipolar	[165,166]
Magnetospirillum magneticum (AMB-1)	Spirillum	3–4	49 ± 20	45	Cuboctahedral	2	Axial	[167,168]
Magnetovibrio blakemori (MV-1)	Vibrio	1–3	8.5 ± 2.3	60	Elongated octahedral	1	Unipolar (oxic zone)	[165,166,169]
Magnetospirillum magnetotacticum (MS-1)	Spirillum	5.2 ± 0.5	44	30 ± 8	Cuboctahedral	2	Axial	[165,170]
UT-4	Spirillum	2–4	25.9 ± 1.4	10–50	Cuboctahedral	2	Dipolar	[165,171]
PR-1	Spirillum	1.6	50.5 ± 5.3	31–57	Elongated octahedral	2	Mix of axial and unipolar (oxic zone)	[165,166,172]
PR-2	Vibrio	No info	23.7 ± 3.6	Around 50[b]	Elongated octahedral	1	Dipolar	[165,166]
LM-1	Vibrio	3–5	20.7 ± 1.5	20–60	Elongated octahedral	1	Dipolar	[165,166,173]
SS-5	Rod	4–5	32.1 ± 2.2	86	Elongated octahedral	1	Unipolar (oxic zone)	[165,166,174]
Magnetospira thiophila (MMS-1)	Spirillum	0.5	49.7 ± 10.6	22–85	Elongated octahedral	2	Dipolar	[165,166]
SS-1	Cocci	No info	111.6 ± 21	No info	Elongated octahedral	2 × 7	Dipolar	[165,166]
PR3	Cocci	≈MC-1[b]	109.9 ± 13.2	Around 50[b]	Elongated octahedral	2 × 7	Dipolar	[165,166]

[a]Average speed at the anoxic zone; [b]Info provided by courtesy of Dr. C. T Lefèvre. Aadopted with permission.[173] Copyright 2020, Wiley-Blackwell.

magnetosomes align forming chains that provide a "compass" or "navigation system" by which the bacteria follow the Earth's magnetic field lines. The MTB compose a large, diverse and phylogenetic group of aquatic bacteria, its motility is powered by its flagella. An overview of different commonly found strain types and their corresponding reported properties is provided in **Table 1**. Some typical bacteria cellular structures are shown

Figure 16. TEM images of environmental magnetotactic bacteria with A) rod, B) coccoid, or C) vibrio cell shape. In addition, different shaped magnetosomes are distinguished: A) elongated octahedral, B) cuboctahedral, and C) rectangular morphologies. Courtesy of Dr. Christopher T. Lefèvre. Adapted with permission.[173] Copyright 2018, Wiley-Blackwell.
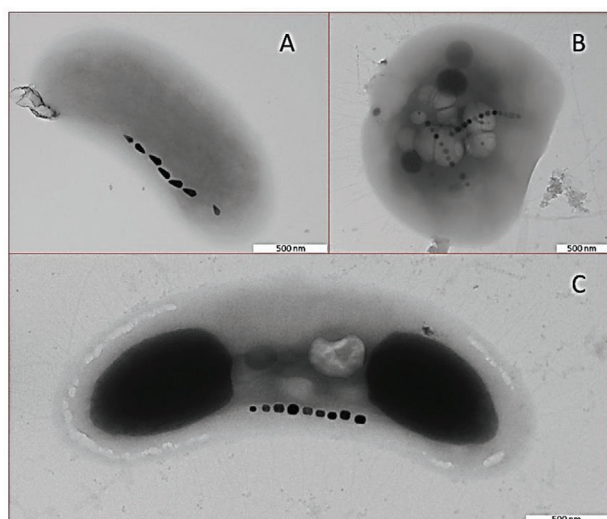
in the TEM images of **Figure 16**. Even though the collection of MTB from their natural environments may be relatively easy to achieve, the MTB are not easy to isolate or cultivate. Different strains might need different cultivation conditions.[164] A large number of magnetosome-producing microorganisms exist and are classified.[163]

Salvatore Bellini in 1963 found aquatic microorganisms that always moved in the same direction under his microscope.[175] In addition, he remarked that there must exist a biomagnetic "compass" in their body.

Independently, Richard Blakemore found similar microorganisms as Salvatore Bellini in 1975.[176] In his findings, he introduced the term magnetotaxis to describe the observed phenomenon. He was the first to present TEM images of the bacteria showing its flagella and the iron-rich nanoparticles in the cell body confirming so the hypothesis of Bellini that indeed particles in the cell internal structure act as a compass needle.[177]

4.3.1. Characteristics of MTB

A set of proteins control the biomineralization of the magnetosomes defining their size and shape. The exact biomineralization process is unknown, in the sense that not all discovered gene´s functionality, i.e., their actual roles in the process, are known. In addition, the existence, nature, and location of possible mineral precursors of magnetite are not clear. Recently it was showed that ferritin-like proteins, that were initially thought to be part of the magnetite biomineralization process involved storing excess iron as an inert iron phase to avoid Fenton Chemistry, are potentially not essential

ADVANCED
SCIENCE NEWS
www.advancedsciencenews.com

ADVANCED
FUNCTIONAL
MATERIALS
www.afm-journal.de

for the biomineralization process occurring in MSR-1 but involved in the resistance to oxidative stress.[178] It is known that the genes encoding magnetosome production are clustered within an about 130 kb sized genomic region called the Magnetotactic or Magnetosome Island.[179] Among different species, a common group of around 30 genes is identified (referred to as *mam* and *mms* genes) and is not present in nonmagnetotactic bacteria. This set of genes is thus expected to play an important role in the formation of the magnetosomes. The magnetic material needed for the formation of the magnetosomes is generally iron and taken up from the growth medium (or from the environment). A cytoskeletal structure composed of the MamK protein, which is a relative of the eukaryotic cytoskeletal protein actin; together with MamJ attaches the magnetosomes in a chain like structure.[180,181] Recently, the MamY protein was associated to the magnetosome alignment strategy.[182] More detailed information, on the genes involved in the biomineralization of magnetotactic bacteria, can be found, e.g., in refs. [183,184].

From a biological context, the steering of an entity to provide directed motion by means of an external signal is called taxis.[185] When the motion pattern is altered due to internal energetic condition it is called energy taxis.[186] The external signal can differ of nature being generally chemical (chemotaxis), light (phototaxis), or other like gravity (gravitaxis), magnetic (magnetotaxis), etc. In the specific case of the MTB, it uses a magnetically assisted aerotaxis (magnetoaerotaxis) allowing the MTB to locate and maintain an optimal position in vertical chemical concentration gradients (oxygen) thus minimizing its search area to a single dimension.[187] MTB may be found in sediments or chemically stratified water columns at the oxic–anoxic interface or in the anoxic regions. It is important to understand the MTB taxis as we could benefit or be inspired by its mechanism for application purposes.

A microcapillary assay is typically used in the lab to simulate the oxygen gradient encountered in the environment.[188,189] For this method a suspension of bacteria is loaded into a microcapillary, which is sealed at one end using a petroleum jelly plug and open at the other end. Directly a gradient forms by either the consumption of oxygen by the bacteria or due to the presence of the reducer in the plug. A magnetic field orientated antiparallel to the oxygen gradient is then applied. Migration toward the preferred oxygen concentration in the capillary and the orientation of the magnetic field promotes the initially homogeneously dispersed suspension of bacteria to organize into a densely populated band denominated as the aerotactic band. The insertion of oxygen microprobe into the capillary or a fluorescent dye sensitive to oxygen detects the actual oxygen gradient present in the capillary.[190]

Regarding Flagella, one has to bear in mind that for MTB, the magnetic field provides the directionality. In a homogenous magnetic field, the bacteria will align, as would a compass needle do, but it needs motility in order to propel. Instead of the typical run-and-tumble known for *E. coli*, a run and reverse is typically observed for MTB.[191] This is, without any U-turn of the cell body, the bacteria inverse their propulsion direction while simultaneously maintaining the direction of their magnetic moment. An overview of flagella apparatus from a set of typical bacteria species is provided in Table 1. The average

observed speed can partly be correlated to the different types of flagella they possess. For example, the two sheath of seven flagella that MC-1, PR-3 and SS-1 possess provide the fastest motion compared to the single and biflagellate bacteria. Detailed description on flagella and MTB is available[187] as specific studies for the MC-1 strain.[192]

Regarding sensing, each MTB species exhibit a different mechanism. The magnetotactic behaviors are described by either one or a combination of dipolar, axial, and unipolar mechanism.[165] In the previously described microcapillary assay, dipolar magnetotactic bacteria produce a microaerotactic band and by reversing the magnetic field, the cells swim persistently move away from the initial band. The swimming mode of polar magnetotactic bacteria is a two state sensory mechanism, the activation of either state is determined by the concentration of dissolved oxygen sensed by bacteria and not by the gradient. The direction toward where the bacteria swim is determined if they sense a concentration above or below a given threshold. Above this threshold, north-seeking dipolar bacteria will swim toward the North Pole and below this threshold, they will swim toward the South Pole.[165]

In some population of bacteria, such as, e.g., MS-1 and MSR-1, no apparent distinction between north- and south-seeking bacteria arises. They move back and forth without any unidirectional motion. This behavior corresponds to axial magnetotaxis, and is only found in pure cultures and not within environmental isolates. In the microcapillary assay, they are not dispersed upon changing the direction of the magnetic field.[165]

The unipolar magnetotactic behavior can only be distinguished in the microcapillary assay when the magnetic field is reversed. The microaerotactic band formed by unipolar magnetotactic bacteria swim as a single population either persistently toward north (MV-1, SS-5, PR-1) or south (RS-1).[165] Those swimming north can upon field reversal sense the dissolved oxygen concentration. When present at the region with high levels of dissolved oxygen (oxic side of the band), they sense and follow the magnetic field, and nevertheless at low oxygen levels (anoxic side of the band) they sense and follow the oxygen gradient.

MTB have been shown to be able to overcome tortuous flow fields. Studies of AMB-1 navigation in complex flow environments in a microfluidic chip showed that MTB overcome 2.3-fold higher flow velocities when directed to swim perpendicular to a given flow as compared to upstream, as the latter orientation induces higher drag. Magnetotaxis enables MTB to overcome counterdirectional flow at threshold values of drag (9.5 pN) and flow velocity (550 μm s^{-1}).[193] In addition, MTB migration in porous media is such that MTB circumvent obstacles by repeatedly switching between forward and backward runs.[194] Finally, evidences of a genetic link between aero- and magnetotaxis and magnetotactic polarity were reported.[195]

4.3.2. Applications of Magnetosomes and Bacteria

The same way the bacteria uses these magnetosomes to guide themselves, they can interact with any external magnetic field allowing remote control of their navigation, an easy detection,

and a means to visualize them. The bacteria are biocompatible, allow easy chemical functionalization and the individual magnetosomes can be harvest and chemically modified. All these properties make both bacteria and magnetosomes potential candidates for a variety of applications.

Regarding magnetosomes, their highly desirable single domain magnetic domain, the ability to functionalize their lipid membrane, and their biocompatibility has allowed their usage in several fields such as contrast agents for Magnetic Resonance Imaging (MRI),[196,197] separation of biomolecules,[198–200] cellular homeostasis disorder,[201] hyperthermia therapy,[202,203] photothermia therapy,[204] immunoassays,[205] drug delivery,[206] biosensing (Peroxidase-like activity),[207] and stain removal.[208]

Living MTB are also used in a variety of application varying from separation of biomolecules,[209] MRI,[210,157] detection of biological entities,[211] hyperthermia therapy,[212] immunoassays,[213] drug delivery,[155] biosensing,[214] pathogen killing,[215,216] domain analysis of soft magnetic materials,[217] waste treatment,[218–222] electromagnetic induction,[223] to model for Human CDF-related type-II diabetes.[224]

However, the aim of the present review is to analyze the magnetotactic bacteria in robotics. Using the bacteria as a micro/nanorobot is easily justified if we analyze the general requirements for a nanorobot designed for nanomedicine. The micro/nanorobot should be able to selectively target a region of interest transporting a given payload. Even more, the micro/nanorobot should be self-propelled, thus present motility, to reach larger area, be able to sense, and interact with the local environment. They must be detectable in order to track and analyze them. Furthermore, the micro/nanorobot should be programmable or remotely controlled.

This is important not only for nanomedicine applications but even in the broader robotic context. If we consider the basic components of a generic robotic system, i.e., sensory system, control system, and actuation system, the MTB perfectly complies them. A simple schematic of the bacteria highlighting each component is presented in **Figure 17**.

Overall, to use the bacteria as a microrobot or bacteriabot, there is thus a need to understand their sensing mechanism and control their motility (Taxis) remotely. In addition, their detection is needed for analysis purposes. An overview of engineered systems and strategies for this end are given in the following section. In addition, as for closed loop control, the magnetic moment is of importance. Accordingly, a rapid overview on different ways to measure the magnetic moment is provided. For application purposes, loading a cargo is essential and therefore works with different functionalization strategies are also discussed.

4.3.3. Microrobotic Applications of MTB

For utilizing the MTB in technological application, a key feature needed is the ability of steering them from a remote distance. Many of the pioneering work on developing a programmable guiding system for MTB for applications in robotics/drug delivery is done by a well-designed magnetic guiding system. For example, it was shown that using a custom-made electromagnetic grid it is possible to manipulate the MTB in a programmable fashion, to make them follow paths to manipulate other objects.[225] MTB can be programmed to pick-up a microbead and to move along an externally programmed magnetic field line. For this, a mixture of MTB and microbeads is dispersed over a glass slide and by applying thereafter a current makes 1% of the bacteria to attach to the microbeads and start pushing after 5 min.

In vivo experiments in the carotid artery of a living swine, show that the MTB can propel and steer a ferromagnetic bead of 1.5 mm in vivo using a magnetic resonance imaging platform (MRI).[226]

Controlled MRI propulsion and steering of MTB strain MC-1 has been shown, this method allows additionally to visualize the MTB.[157] This research was the first report on how to control MTB without addition of chemicals. Many works have since
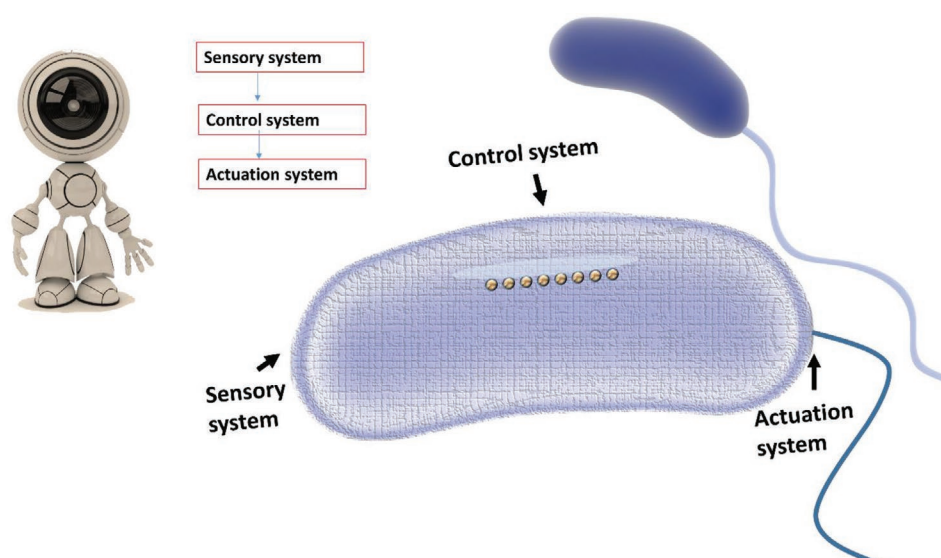
Figure 17. Schematic showing the basic components of a robotic system and highlighted in a magnetotactic bacteria.

**ADVANCED
SCIENCE NEWS**
www.advancedsciencenews.com

**ADVANCED
FUNCTIONAL
MATERIALS**
www.afm-journal.de

then been published which used similar MRI guiding systems. The most important is perhaps the one where MTB deliver drug-containing nanoliposomes to localized tumor hypoxic regions by the MRI guiding system.[155]

Other approaches to generate magnetic fields as guiding systems has been studied by combining Helmholtz coils and Maxwell coils, using permanent magnets or by customized electromagnetic coils. For all of these, a closed-loop control system is required for accurate positioning and different models predict the relation between the applied current and generated field and can be categorized by their actuation.[17] However, common methods like the linear proportional-integral-derivative (PID) method does not take in to account uncertainties and nonlinearities of the microrobot motion. A robust control of a given microrobot trajectory with no chattering to follow step inputs was done by the implementation of a time-delay-estimation model as method to enhance the closed-loop control system.[227] Despite this progress, when testing in mice by injecting a swarm of bacteria, only a low percentage of bacteria was found around the targeted tumor. Many cells stray off due the heavy current and never reach calmer capillaries. A further improvement on closed loop control systems for point-to-point positioning of microrobots is to introduce a null-space control system to closed loop system.[228] The MTB is guided to a reference point and its magnetic moment is obtained by the U-turn approach under reversal of the magnetic field and used to readjust its position. Thus, first the MTB orientation is controlled and thereafter a field with alternating directions is applied to decrease the MTB velocity allowing thus to control the MTB positioning. This approach allowed to control the MTB along a microfluidic maze.[229]

Antibiotics were successfully delivered to a an infectious biofilm by a MTB powered bio hybrid composed of MSR-1 integrated in a silica microtube.[215] This biocompatible encapsulation allowed the successful cargo loading of antibiotics and the MTB motility increased the effective targeting disrupting the biofilm.

In digital microfluidics (DMF), discrete droplets containing samples and reagents can be controlled to implement a series of operations via electrowetting on dielectric, magnetic, surface acoustic wave, and other stimuli, depending on the mechanism of droplet actuation.[230] This typically works on (super) hydrophobic surfaces. On the contrary to microchannel, DMF provides simple and precise control over multiple reaction processes in where each droplet is actuated independently allowing multiple functionality. Their applications span from chemical and enzymatic assays, immunoassay, cell based-operation (culture, sorting and purification), DNA-based applications (extraction, purification, amplification, and detection), and protein analysis.[231] MTB are used to provide actuation of aqueous droplets on a superhydrophobic surface for DMF.[232] A whole drop containing MTB can follow a set of trajectories and effectively apply DMF to perform a microfluidic phosphatase assay. Here the MTB in addition acts as a source of enzymes that generates a color reaction when the bacteria was merged and mixed with a droplet containing the substrate (p-nitrophenyl phosphate) to analyze.

The MTB self-assembly process can also be a tool for robotic applications.[233] For this, understanding the role of the hydrodynamics and magnetism involved is essential. The hydrodynamically self-assembled magnetic bacteria orients perpendicular to a surface and are self-limiting, reaching a quasi-static state. This phenomenon leads to the analogue observed in inactive colloidal systems called "self-focusing regime." Therefore, it can be used in a more general model for the design of self-assembled systems, allowing stable structure formation in designed artificial systems. In addition, MTB clusters may be directed along controlled paths or distorted under the influence of in-plane fields. This allows to controllably assemble/disassemble MTB clusters and potentially use them to transport cargo to specific locations.

More information on the progress of different guiding system for drug delivery, magnetic manipulation, and actuation are available in the following chapters.

Many researchers are inspired by microorganisms and try to mimic their main properties or combine microorganisms with other engineered strategies to form so-called bio hybrids. Specifically the swimming capabilities of bacteria at low Reynolds number, in where viscous forces dominate, are of great interest. Combining a biological component with another material to modify their properties is in fact present in some of the works previously presented. For example, the bio hybrid system of the MTB in a silica microtube that allowed facile cargo loading, antibiotics, and its targeted transport to disrupt a biofilm.[215] Another MTB based bio hybrid is the system in where AMB-1 was combined with iron oxide nanoparticles to change its magnetic properties and ease the control of the MTB magnetotaxis.[234] The functionalization herein was of great interest, as we will discuss later on. Besides these examples, there are many more bio hybrid systems with magnetic control, which have successfully been achieved and some are highlighted in the following.

We shortly discussed the role of the bacteria flagella earlier in this section, where a molecular motor rotates the helical flagella for forward propulsion. In microalgae (as in all eukaryotes), the two flagella produce planar waves, such as breaststroke waves in C. reinhardtii, by bending.[235] An increase up to 100% efficiency is proposed for the planar wave compared to the single helical flagella.[236] However, the microalgae lacks magnetic properties and therefore an adequate steering mechanism for its usage in robotics is missing. An approach to provide magnetic properties to the microalga species C. reinhardtii is to culture them in a media containing terbium ions (Tb_3^+).[237] These ions are known to possess magnetic properties and to present photoluminescence and could therefore potentially be used as a biomarker. The grown microalgae presented superparamagnetic properties and their motion could be controlled by magnetic fields and tracked by their photoluminescence.

Another MTB inspired robotic microswimmer was designed by isolating flagellar filaments from Salmonella typhymurium and magnetic nanoparticles.[238] By using avidin–biotin linkages, a magnetic nanoparticle was conjugated to a polystyrene microbead. The construction consisted of 3 phases. First, biotinylated monomers were utilized in a flagella repolymerization reaction to produce flagellar filaments that had biotin groups at both ends of the filament. Second, the microbeads and magnetic nanoparticles were functionalized with avidin. In the last step, all components were mixed yielding the magnetic biomimicking microswimmer. Their motion could be controlled by a set of Helmholtz coils.

Magnetic bio hybrid capable of moving large superparamagnetic beads are designed by randomly attaching multiple *Serratia marcescens* (*S. marcescens*) bacteria a 6 µm diameter streptavidin coated superparamagnetic bead through streptavidin–biotin binding.[156] The modified beads where added to the bacteria motility medium, mixed with LB, and incubated for 5 minutes to allow for bacterial attachment to the beads by means of surface protein binding to the biotin–streptavidin bead coating. Remote control of their motion was successfully shown by applying weak magnetic fields.

Motivated by developing new fertilization methods, where the transport of a single spermatozoon to the egg cell location is required, successful encapsulation of motile sperm cells in microtubes demonstrated the first sperm-driven magnetic microrobot.

4.3.4. Determining the Magnetic Moment of MTB

Determining the magnetic moment of MTB is of interest for closed loop applications as the region of convergence (which is the region around a reference point of interest), depends directly on the magnetic dipole moment.[239,240] The larger the dipole moment, the higher the positioning accuracy through the closed loop control will be. There exist several techniques for the MTB magnetic moment determination, and could be categorized as indirect and direct magnetic moment measurements.[184]

The counting of magnetosomes, by direct visualization with electron microscopy, and knowing the magnetic moment per unit of volume of the magnetic material allows estimating the total magnetic moment

$$M_{total} = n_{Mag} \cdot V_{Mag} \cdot M_V \qquad (1)$$

where n_{Mag} is the number of magnetosomes, V_{Mag} corresponds to the volume of each magnetosome, and M_V corresponds to the magnetic moment per of volume of the magnetic material. For the case of magnetite $M_V = 480 \times 10^{-3}$ A m^2 cm^{-3}.

Due to the sizes of the magnetosomes, they act as superparamagnetic particles or stable single domain (SSD) ferrimagnets.[241] When an external magnetic field is applied to these magnetosomes, their average magnetization orientation follows the average in fluctuations along the cosine of the angle between bacteria velocity and external applied magnetic field. Mathematically, this is described by the Langevin function that relates the bacteria magnetic moment and applied field with the thermal fluctuations. In this way by analyzing either the velocity or orientation of a single bacterium, its magnetic moment is estimated.

Another indirect way is by analyzing the U-turn the bacteria performs when applying an external magnetic field and changing the direction (Bean model). In this case, exactly at the point where the bacteria trajectory is changed, the sum of magnetic torque and viscous torque are equal in magnitude when considering low Reynolds number and ignoring flagellar forces. The helical radius (L) is determined as a function of the magnetic field, particle shape and magnetic moment. In addition, the turning time (τ) as a function of the magnetic field

can be calculated and compared to the experimental observed turning time to validate the magnetic moment or to determine the same

$$\tau = \frac{8\pi\eta R^3}{mB_0} \ln\left(\frac{2mB_0}{k_B T}\right) = \frac{L}{\pi v_0} \ln\left(\frac{2mB_0}{k_B T}\right) \qquad (2)$$

Here, B_0 is the magnetic field, R is the radius of the cell, η is the viscosity k_B is the Boltzmann constant, T is the temperature, and m is the cell magnetic moment.

Using this method Esquivel and Lins de Barros analyzed a set of MTB.[242]

Based on the same method, by applying rotating fields and finding the maximum frequency (f_C) for which the bacteria maintains its circular trajectory it is possible to calculate the magnetic moment as they relate by the following equation

$$M_{total} = c\eta 2\pi f_C l^3 / H \qquad (3)$$

where H is the applied magnetic field intensity, c is the shape factor, η is the viscosity, and l is the bacterium length. This method allowed to provide the magnetic moments of MYC-1 MTB strain.[243]

Of course, alternative methods and other parameters can be extracted by analyzing bacteria trajectories and are encouraged to be revised also.[244]

The superconducting quantum interference device (SQUID) allows direct determination of the magnetic field generated by a given element. It consists in two superconductor magnets separated by an insulating layer, when a DC current is applied to the device, the voltage oscillates with a frequency that is proportional to the change in magnetic flux passing the device. Counting the oscillations allows calculating the flux change, which has occurred. The SQUID is a reliable method for determining the average magnetic moment of small samples of magnetotactic microorganisms collected directly from the environment.[245]

Another technique that allows direct detection of the magnetic moment is the vibrating sample magnetometer (VSM). Here, as indicated by its name, the sample of interest is vibrated in a detection coil space. The induced voltage in the coil is proportional to the magnetic moment following Faraday´s law of electromagnetic induction. The sensitivity is typically around the 10^{-6} emu. The VSM easy usage and setup allows to study samples in different configurations such as the MTB, AMB-1, dispersed in a silica gel matrix.[246] The immersion in a silica gel allowed constraining the role of an external applied magnetic field on the alignment of magnetosome chains. This permits to study reorientation of the chains within living magnetotactic bacteria exposed to an external magnetic field dirrectly. A stable deviation is observed of the chain orientation within living cells suggesting that the assembly of cytoskeletal proteins are the responsible for the regulation of the nanocrystal organization and possess a dynamic character.

Optical techniques are used in where the optical properties changes are proportional to the presence or changes of magnetization of the sample. In general, these optical measurements have fast, reliable output and are relatively less expensive compared to the SQUID or electron microscopy.

Near field scanning optical microscopy (NSOM) together with the magneto-optical Kerr effect (MOKE) can be used to visualize and analyze the magnetic properties of the MSR-1 bacterial cells.[247] The combined techniques allows visualizing and magnetically characterizing both magnetosomes and cells directly. Light scattering can be used to determine average lengths and magnetic moments of the MS-1 bacteria.[248] Obtained MTB magnetic moments by this technique are comparable with those obtained from electron microscopy. Magnetic induced birefringence also allows to determine the magnetic moments of MTB.[249] The techniques is a fast and reliable method and comparable to results obtained by light-scattering determinations and estimates made from electron microscopy. The orientation of the bacteria, upon applied magnetic field, follow an angular distribution, which affects the structure factor in the scattered light intensity. This phenomena was used to characterize south and north seeking MTB in both AMB-1 and MO-1.[169]

4.3.5. Loading a Payload/Cargo to MTB

Another critical step toward the efficient use of MTB for delivering therapeutics or nanorobotics is to develop a method of loading the bacteria while maintaining its overall properties unchanged. In this sense, the modification of MTB with nanoliposomes for MRI targeted drug delivery had great impact[155] and the MTB encapsulated in the silica microtube[215] also allowed to maintain the MTB properties. However, the modification of MTB with nanoliposomes had been accomplished before by covalent binding through carbodiimide chemistry.[250] In this case, amine-containing molecules of bacteria covalent bind to carboxylated liposomes. Also, other cargo binding to bacteria based microrobot are done through immunoreactions.[251] Whereas, the work discussed in the bio hybrid section in where Fe_3O_4 magnetic materials are deposited on the MTB surface was even achieved through electrostatic interaction and shown that the overall MTB surface charge is negative allowing to effectively immobilizing positively charged molecules.[234] MSR-1 could so be modified with positively charged DNA coated gold nanoparticles to mimic transmembrane proteins. Increasing the loading efficacy and as a means of visualization.[252] Several attachment strategies via physical synergies are thus available and in general they can be classified by hydrophobic/electrostatic interaction, inherent response and chemical interaction such as streptavidin, biotin, and covalent binding.[102,103]

5. Electromagnetic Soft Actuators

Electromagnetic actuators (e.g., DC motors, solenoids, voice coil motors, etc.) are, by far, the most widely being used type of actuators in the traditional robotic applications. This is due to their ease of operations, simplicity in control and efficiency in converting electrical power into mechanical actions, but they are made of rigid elements. The problem is, rigidity in the materials of an actuator limits its performance in many robotic applications, especially when the robotic platform is supposed to physically interact with humans. In these scenarios, in order to guarantee safety of humans with whom the robot is physically interacting, the body of the robot, an especially its actuators as sources of providing energy, should be soft. The question is how to make an electromagnetic actuator with soft materials.
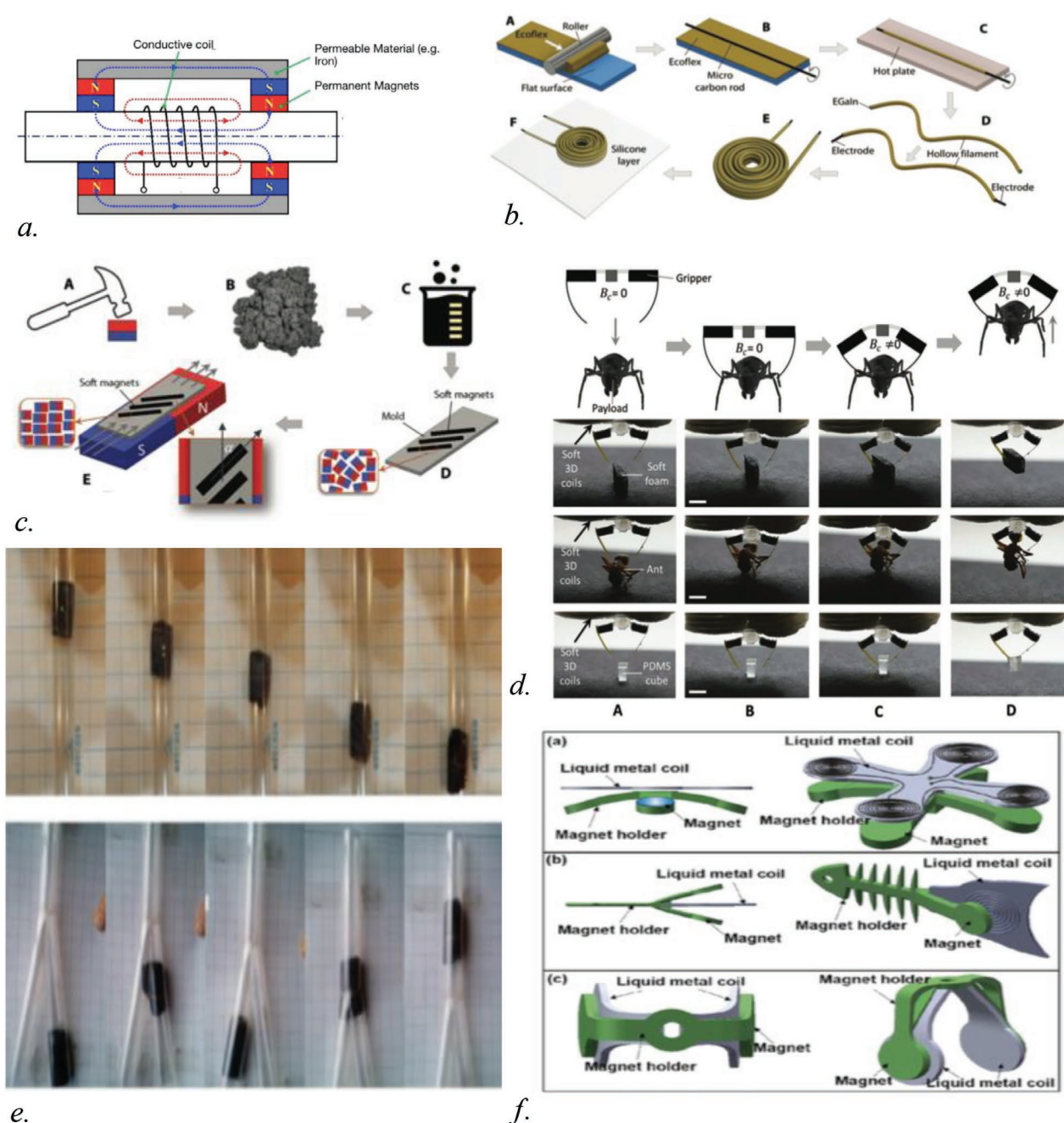
5.1. Fabrications

In order to fabricate electromagnetic soft actuators, the working principle and essential components of such actuators have to be identified and then realized with soft matters. The fundamental working principle of all electromagnetic actuators is based on interaction forces between two magnetic fields: a magnetic field due to presence of a permanent magnet and another magnetic field created by an electromagnet (i.e., current through a conductive coil).

Therefore, in order to build a soft electromagnetic actuator, we need to realize a permanent magnet as well as a conductive coil with soft matters. In addition, we would need a soft material that can get magnetized when it is exposed to an external magnetic field and keep its magnetization for a while when the external magnetic field is removed, a property that is defined as permeability. In traditional rigid electromagnetic actuators, usually Iron is being used as a return path for the magnetic field as it has high permeability. A representative example of an electromagnetic actuator (solenoid)[253] is shown in **Figure 18**a with its fundamental components.

To realize conductive wire, researchers have used conductive liquids such as Eutectic Alloys Galinstan (68% Ga, 21.5% In, and 10% Ti)[257] and Eutectic Gallium Indium Alloy (EGaIn, 75% Ga, 25% In by mass).[258,259] These liquids can be injected into soft micropipes or microchannels made of rubbery-like materials, that are usually made of PDMS, also known as dimethylpolysiloxane or dimethicone,[260,261] belong to a group of polymeric organosilicon compounds that are commonly referred to as silicones. The PDMS body of the micropipe or microchannel plays role of an insulator for these soft wires. Micropipes can be realized using extrusion fabrication techniques or by a method Do et al.[254] where a thin layer of Ecoflex[262–264] (a blend of recycled polymers and wood byproducts that exhibits characteristics of the polymers and wood) powder is laminated on a flat surface using a stainless-steel roller and then a fine carbon fiber rod is rolled onto the thin polymer layer. The laminated layer and rod are then heated and then the rod is pulled out and EGaIn is injected and then the whole filament will be formed as a coil (Figure 18b).

The other method to realize a soft conductive coil is creating microchannels with 3D printing techniques.[265,266] The advantage of 3D printing microchannels over the previously described method of realizing microtubes is achieving higher-dense, more compact coils with smaller cross-section area. This would lead to generating larger amount of forces as the electromagnetic force that can be generated is a function of number of the conductive loops. However, the fabrication of these microchannels requires high-end 3D printers such as Nanoscribe[267,268]that are extremely expensive.

Figure 18. a) Fundamental components of a Solenoid (permanent magnet, permeable material and conductive coil).[253] b) Fabrication process for the soft, 3D helical coil inductor. A) A thin layer of liquid silicone elastomer (Ecoflex 0030) is laminated onto a flat surface using a stainless-steel roller. B) A fine, carbon fiber rod is rolled onto the thin silicone layer. Adapted with permission.[254] Copyright 2018, Wiley-VCH GmbH. c) Fabrication process of soft permanent magnets: A) crush a permanent magnet into B) powders which then C) mixed with liquid silicone polymer using a mixture machine. D) Pour the suspension of magnetic particles and PDMS into a 3D printed mold and E) align the mold above a permanent magnet to elicit a specified magnetization orientation. Adapted with permission.[254] Copyright 2018, Wiley-VCH GmbH. d) Manipulation process steps and experimental validation for the miniature gripper with a soft foam cube, an ant, and a PDMS cube. A) Initial position of the gripper. B) The gripper approaches vertically from the top to the payload. C) The gripper holds and lifts the payload. D) The gripper moves back to its original position. The objects are ≈2 mm wide. Videos for real-time experiments are presented in the Supporting Information. Scale bar: 2 mm. Adapted with permission.[254] Copyright 2018, Wiley-VCH GmbH. e) Top: First trials along X axis of WSL robot. Bottom: Steering motion of WSL robot. Adapted with permission.[255] Copyright 2014, American Institute of Physics. f) The structure of the soft mechanical devices. a) The structure diagram of the jellyfish soft robot, b) the structure diagram of the soft fishtail, and c) the structure diagram of the soft manipulator. Adapted with permission.[256] Copyright 2018, Springer.

Compared to traditional copper wire that is being widely used in almost any electromagnetic actuator, the use of conductive soft wire with conductive liquid inside PDMS has some limitations as well as some advantages. First of all, the specific resistivity of copper (1.68×10^{-8} Ω m, at 20 °C[269]) is less than that of any conductive liquid, for example EGaIn (24.9×10^{-6} Ω m, at 20 °C[254]).

**ADVANCED
SCIENCE NEWS**

www.advancedsciencenews.com

**ADVANCED
FUNCTIONAL
MATERIALS**

www.afm-journal.de

This means smaller input voltage is required to achieve same amount of electric current through a copper wire compared to a case for EGaIn-based soft wire at the same length and diameter, and therefore using copper wire, is more energy efficient way of generating electromagnetic force, as the force is function of electric current. However, copper wires are very sensitive to the magnitude of the current going through them. As the current increases, the heat increases and that can burn out very tiny insulator cover of the copper wires. However, using soft wire has more robustness against the generated heat, as EGaIn is already liquid with very high vaporing temperature[258] and also PDMS has also very high melting point.[270] This means that the current limitation using a soft wire is much higher than that of a copper wire and as a result larger amount of force can be generated using soft wires, however, that would be at the cost of energy efficiency.

Fabrication of permanent magnets from soft materials is very challenging. Permanent magnets are usually made of from "hard" ferromagnetic materials such as Alnico and Ferrite[271] that are subjected to special processing in a strong magnetic field during manufacture to align their internal microcrystalline structure, making them very hard to demagnetize.[272] Here, the word "hard" refers to ferromagnetic materials that can be easily magnetized but hardly get demagnetized, in other words they can keep their magnetism for a long period of time. The problem is magnetically hard materials such as Iron and Alnico, are also mechanically hard.[14] In order to make mechanically soft permanent magnets, there are basically two main techniques: extrusion and molding. The extrusion technique is usually used for fabrication of rubber magnets where the granular material (such as NdFeB granule neodymium) is heated until it starts to melt and then forced under high pressure using a screw feeder through a hardened die where it is mixed with rubber. The die has been electrical discharged and eroded to have the desired shape. As materials continually flows from the die, it cools and passes over a magnetism fixture that magnetize the granule.[273]

Another method of fabricating soft permanent magnet has been proposed by Do et al.[254] (Figure 18c) where a permanent magnet is hammered and crushed to powder. The powder is then mixed with liquid Silicone polymer and then poured into a 3D printed mold. The mold is then placed inside a strong external magnetic field so that the magnetic particles align during the curing process. Once completely cured, the magnetic particles will stay aligned even if the external magnetic field is removed. The advantages of this molding fabrication technique over the extrusion one, are 1) the direction of magnetic field with respect to the base material can be easily adjusted by simply tuning the direction of external magnetic field and 2) it is cheap and doable in a lab environment. However, the flexible magnets made through extrusion technique have stronger magnetic field. Nevertheless, the magnetic fields of flexible magnets ae not as strong as those of commercially available, traditionally hard magnets.

Fabrication of magnetically permeable soft materials can be simply done by replacing Iron oxide Fe_3O_4 particles with magnetic particles in the aforementioned molding process.[274] The existence of the Iron oxide particles will allow the magnetic field to have a return path while being exposed to an external magnetic field. It is important to mention that the permeability of these materials is obviously less effective than those used in traditional rigid electromagnetic actuators as the percentage of Iron is less in soft permeable materials. By increasing the percentage of Iron, the permeability will increase, however, the flexibility of the material will decrease. Ebrahimi et al.[275] have experimentally tested different percentage of Iron oxide mixture with PDMS regarding tension force, maximum elastic elongation and yield point. It was concluded that around 35% of Iron oxide mixed with PDMS would lead to 70% increase in tension force to achieve same amount of elastic elongation, while the yield point is almost 80% as for a sample made of pure PDMS. Interestingly, adding only 5% Iron oxide (i.e., 40% iron oxide–60% PDMS) to the mixture resulted in dramatically decrease in the yield point (less than 30% of pure PDMS sample), while tension force for the same amount of elongation as compared to a pure PDMS sample stayed at around 65%. This means that adding more Iron oxide does not considerably affect the elasticity of the mixture but would make it very fragile.

5.2. Applications

Leon, et al. presented an application based on the bio-inspired motion of the Amoeba.[255] Their research was focused on development a soft microrobot based on the Amoeba locomotion which they called it: whole skin locomotion (WSL) as it is shown in Figure 18e.

The WSL robot was created using the fluid filled toroid method that acts as a body shaping feature with Ferrofluid material[276] placed within that is delivered to create the driving force. The passive fluid switch acts as an active sensitive liquid when a magnetic field is applied. Therefore, based on this behavior, in order to produce the driving motion, external electromagnetic coils were arranged as a wireless control and actuator. A number of motions and hindrances were then presented to insure the principal motions of the robot. Some other approaches of Ferrofluid soft-robot biomimetic inspired were also presented as well.

Using the movement of one single cell like amoeba animals move implemented as a biomimetic soft robotic and using a Ferrofluid as passive/active actuator, the movement motion of WSL was confirmed through various experiments. Fluid-filled toroid in the human digestion system is a potential application for drug delivery system or if possible further miniaturization movement in the vessel is also expected to be achieved through the control of an external magnetic field in intravascular applications. As a main advantage of the WSL robot proved that is possible to achieve the 2D movement and not a simple linear motion. Where, ferrofluids can offer remarkable actuation response in soft robots for future applications and improvements. However, to obtain a precise control, it requires further analysis as nanoparticles for molecular motion. Also, the ferrofluids could be considered as neutral monopole or magnetized dense liquid that follow the magnetic field with capillarity restrictions forces.[277]

Additional challenges arose from the tests, such as the difficulty to trace concentration material of ferroparticles in specific areas in order to improve the performance and also create

**ADVANCED
SCIENCE NEWS**

www.advancedsciencenews.com

**ADVANCED
FUNCTIONAL
MATERIALS**

www.afm-journal.de

a microbuoyancy space to execute a rotational motions its horizontal displacements for the underwater applications. However, microchannels as alternative of powered the Ferro-fluid is also possible in other to used its hydrodynamics properties.

Do et al. developed and fabricated soft electromagnetic actuators (SEMA)s,[254] which are actuated based on the Lorentz force principle, via electrical current. The central innovation of their devices was a soft electromagnetic inductor made from 3D helical coils formed from fine, stretchable hollow filaments that are filled with a liquid metal conductor. By fabricating these filaments from a colloid of silicone polymer and EGaIn microdroplets, they achieved high thermal conductivity, facilitating greatly increased current handling, and commensurately higher magnetic fields, and forces. Using these technologies, they demonstrated small scale cylindrical actuators capable of linear high-frequency motion as shown in Figure 18d.

The performance of these devices exhibited close quantitative agreement with predictions of a mathematical model based on the Lorentz force principle. They were capable of operating over a scalable range of voltages or currents, here ranging from 50 mA to >1 A, or 50 mV to 1 V, yielding displacements of up to 1 mm, and retained most of their performance when stretched up to 100%, or bent to angles of 38°. They applied these actuators in multipoint arrays, which are suited to providing tactile feedback in wearable devices, even as they stretch to conform to the skin. They also demonstrated multi degree-of-freedom devices that are capable of articulated motion and demonstrate their application in a unique miniature soft robotic gripper, which proved capable of manipulating (grasping, lifting, and releasing) miniature loads.

The proposed SEMAs by Do et al. have several key advantages: they were fast, capable of operating at high frequencies, they were operated at low voltages, were thermally efficient, enabling them to achieve high transient or sustained displacements. They were operated even when bent or stretched. They also offered theoretically predictable performance that was scalable in size and force, and finally, they were polymodal, suited to integration in simple arrays or articulated structures. These actuators shared a disadvantage that is common to other electromagnetic actuators, which is that higher forces require proportionally higher currents, with the feasible current limited by heating. As introduced by Do et al., these devices mitigate this through the use of thermally conductive polymers that greatly reduced heating. They also have the disadvantage of relatively small displacements, although this could be improved through mechanical design. In a broader context, owing to the attractive properties (including stretchability, speed, ease of driving, and scalability), these actuators could prove useful in applications benefitting from integration in wearable electronics,[278] microsurgical robotic instruments,[279] soft MEMS,[280] acoustic actuators,[281] microfluidics,[282] and autonomous soft robotics.[283] They are more complex to fabricate than simpler pneumatic soft actuators, but are faster, simpler to drive with microelectronics, and easily adaptable to proportional control over a wide dynamic range.

Rui et al.[256] fabricated liquid metal electromagnetic actuators via liquid metal spraying technology to develop soft jellyfish robots as shown in Figure 18f.
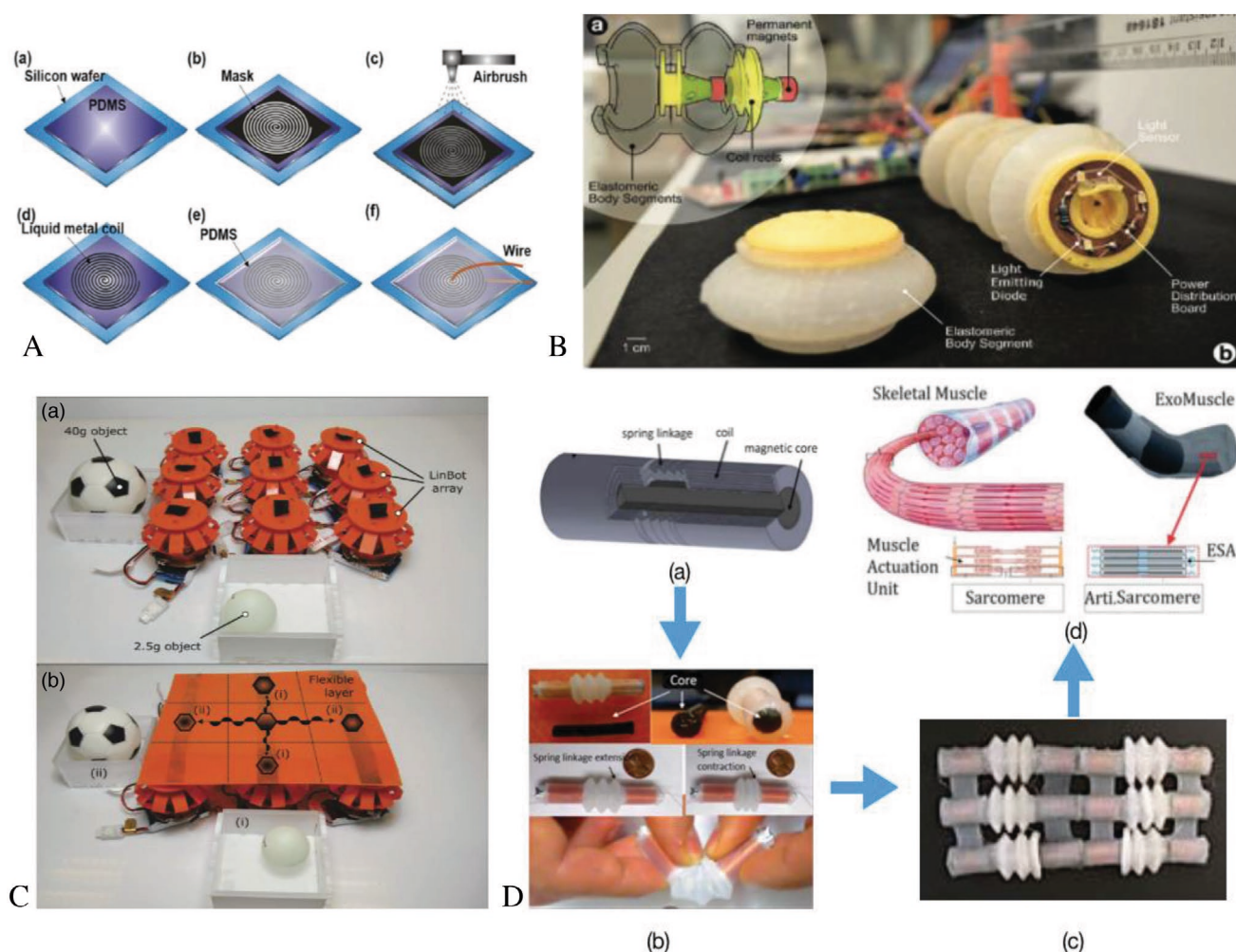
In this method, they first spin a layer of PDMS membrane with thickness around 0.5 mm on a smooth Silicone wafer. The PDMS substrate was then cured in an oven. Subsequently, cover the film with a particular shape mask plate, using liquid metal spraying gun to print liquid metal evenly on the PDMS membrane. They then removed the mask plate, and made some holes with diameter of around 1 mm on the location of the coil endpoints and then filled the liquid metal in these holes. Finally, evenly spin coated a layer of PDMS membrane on the pattern and then cured the PDMS in an oven (**Figure 19**A).

The preparation technology proposed by Rui et al.[256] showed evident advantages such as short production cycle and low cost. However, certain uneven distribution of liquid metal drops on PDMS membrane was noticed that required repeated spraying. In their designs, the electromagnetic interaction between the magnet and liquid metal coil is the main driving principle of the actuators. However, due to the imitation of the electric current, the size of the coils and magnetic field intensity, the Lorentz force between the liquid metal coils and the magnets was very small. Nevertheless, this range of force was enough to propel the light weight of the robot.

McKenzie et al.[284] presented a soft, modular robots that were explicitly designed for manufacturability as they called them Linbots. Linbots use multifunctional voice coils to actuate linearly, to produce audio output, and to sense touch. When used in collectives, the Linbots can communicate with neighboring Linbots allowing for isolated behavior as well as the propagation of information throughout a collective. They demonstrated that these collectives of Linbots can perform complex tasks in a scalable distributed manner, and showed transport of objects by collective peristalsis and sorting of objects by a 2D array of Linbots (Figure 19B).

In a similar work, Nemtiz et al. presented a modular worm-like robot (Wormbot),[285,287] which utilized voice coils as a new paradigm in soft robot actuation. Drive electronics were incorporated into the actuators, providing a significant improvement in self-sufficiency when compared with existing soft robot actuation modes such as pneumatics or hydraulics (Figure 19C).

The body plan of this robot was inspired by the phylum Annelida and consists of 3D printed voice coil actuators, which were connected by flexible silicone membranes. Each electromagnetic actuator engages with its neighbor to compress or extend the membrane of each segment, and the sequence in which they are actuated results in an earthworm-inspired peristaltic motion. They found that a minimum of three segments is required for locomotion, but due to their modular design, robots of any length could be quickly and easily assembled. In addition to actuation, voice coils provided audio input and output capabilities. They demonstrated transmission of data between segments by high-frequency carrier waves and, using a similar mechanism, they noted that the passing of power between coupled coils in neighboring modules—or from an external power source—was also possible. Voice coils are a convenient multifunctional alternative to existing soft robot actuators. Their self-contained nature and ability to communicate with each other are ideal for modular robotics, and the additional functionality of

**ADVANCED
SCIENCE NEWS**

www.advancedsciencenews.com

**ADVANCED
FUNCTIONAL
MATERIALS**

www.afm-journal.de

Figure 19. A) Fabrication process of the liquid metal electromagnetic actuator based on the spraying technology. Adapted with permission.[256] Copyright 2018, Springer. B) Peristaltic sorter and addressing system. a) The peristaltic sorter without the flexible layer on top of it, showing the Linbot array. b) The peristaltic sorter with the flexible layer attached. The behavior of the sorter is shown with the central Linbot detecting the weight of an object and its neighbors actuating to roll the object in the desired direction based on weight. Adapted with permission.[284] Copyright 2019, Mary Ann Liebert. C-a) A cutaway sketch of one module from Wormbot, showing the connecting elastomeric body segments and a voice coil actuator. b) A photograph showing Wormbot with the rearmost body segment removed to reveal the power distribution board. Adapted with permission.[285] Copyright 2016, Mary Ann Liebert. D-a) Details of an Electromagnetic Soft Actuator ESA, b) mgnetic flexible core and spring linkage connection, c) a 3 × 2 network of ESA, and d) future artificial ExoMuscles based on networked ESA inspired by anatomy of skeletal muscles.[286] Adapted with permission.[275] Copyright 2018, Elsevier.

sound input/output and power transfer will become increasingly useful as soft robots begin the transition from early proof-of-concept systems toward fully functional and highly integrated robotic systems.

Ebrahimi et al.[275,286] presented another novel highly scalable electromagnetic soft actuator (ESA) based on the principle of solenoids. The actuator was made mostly of silicone rubber so that it can have low stiffness. The major components of the soft actuator included helical coil, soft silicone ferromagnetic core, inner layer, spring linkage, and outer layer as shown in Figure 19D. The helical coils are made of 100 turn of soft wire. The outer layer of ESA which is included to shield and boost the resultant magnetic field consists of a mixture of 40% iron oxide and 60% silicone rubber. This part is included to make a layer of electromagnetic suspension to strengthen the generated field and increase the force.

Interestingly, they found that by scaling down the ESA size, the force/volume ratio increase. Therefore, by miniaturizing the size of the actuator and attaching them as a network, the total resultant force can be greatly enhanced, the same arrangement of linear tiny actuators (actin and myosin filaments) in skeletal muscles.[288] The idea is to create an ExoMuscle that can be worn around joints such as elbow or knee to help mobility impaired patients with movement of their limbs.

6. Biomedical Magnetic-Driven Robots

Magnetic actuation can provide substantial benefits in activating and controlling of biomedical robots. This section provides a review on magnetic-driven soft robots for three different biomedical applications; capsule endoscopy, drug delivery and steerable catheters.

**ADVANCED
SCIENCE NEWS**

www.advancedsciencenews.com

**ADVANCED
FUNCTIONAL
MATERIALS**

www.afm-journal.de

6.1. Magnetically Guided Capsule Endoscopy

Magnetic locomotion of capsule endoscopes has been investigated and proposed in literature through either external permanent magnet or electromagnets. A comprehensive review of magnetic actuation principles and magnetically driven activation strategies, applied to medical robots and classified by different clinical applications, has been presented by Sliker et al. in ref. [289], and a recent review, worth to be mentioned, on magnetic methods for remote-manipulation and wireless-actuation tasks in robotics has been presented by Abbott et al. in ref. [290].

In general, if compared to electromagnets, permanent magnetic field sources allow for the generation of a high strength-to-size ratio magnetic field; in other words, given a comparable size and volume, permanent magnets generate lager interaction forces than electromagnets. Another important feature of permanent magnets is related to their intrinsic permanence, i.e., the magnetic field is generated through the material without the need of a power supply, thus offering a wireless nonactive magnetic field generator. However, due to possible interference with other equipment in the operating room and interaction with ferromagnetic instrumentation, the latter feature can be considered also in terms of disadvantage since permanent magnets cannot be switched off or controlled in terms of magnetic field direction and strength; shielding is only possible using high-permeability materials to redirect lines of magnetic flux.[291] Contrarily, permanent magnets can be easily customized in terms of remanence, dimensions, shapes and magnetization directions, making them suitable for different applications.

Electromagnetic field sources, on the other hand, provide the substantial advantage of the controllability of the generated magnetic field (i.e., from turned on to turned off, modulating the generated field strength and direction), contributing to the safety, flexibility and applicability of the systems in the operating room. However, the main disadvantages are: 1) their high size-to-strength ratio, if compared to permanent magnets; 2) the need of implementing control strategies for modulating, through the supplied current, the electromagnetic field; and 3) the need of a power supply and, frequently, of a cooling system to generate a magnetic field, which usually contributes to a more bulky equipment in the operating room, higher device cost and design complexity, and electrical power demands. Finally, mainly in the case of magnetically driven locomotion, large electromagnetic sources present a physical limit, since the larger magnetic field that is created along the N–S poles direction can be far from the external surface of the electromagnet, and thus from the medical device if placed parallel to the magnetization direction; this is due to the high number of windings between the center of the electromagnet and the external surface and to the use of a bulky cooling system.

One of the most noteworthy and a first example of a magnetic-based robotic navigation approach applied to gastrointestinal (GI) endoscopic pill-size robots was first explored between 2008 and 2009 in the framework of a European FP6 project, called "Versatile Endoscopic Capsule for GI Tumor Recognition and therapy (VECTOR project)," coordinated by novineon Healthcare Technology Partners GmbH (Tuebingen, Germany).[292] In the framework of this European project,

Ciuti et al. at the Scuola Superiore Sant'Anna (Pisa, Itay) proposed the development of an active locomotion robotic platform based on mutually-interacting permanent magnets, i.e., above the patient body acting as the external magnetic driving source and inside a first prototype of a wireless endoscopic capsule. The developed robotic platform for wireless and wired capsule GI endoscopy combined the benefits of permanent magnetic field strength and limited encumbrance, demonstrating an accurate and reliable control through the use of an external teleoperated anthropomorphic robotic arm and an accelerometer-based localization strategy.[293–295]

A similar robotic platform has been developed, since 2011, by the research team lead by Prof. J. Abbott at the University of Utah (Salt Lake City, UT, USA), and it is composed of a 6-DoFs industrial robotic arm with an active-rotatable permanent magnet as the end-effector. The robotic platform has been demonstrated to effectively control and navigate several untethered magnetic devices, e.g., threaded capsule endoscopes and helical microrobots, to operate in natural lumen pathways of the bodies, such as GI, ENT, nervous, and vascular systems.[296–300]

Apart from the aforementioned multipurpose robotic platforms for applying magnetic fields for endoscopic capsule locomotion, looking at the research- and industrial-oriented state of the art, it is worth mentioning that magnetic locomotion for capsule endoscopy was mainly applied to the upper (i.e., esophagus and stomach) and lower (large bowel, mainly) GI tracts. It is worth mentioning that only the most recent and relevant studies will be mentioned in this section of the review paper for the sake of brevity but with the aim of providing a comprehensive overview of the main milestones in this research field; detailed reviews of magnetically guided capsule endoscopes can be found in refs. [301–303].

Starting with a proof-of-concept developed in 2016, Carpi et al. proposed an external magnetic add-on (i.e., elastic shells made of silicone elastomers mixed with magnetic particles) to provide active magnetic control of a commercially available wireless capsule endoscope (WCE, M2A Capsule, Given Imaging Ltd., Yoqneam, Israel— today, Medtronic Inc., Minnesota, USA) using hand-held external permanent magnets. Tests, performed in ex vivo simplified experimental conditions, demonstrated controlled translations, rotations, and roto-translations of the modified WCE.[304,305] In 2008, Carpi and Pappone improved the WCE controllability, proposing the use of a commercially available magnetic robotic platform, originally applied to magnetically-enabled interventional catheter-based cardiovascular procedures, i.e., Stereotaxis Niobe Robotic Magnetic Navigation System (Stereotaxis Inc., St. Louis, MO, USA), for the active control of the modified commercially available WCE housing, this time, an external magnetic add-on composed of two solid neodymium-based magnetic semicylindrical shells. Effective magnetically controlled capabilities were experimentally assessed inside a stomach-like cavity into a human-sized plastic phantom under fluoroscopy.[306–308] Finally, the same authors demonstrate in 2010 in vivo accurate robotic steering (omnidirectional steering accuracy of 1°) and noninvasive 3D localization (error of 1 mm) of the same magnetically modified commercially-available WCE within each of the main regions of the upper and lower GI tract (esophagus, stomach, small bowel, and colon) in a domestic pig model.[309]

ADVANCED
SCIENCE NEWS
www.advancedsciencenews.com

ADVANCED
FUNCTIONAL
MATERIALS
www.afm-journal.de

In 2010, Given Imaging Ltd. in collaboration with Prof. Paul Swain, conducted the first in vivo human magnetic manipulation trial of a modified WCE, i.e., PillCam COLON Capsule embedding neodymium–iron–boron magnets, in the upper GI tract (esophagus and liquid-filled stomach), through an external hand-held permanent magnet; the study demonstrated the feasibility of the remote manipulation of a modified WCE in humans and larger clinical studies, involving ten healthy participants, were conducted successfully in the esophagus[310] and stomach.[311] A similar research-oriented study, including a hand-held rotary magnet to navigate a magnetic capsule in ex vivo trials, has been presented by Lien et al. in 2012.[312] On the other hand, commercially-available hand-held magnetic field-based systems have been developed by the companies Jianshan Science and Technology (Chongqing, China) and Intromedic Ltd. (Seoul, Korea) with the OMOM Controllable Capsule System and MiroCam Navi MC1000-WM, respectively, demonstrating upper GI tract manoeuvrability in human models.[313,314]

In 2010, Siemens Healthcare AG (Erlangen, Germany) and Olympus Medical Corp. (Tokyo, Japan) developed the first electromagnetic capsule manipulation system successfully validated in in vivo gastric clinical trials, using 12 body-external electromagnetic coils. The proposed MRI-based Siemens Healthcare AG external platform allows 5-DOFs control of a single-use modified Olympus Medical Corp. WCE (31 mm in length and 11 mm in diameter) embedding a small permanent magnet.[315–317] Other significant examples of electromagnetic navigation systems, using modified MRIs or complex electromagnetic-based platforms, for meso- to nanoscale robots, have been proposed by the research teams led by Sitti,[318] Martel,[319] and Nelson;[65] comprehensive tutorials of "robotics in the small" have been presented in refs. [320,321].

A commercially-available platform dedicated to robotic capsule gastroscopy, worth to be mentioned in the section of this review, is the robotic magnetic capsule guidance system produced by Ankon Technologies Co., Ltd. (Wuhan, China). The platform is composed of a 5-DoFs arm that controls an external single spherical permanent magnet able to generate a 200 mT static magnetic field in a 500 mm³ working volume. The generated permanent magnetic field teleoperates an endoscopic pill-size capsule, embedding a small permanent magnet. The platform, patented and clinically approved with CFDA clearance in 2013, has been installed in over hundreds of medical centers in China and successfully clinically validated in humans for gastric examination.[322,323] A similar platform, to date at a research/validation phase, has been proposed in 2019 by Cheng et al. and preliminary tested in a cohort of 31 healthy volunteers for gastric examination; the main different is that the examination is conducted in standing than supine position with the aim to improve manoeuvrability in the stomach. The study demonstrated feasibility, safety and satisfactory manoeuvrability of the magnetically modified WCE in a standing position.[324]

In the lower GI tract, i.e., into the colonic district, a first significant example of magnetically guided endoscopic capsule derived from the previously mentioned European FP6 VECTOR project. Even if the project focused on the developed of magnetically guided wireless capsule robots, an interesting derivative

device of the project consisted of a soft-tethered magnetically driven capsule for colonoscopy. A proof-of-concept of the robotic colonoscope, presented by Valdastri et al. in 2012[325] as a trade-off between capsule and traditional colonoscopy combining the benefits of low-invasive propulsion (through "front-wheel" locomotion) with the multifunctional tether for treatment; was the capsule n.0 and the forerunner of a significant number of derived improvements, new implementations and allied magnetically guided endoscopic devices. Indeed, the system has been improved in the subsequent years, for instance, in terms of modelling,[326,327] tracking and localization,[328–330] and control,[331–333] toward autonomous locomotion strategies[334] and other applications.[335] In the recent years, a derived novel soft-tethered magnetically guided colonoscope was designed within a European H2020 project, called "Endoscopic versatile robotic guidance, diagnosis and therapy of magnetic-driven soft-tethered endoluminal robots (Endoo project)," coordinated by Scuola Superiore Sant'Anna (Pisa, Italy).[336] The soft-tethered robotic colonoscope is featured by a high-definition stereoscopic camera with custom-made optics, navigated by an external permanent magnet, precisely controlled by a collaborative anthropomorphic robot (COMAU SpA, Turin, Italy).[337] A noteworthy outcome of the EU project was the development of artificial intelligence algorithms to perform 3D lumen visual reconstruction, vision-based closed-loop control strategies and autonomous detection and measurement algorithms of colonic lesions, e.g., polyps.[338–342]

A hand-guided external electromagnetic system for a wireless colonoscope was designed in the framework of a European FP7 project, called "New cost-effective and minimally invasive endoscopic device able to investigate the colonic mucosa, ensuring a high level of navigation accuracy and enhanced diagnostic capabilities (SUPCAM project)," coordinated by S.E.D. Srl (Certaldo, Italy), under the supervision of Dr. Alessandro Tozzi, inventor of the novel capsule spherical concept. The external electromagnetic source, supported by a gravity-compensated arm, navigates, through a generated static magnetic field, a colonoscopic spherical-shape capsule provided with an internal permanent magnet, able to perform a 360° inspection through inner camera rotation.[343,344]

Another significant example of a WCE driven in the colonic tract using electromagnetic fields, in this case alternated, has been presented by Nouda et al. in 2018. A self-propelling capsule endoscope composed by a PillCam SB2 Capsule (Medtronic Inc., Minnesota, USA) modified with a silicone fin and embedding a permanent magnet attached to it (45mm in length and 11mm in diameter), has been tested for the first time in a human healthy volunteer. An external platform generates an alternating magnetic field that make the fin shaking and thus propel the capsule with a 3D control. The capsule, inserted in the anus and transported with endoscopic forceps in the descending colon, was able to swim in the lumen in antegrade and retrograde directions without any damage to the mucosa.[345]

Examples of the use of magnetic fields, both permanent and electromagnetic, not for locomotion purposes but as activation means for endoluminal treatment or therapy of mesoscale robots have been widely explored and designed in the last years. Being out of the main topic of the section, i.e., magnetically

**ADVANCED
SCIENCE NEWS**

www.advancedsciencenews.com

**ADVANCED
FUNCTIONAL
MATERIALS**

www.afm-journal.de

guided capsule endoscopy, the most significant examples are delegated to this comprehensive review paper published by Sliker et al. in ref. [289]; recent and significant examples have been developed in 2020 by Son et al.[346] and Kim et al.[347]

6.2. Magnetic Drug Delivery

Magnetic Drug delivery is a promising approach to deliver drugs to the site of disease without effecting other healthy tissues and organs. Magnetic drug targeting has received increased interest among scientist and researchers for delivering drug compounds to their target cells. For two decades, the need for improving therapy efficiency with increasing the uptake of drug while decreasing the dosage has been a primary goal in magnetic drug delivery. Magnetic drug targeting is a technique that uses magnetic nanoparticles (MNPs) to carry drugs within blood stream and guides them through their way using an external magnetic force. The target location could be a cancerous tissue, tumor or an infectious region, or any malignant tissue.

Magnetic Particles are highly biocompatible, functional and versatile nanoparticles therefore making them promising candidates for a successful drug carrier. Moreover, their small size (1–100 nm) makes them feasible to enter cells with endocytosis and deliver their contents directly to cells. One of the most widely used magnetic drug delivery is hyperthermia which is killing cancerous tissue by agitating MNPs with external magnetic fields and killing cancer cells at the site of tumor.

Two major issues that magnetic nanoparticles and microspheres can overcome that are present with nonmagnetic microcarriers are the reticuloendothelial system clearance and poor site specificity.[348]

However, recently scientist have developed a new avenue of smart magnetic drug targeting. In this approach, MNPs react smartly by external stimuli for targeting, releasing or reacting with specific molecules. MNPs have been used as the carrier of drug molecules themselves or in combination with other encapsulation techniques, to increase the efficiency of drug targeting. Examples of a combined systems are MNPs combined with electrospun nanofibers, layer by layer capsules (LbL), and other nanoparticles.

Habibi et al. used MNPs combined with electrospun nanofibers loaded with 5-FU drug molecules. The fibers were then exposed to an alternating magnetic field for different time intervals and different frequencies. The SEM results showed a complete breakdown and swelling of fibers and a burst release of drug molecules after exposure to alternating magnetic fields. This approach is a promising method for achieving controlled release of drug at specific cells.[349] MNPs combined with chitosan nanoparticles were also exposed to an alternating magnetic field. The challenge in using chitosan capsules is the ability to break the carrier or release the drug content once the capsule has reached its target. MNPs showed to be a smart approach for this purpose, since they can drive the capsule to target, and break the content once being exposed to alternating magnetic field.[350]

One of the most challenging efforts in drug delivery is the targeting of the eye. This is mainly to the eye structure and barriers rendering this organ being permeable to drugs. It is just

to recently that nanoscience has entered ocular drug delivery to improve penetration and half-life of drugs, specially to anterior eye chamber. In a study MNPs were used a s a nanotool for ocular drug delivery that is capable of special localization in the retinal pigmented epithelium (RPE) layer where is the responsible region for the majority of blindness both in childhood and adulthood. They demonstrate that, following intraocular injection in Xenopus embryos, MNPs localize specifically in RPE where they are retained for several days. This targeting was not specific, or dependent on particles size and surface properties. Using MNPs in ocular drug delivery has entered the avenue of translational drug development due to their promising and excellent properties.[351]

Magnetization effect can also help other nanoparticles to self-assemble into accurate ordered micro-nanostructures via controlled magnetic effect. Nanoparticles have shown to self-align into parallel chains under magnetization with the aid of MNPs. This approach developed micro- and nanoscale robotic swimmers that are very promising to significantly enhance the capability of particulate drug delivery by providing high accuracy at very small scale. A rotating magnetic field supplied by Helmholtz coils, were applied that effected the nanoparticles to deform into chiral structures, thereby giving them the prerequisite for nonreciprocal motion to move about at low Reynolds number. The size of nanoparticles can significantly effect this motion, as nanoscale swimmers are sensitive to Brownian motion, and microswimmer with the size of three time larger, are less vulnerable to Brownian motion.[352]

One of the challenge in targeted drug delivery is precisely steering MNPs to the target region and especially to the deep tissues. MNPs can't get captured in deep regions using existing permanent magnets. Hamdipoor et al. developed a real-time steering and magnetic particle imaging system (MPI) for real time tracking and steering of specific MNPs.

They used a novel intelligent haptic guidance scheme for steering a number of magnetic nanoparticles (MNPs) using forbidden region virtual fixtures and a haptic rendering scheme with multi particles. Forbidden region virtual fixtures are a general class of guidance modes implemented in software, which help a human–machine collaborative system accomplish a specific task by constraining a movement into limited regions. The results suggested improved targeting efficiency of MNPs by using this smart system.[353]

There are several essential rules which need to be taken in consideration for the development of successful of magnetic drug delivery carriers. The magnetic particles need to be large enough to possess high magnetization for efficient magnetic targeting. After targeting, they have to increase drug uptake and efficient drug release. Finally, they have to possess theranostic features (both diagnostic and therapeutic) to enhance the delivery and the drug action. The other key feature of promising magnetic drug delivery vehicles is long-circulating, stealthy systems which will not be cleared by a phagocyte system.[348]

6.3. Magnetically Actuated Steerable Catheters

Magnetic actuation has attracted increasing attention in those application fields where dimensional constraints significantly

hamper the employment of standard actuation technologies. In this regard, the fields of surgical robotics, medical devices, interventional systems, and microrobotics have greatly benefitted from the use of magnetic fields for wireless actuation, either steering or locomotion. Reducing invasiveness and pursuing direct target reaching to deliver the therapy in a more efficient way while reducing side effects is one of the challenges in medical robotics and interventional procedures.

The current best practice in interventional vascular procedures is represented by manual catheter control (catheter push and pull to enable target reaching) and time-consuming interventional procedures typically guided by x-ray imaging. Whilst catheters insertion can be performed through dedicated cable-driven advancing systems, finely controlling their bending and the force exerted on vessels wall is extremely challenging and typically performed manually.

Wireless magnetic actuation can be particularly beneficial for catheter steering in light of the complex and tortuous nature of the vascular tree and of the small vessels caliber. Furthermore, the possibility to exert a stable force on a magnetic component can be particularly useful to overcome the wide fluctuations experienced in manual catheters when in contact with moving tissues, e.g., the beating heart in applications such as radiofrequency ablation.

Significant advances have been recently made in magnetic navigation systems and magnetically steerable catheters/guidewires, showing potential benefits such as reduced radiation doses and improved access to hard-to-reach and tortuous anatomies.[354]

In order to enable catheter remote magnetic control, it is necessary to establish a magnetic link between an external magnetic field source (a set of magnets or electromagnets) and a magnetic element mounted on the catheter. When a magnetic object is exposed to a magnetic field, it can experience a certain magnetic force F_m and torque T_m that can be expressed as follows in Equations (4) and (5)

$$F_m = \int_V (m \cdot \nabla) B \, dV \tag{4}$$

$$T_m = \int_V (m \times \nabla) B \, dV \tag{5}$$

where m is the catheter magnetization, V is the volume of the magnetic element included in the catheter, and B is the magnetic flux density.[355] In order to enable establishing the aforementioned magnetic link, endovascular catheters and guidewires both including ferromagnetic components, permanent magnets, coils, or based on innovative magnetic materials have been reported both as commercial and research systems.[356] We will analyze in the following all these solutions by reviewing the most significant examples reported in the state of the art.

The inclusion of one or more small permanent magnets on the catheter tip to enable tip steering and controlled vessel contact is undoubtedly the most straightforward solution and the strategy adopted by many research groups and companies. Biosense Webster commercializes a 8F magnetic endocardial catheter for atrial fibrillation ablation (CARTOTHERMOCOOL RMT) suitable for navigation with the Niobe (Stereotaxis)

system, a commercial magnetic navigation system based on two rotating strong permanent magnets. Consisting in a flexible body, the catheter includes a magnetic tip and multiple radiofrequency electrodes for ablation. A small magnet embedded in the catheter tip causes the catheter to align and to be steered by the external magnetic field whereas a motor drive advances or retracts the catheter, enabling complete remote navigation. Similarly, a 0.36 mm diameter magnetic guidewire (Cronus, Stereotaxis) suitable for navigation with the Stereotaxis system was proposed. The guidewire includes a coiled distal segment to which a gold-encapsulated NdFeB magnet is attached to enable guidewire steering.[357] Choi and co-workers extended this concept by proposing a soft microrobotic system to be mounted on the tip of conventional guidewire to increase their steerability. The microrobot is fabricated via replica molding and features a soft body made of polydimethylsiloxane, two permanent magnets, and a microspring for an overall 500 μm diameter. The angulation of the microrobot can be controlled from 21.1° to 132.7° by using a magnetic field of an intensity of 15 mT.[358] Permanent magnets have also been employed in combination with smart materials to enable stiffness control. Nelson and co-workers recently reported about a variable stiffness multiple segments magnetic catheter combining a permanent magnet placed on the catheter tip and a low melting point alloy allowing to independently change the stiffness of each module through electrical currents. The resulting system matches the precision of magnetic navigation with additional degrees of freedom provided segments stiffness variations. The catheter has a 2.33 mm diameter and includes a working channel for additional tools insertion.[359]

A different approach to be pursued while trying to provide a catheter or a guidewire with magnetic properties is to include ferromagnetic components. However, this kind of approach calls for two different magnetic excitation fields to accomplish catheter orientation and steering: a permanent magnetic field to magnetize the ferromagnetic element to its saturation and a magnetic gradient to produce deflections.

MRI systems combining strong static fields and additional gradients have been successfully employed in this kind of application together with catheters and guidewires equipped with ferromagnetic beads on the tip. This approach was mainly pursued by Martel and co-workers by including one or more ferromagnetic beads either on catheters,[360,361] or guidewire tips,[362] to produce controlled steering in a clinical MRI system. Feasibility of such approach was demonstrated in vivo on swine model. Particularly interesting is the recent work by Martel and co-workers who used the fringe field of clinical MRI to combine catheter push and pull in order to better counteract friction forces and enable better steering also in small diameter vessels.[363] MRI-based navigation was proposed also in combination with clinical-grade microcatheters with a solenoid coil at the distal tip.[364] In this case, the local magnetic field produced by the tip coil interacts with the main field of the MRI system thus steering the catheter. However, heating issues with consequent blood vessels damage risks, are associated with such strategy.

Last but not least, innovative flexible magnetic materials have been employed in endovascular applications to cope with the bottleneck of size imposed by permanent magnets manufacturing. Zhao and co-workers presented a submillimeter-scale,

**ADVANCED
SCIENCE NEWS**

www.advancedsciencenews.com

**ADVANCED
FUNCTIONAL
MATERIALS**

www.afm-journal.de

self-lubricating soft continuum robot with omnidirectional steering and navigating capabilities based on magnetic actuation, which are enabled by programming ferromagnetic domains in its soft body while growing hydrogel skin on its surface. In particular, a composite polymeric matrix based on polydimethylsiloxane and silica-coated NdFeB particles was permanently magnetized and printed in the desired shape while selectively orienting the premagnetized particles to accomplish the desired magnetization pattern. The obtained magnetic guidewire was then provided with an hydrogel skin to reduce navigation friction.[365]

Most of the catheter and guidewire systems reviewed in this section were aimed at interventional procedures such as ablation. However, smart permanent magnets-based catheters have been recently proposed also for liquid biopsy and for enhancing the safety of micro and nanorobots based therapeutic paradigms. Vermesh et al. reported the development of a flexible magnetic wire to be inserted and removed through a standard intravenous catheter to capture biomarkers that have been previously labelled with injected magnetic particles. The MagWIRE's consists in a simple string of 60 cylindrical NdFeB magnets (N50-grade, 0.75 mm in diameter by 1 mm in length) encapsulated within a Polytetrafluoroethylene (PTFE) tubing with an inner diameter of 0.81 mm and wall thickness of 38.1 µm. This kind of magnetic arrangement enables to produce a large magnetic field gradient and attractive force thus to maximize specific biomarkers capture.[366]

Iacovacci et al. extended the concept of magnetic micro-objects capture to the field of micro/nanorobotics and nanomedicine with the aim to increase the safety of such therapeutic procedures. To become fully acceptable in fact medical microrobots should be either biodegradable or removed after task execution, to not raise short- and long-term side effects. To this aim an intravascular catheter able to efficiently retrieve from the bloodstream magnetic micro and nanorobots was proposed. The device consists of a miniature module, based on 27 permanent magnets arranged in two coaxial series, integrated into a clinically used 12 French catheter provided with a tip balloon for blood canalization within the retrieval catheter. This device can capture ≈94% and 78% of the unused agents when using as carriers 500 and 250 nm nominal diameter superparamagnetic iron oxide nanoparticles, respectively.[367,368]

7. Discussion and Future Works

Despite extensive body of research in magnetic actuation for bio/soft robots, exploration into these actuation methods is still at an early stage and many remaining challenges and opportunities require further investigation. For instance, ongoing advances in the study of biological microswimmers, such as the recent use of high-speed 3D microscopy to analyze the asymmetric and anisotropic flagellar controls of human sperm,[369] can be leveraged to inspire the next generation of bioinspired magnetic microrobots with improved stability and steering control. Further efforts should be made to track the position and state of magnetic microrobots inside the living organs, so we may gain additional data on their performance in vivo. Some preliminary research on this have been demonstrated, and

needs to be proposed in the future to confirm the fidelity of soft microrobots.[370,371] The rapidly emerging use of biodegradable and nontoxic materials to develop magnetic microrobots is also anticipated to continue to accelerate so that new biomedical applications can be delivered.

Furthermore, while tumbling/rolling locomotion has been demonstrated for both fluid and dry environments, crossing through the liquid–air interfaces between environments and the ability to break strong surface tension forces remain difficult. Electrostatic forces in dry environments can also vary substantially depending on local humidity and substrate surface properties, imposing external forces on the microrobots that can be strong enough to overpower actuation efforts. Predictable microscale locomotion in dry environments is difficult in general due to the lack of significant damping forces in air at low tumbling/rolling speeds and the miniscule inertia of microrobots. Losing surface contact while tumbling can result in the microrobot landing several body lengths from its original location. Small surface variations and dust can significantly alter a microrobot's planned trajectory, necessitating the use of controlled environments for repeatable performance. Electrostatic forces, if controlled, could allow for artificial surface adhesion of the microrobots to vertical and upside-down planes, opening up new mobility possibilities in dry air. In highly viscous fluids, fluid drag limits the rotational frequency and resulting translational speed of the microrobots. High viscosity can also suspend the microrobots within the fluid, preventing them from gaining traction on a solid substrate and rendering them immobile. In all environments, careful tuning of the tumbling/rolling microrobot design is needed to maintain enough surface traction to sustain a net forward motion while ensuring that actuation force is still sufficient to break surface adhesion forces. Opportunities exist for new microrobot geometries, surface treatments, and magnetization configurations that would help further iterations of tumbling/rolling microrobots overcome these mobility challenges. The use of compliant outer materials, for example, could help improve traction in viscous fluids where surface adhesion is poor. The introduction of real-time, high-resolution imaging combined with closed-back feedback control would also allow for more precise guidance of microrobots to target locations over rough terrain. In uncontrolled dry air environments where unpredictable microrobot jumps can occur in a fraction of a second, a combination of control algorithms and design features that mitigate jerky movement may be necessary. Actuated by global rotating magnetic fields, it remains to be seen how swarms of tumbling/rolling microrobots can be manipulated independently. While methods of having individualized rotational axes and rotational frequencies are available, motion between all microrobots remains coupled to the global field. The development of local, independent rotational fields or a way to decouple individual microrobots would create many new possibilities in workflow. Additionally, the question of how to integrate end-effectors into tumbling/rolling microrobots for executing more complex functions than direct pushing of micro-objects of microrobots or dissolution drug delivery is still an open design area. Such end-effectors may need to maintain fine positional control while still accounting for the constant change in microrobot orientation during tumbling/rolling locomotion.

ADVANCED
SCIENCE NEWS

www.advancedsciencenews.com

ADVANCED
FUNCTIONAL
MATERIALS

www.afm-journal.de

Magnetic biohybrid microrobots such as bacteria or sperm cells hold great promise for biomedical applications due to their high biocompatibility and propulsion mechanisms that are optimized for operating under physiological conditions. Their biological components do not require external power sources or fuels and offer facile interaction with cells and tissues which make them ideal for applications such as drug or cell delivery, diagnostics or in vivo imaging. Several challenges lie ahead on the road of applying biohybrid microrobots in vivo. First, imaging modalities need to be developed that allow the precise localization and control of the robots. Another challenge that is shared by all microrobots, is the investigation of the biocompatibility, toxicity and immune response by the organism in which they operate. Further, the clearance or degradation of the robots after their use needs to be solved. Many biohybrid robots rely on living components. In these cases, it is important to extend their lifetime as much as possible and enable affordable and reproducible production of such robots.

All magnetic microrobots have in common the problem of independent control. Ideally, microrobots should operate in swarms, since single robots will not be able to achieve much. Magnetic control offers the ability to control all microrobots simultaneously. However, the microrobots should also be able to perform different tasks independently from each other. Thus, the interaction between single robots and collective behavior of robots is a major future challenge. A possible approach for this is the exploration of taxis mechanisms found in nature (chemotaxis, thermotaxis, phototaxis, etc.), as discussed above in this article. Another approach is to use shape reconfiguration or geometrical differences that lead to differential response to the magnetic field and thereby results in individual control.

Although many works have shown potential usage of MTB in robotics, there still are many open questions and space for improvements. For example, in the case of drug delivery applications, we could ask ourselves what concentration of bacteria would be needed to effectively eradicate the tumor? In addition, how cytotoxic are these bacteria actually? Also, when used in the human body, will a new immune defense rise? Recent study on magnetosomes with HELA cell have shown promising results regarding their cytotoxicity showing biocompatibility and suffering no chemical nor physical changes after internalization by the cells.[372] Magnetosomes degradability in human stem cells has also recently been studied showing that after degradation from magnetite to ferrihydrite, the human stem cell are re-magnetized entirely biosynthesizing magnetic nanoparticles anew forming again magnetite.[373]

More generally, the release of a given cargo is still not well controlled although there exist many promising strategies their actual application is limited or not yet tested on MTB.[374,375] Regarding the steering mechanism, upon a given application other approaches based on the sensory mechanism, like ratchets[376] or locally, at the microenvironment, control oxygen gradients.[377] Regarding their magnetic properties, interaction with other materials like antiferromagnetic nanomaterials could bring new behaviors into light. Theoretically it is shown that MTB might present original magnetorheological properties and present novel collective behavior.[378–381] Experimentally, the MTB were shown to behave as rotary motors in oil–water emulsions for example and therefore their behavior in complex

medium is an open field.[382] In this line, taking into account that among MTB strains they have different properties and needs, the same diversity is most likely to be translated to different collective behaviors which if controllable are of interest for the field or robotics.

Regarding electromagnetic soft actuators, the generated output force is still the main concern. While employing soft wires can greatly enhance the electric current capacity of these type of actuators, liquid metals still present higher electric current resistance compared to conventional copper wires. Another limiting factor is the coil density in electromagnetic soft actuators, which can greatly affect the output force. A possible solution could be to use high-end 3D printers to create high dense helical channels inside a body of PDMS, instead of using a flexible wire. Creating strong magnetic field using mixture of magnetic particles and PDMS is another vital limitation that requires essential breakthrough in developing advanced materials for flexible magnets.

Magnetically driven capsule endoscopes emerged in the last years as promising solutions for endoluminal GI diagnosis and therapy, combining the benefits of accurate navigation control and wireless activation of internal mechanisms in an ingestible-compliant volume. Shifting from a high-demanding electrical- to a magnetic-based actuation and activation source guarantee saving embedded energy to power multimodal sensors and data transmission modules, approaching the target of an ingestible pill-size medical device. In addition, innovative design of magnetic configurations and mechanisms is at the base of the development of nonelectrical ingestible capsule devices with the benefit of avoiding embedding electrical source, potentially in contact with human tissues and organs;[20] moreover, the embedded magnetic element can also operates as a natural transmitter for external capsule localization units.[383]

At the "cost" of these benefits, magnetic-based capsule endoscopes require a complex modeling and design in order to overcome the challenge of providing adequate interaction forces and torques among relatively compact magnetic sources with a high dependence on magnet-to-magnet alignment and, often, significant magnet-to-magnet distances due to anatomical barriers.[290] In addition, permanent magnets cannot be "turned off" and contrariwise, in case of limited intermagnets distances or multiagents configurations, mutual magnetic interactions, or their proximity with external ferromagnetic elements have to be normed to keep patients' safety requirements always at the first place.

Combining smart magnetic materials with high flexibility and magnetic domain programmability possibilities together with novel printing strategies is a new trend in the field of magnetic catheters and guidewires. This approach at the same time opens new development venues and poses new challenges. If on one side, employing soft smart materials enables to push toward miniaturization overcoming both the dimensional limitations imposed by permanent magnets and the wiring/powering ones imposed by electromagnets, providing such materials with suitable magnetic properties to enable their control at working distance compatible with in-body operation is still a challenge. The second challenge is more related to the mechanical properties of such materials. As a matter of fact, if on one side having a soft structure would be beneficial

to prevent damages to blood vessels, this can become a drawback during the push–pull phase for target reaching and when close contact with the tissue (e.g., for ablation procedures) is required. In this framework, to advance in the field of magnetic-guided catheters, investigation on novel materials and fabrication schemes enabling at the same time miniaturization, suitable magnetization profiles, and variable stiffness is desirable and should be addressed in future research.

Conflict of Interest

The authors declare no conflict of interest.

[1] V. Moura, *Magnetically Actuated Multiscale Medical Robots, Presented at the IROS 2012 Full-day Workshop*, Algarve, Portugal **2012**, p. 48.
[2] F. Schmitt, O. Piccin, L. Barbé, B. Bayle, *Front. Rob. AI* **2018**, 5.
[3] M. Riahi, N. Ebrahimi, *Exp. Technol.* **2016**, *40*, 185.
[4] M. Riahi, N. Ebrahimi, *J. Artif. Intell. Instrum.* **2012**, *32*, 9.
[5] Z. Abbasi, J. Hoagg, T. M. Seigler, in *AIAA Scitech 2020 Forum*, American Institute of Aeronautics and Astronautics, Reston, VA **2020**.
[6] Z. Abbasi, J. Hoagg, T. M. Seigler, in *AIAA Scitech 2019 Forum*, American Institute of Aeronautics and Astronautics, Reston, VA **2019**.
[7] U. Enz, *Handbook of Ferromagnetic Materials*, Elsevier, Amsterdam **1982**, pp. 1–36.
[8] M. Evans, F. Heller, *Environmental Magnetism: Principles and Applications of Enviromagnetics*, Elsevier, Amsterdam **2003**.
[9] J. Li, E. S. Barjuei, G. Ciuti, Y. Hao, P. Zhang, A. Menciassi, Q. Huang, P. Dario, *J. Magn. Magn. Mater.* **2018**, *452*, 278.
[10] É. Trémolet de Lacheisserie, M. Schlenker, D. Gignoux, *Magnetism: Materials and Applications*, Springer, Berlin **2005**.
[11] J. M. D. Coey, *J. Magn. Magn. Mater.* **2001**, *226–230*, 2107.
[12] C.-G. Stefanita, *Magnetism: Basics and Applications*, Springer Science & Business Media, Berlin **2012**.
[13] J. Stöhr, H. C. Siegmann, *Magnetism: From Fundamentals to Nanoscale Dynamics*, Springer Science & Business Media, Berlin **2007**.
[14] J. Kaleta, S. Tumański, J. Żebracki, *J. Magn. Magn. Mater.* **1996**, *160*, 199.
[15] M. W. Freeman, A. Arrott, J. H. L. Watson, *J. Appl. Phys.* **1960**, *31*, S404.
[16] Z. Abbasi, A. Sunny, J. B. Hoagg, T. M. Seigler, in *2020 American Control Conf. (ACC)*, IEEE, Piscataway, NJ **2020**, pp. 4951–4956.
[17] T. Xu, J. Yu, X. Yan, H. Choi, L. Zhang, *Micromachines* **2015**, *6*, 1346.
[18] B. R. Donald, C. G. Levey, C. D. McGray, I. Paprotny, D. Rus, *J. Microelectromech. Syst.* **2006**, *15*, 1.
[19] O. Ohmichi, Y. Yamagata, T. Higuchi, *J. Microelectromech. Syst.* **1997**, *6*, 200.
[20] L. Sliker, G. Ciuti, M. Rentschler, A. Menciassi, *Expert Rev. Med. Devices* **2015**, *12*, 737.
[21] J. Sikorski, I. Dawson, A. Denasi, E. Hekman, S. Misra, in *Proc. of the IEEE Int. Conf. on Robotics and Automation (ICRA)*, IEEE, Piscataway, NJ **2017**.
[22] N. Garbin, C. Di Natali, J. Buzzi, E. De Momi, P. Valdastri, *J. Med. Devices* **2015**, *9*, 011005.
[23] M. Rea, D. McRobbie, H. Elhawary, Z. T. H. Tse, M. LampÉrth, I. Young, *IEEE/ASME Trans. Mechatron.* **2008**, *13*, 379.
[24] H. C. Berg, R. A. Anderson, *Nature* **1973**, *245*, 380.
[25] R. Dreyfus, J. Baudry, M. L. Roper, M. Fermigier, H. A. Stone, J. Bibette, *Nature* **2005**, *437*, 862.
[26] M. Roper, R. Dreyfus, J. Baudry, M. Fermigier, J. Bibette, H. A. Stone, *J. Fluid Mech.* **2006**, *554*, 167.
[27] W. Gao, S. Sattayasamitsathit, K. M. Manesh, D. Weihs, J. Wang, *J. Am. Chem. Soc.* **2010**, *132*, 14403.
[28] O. S. Pak, W. Gao, J. Wang, E. Lauga, *Soft Matter* **2011**, *7*, 8169.
[29] E. Diller, J. Zhuang, G. Zhan Lum, M. R. Edwards, M. Sitti, *Appl. Phys. Lett.* **2014**, *104*, 174101.
[30] B. Jang, E. Gutman, N. Stucki, B. F. Seitz, P. D. Wendel-García, T. Newton, J. Pokki, O. Ergeneman, S. Pané, Y. Or, B. J. Nelson, *Nano Lett.* **2015**, *15*, 4829.
[31] T. Li, J. Li, H. Zhang, X. Chang, W. Song, Y. Hu, G. Shao, E. Sandraz, G. Zhang, L. Li, J. Wang, *Small Weinh. Bergstr. Ger.* **2016**, *12*, 6098.
[32] D. J. Bell, S. Leutenegger, K. M. Hammar, L. X. Dong, B. J. Nelson, in *Proc. 2007 IEEE Int. Conf. on Robotics and Automation*, IEEE, Piscataway, NJ **2007**, pp. 1128–1133.
[33] L. Zhang, J. J. Abbott, L. Dong, B. E. Kratochvil, D. Bell, B. J. Nelson, *Appl. Phys. Lett.* **2009**, *94*, 064107.
[34] A. Ghosh, P. Fischer, *Nano Lett.* **2009**, *9*, 2243.
[35] I. S. M. Khalil, A. Fatih Tabak, A. Klingner, M. Sitti, *Appl. Phys. Lett.* **2016**, *109*, 033701.
[36] I. S. M. Khalil, A. F. Tabak, M. A. Seif, A. Klingner, M. Sitti, *PLoS One* **2018**, *13*, e0206456.
[37] Y. E.l Alaoui-Faris, J.-B. Pomet, S. Régnier, L. Giraldi, *Phys. Rev. E* **2020**, *101*, 042604.
[38] J. Li, S. Sattayasamitsathit, R. Dong, W. Gao, R. Tam, X. Feng, S. Ai, J. Wang, *Nanoscale* **2014**, *6*, 9415.
[39] C. C. J. Alcântara, S. Kim, S. Lee, B. Jang, P. Thakolkaran, J.-Y. Kim, H. Choi, B. J. Nelson, S. Pané, *Small* **2019**, *15*, 1970086.
[40] Z. Ye, S. Régnier, M. Sitti, *IEEE Trans. Rob.* **2014**, *30*, 3.
[41] D. Schamel, A. G. Mark, J. G. Gibbs, C. Miksch, K. I. Morozov, A. M. Leshansky, P. Fischer, *ACS Nano* **2014**, *8*, 8794.
[42] S. Schuerle, S. Pané, E. Pellicer, J. Sort, M. D. Baró, B. J. Nelson, *Small Weinh. Bergstr. Ger.* **2012**, *8*, 1498.
[43] X. Yan, Q. Zhou, J. Yu, T. Xu, Y. Deng, T. Tang, Q. Feng, L. Bian, Y. Zhang, A. Ferreira, L. Zhang, *Adv. Funct. Mater.* **2015**, *25*, 5333.
[44] J. Ali, U. K. Cheang, J. D. Martindale, M. Jabbarzadeh, H. C. Fu, M. Jun Kim, *Sci. Rep.* **2017**, *7*, 14098.
[45] S. Tottori, L. Zhang, F. Qiu, K. K. Krawczyk, A. Franco-Obregón, B. J. Nelson, *Adv. Mater.* **2012**, *24*, 811.
[46] K. Kobayashi, K. Ikuta, *Appl. Phys. Lett.* **2008**, *92*, 262505.
[47] A. Barbot, D. Decanini, G. Hwang, *Sci. Rep.* **2016**, *6*, 19041.
[48] P. Satir, T. Heuser, W. S. Sale, *Bioscience* **2014**, *64*, 1073.
[49] J. R. Blake, M. A. Sleigh, *Biol. Rev. Cambridge Philos. Soc.* **1974**, *49*, 85.
[50] B. A. Evans, A. R. Shields, R. L. Carroll, S. Washburn, M. R. Falvo, R. Superfine, *Nano Lett.* **2007**, *7*, 1428.
[51] A. R. Shields, B. L. Fiser, B. A. Evans, M. R. Falvo, S. Washburn, R. Superfine, *Proc. Natl. Acad. Sci. USA* **2010**, *107*, 15670.
[52] S. Kim, S. Lee, J. Lee, B. J. Nelson, L. Zhang, H. Choi, *Sci. Rep.* **2016**, *6*, 1.
[53] S. N. Khaderi, M. G. H. M. Baltussen, P. D. Anderson, D. Ioan, J. M. J. den Toonder, P. R. Onck, *Phys. Rev. E* **2009**, *79*, 046304.
[54] F. Meng, D. Matsunaga, J. M. Yeomans, R. Golestanian, *Soft Matter* **2019**, *15*, 3864.

**ADVANCED
SCIENCE NEWS**

www.advancedsciencenews.com

**ADVANCED
FUNCTIONAL
MATERIALS**

www.afm-journal.de

[55] M. Medina-Sánchez, L. Schwarz, A. K. Meyer, F. Hebenstreit, O. G. Schmidt, *Nano Lett.* **2016**, *16*, 555.

[56] F. Qiu, R. Mhanna, L. Zhang, Y. Ding, S. Fujita, B. J. Nelson, *Sens. Actuators, B* **2014**, *196*, 676.

[57] S. Jeon, S. Kim, S. Ha, S. Lee, E. Kim, S. Y. Kim, S. H. Park, J. H. Jeon, S. W. Kim, C. Moon, B. J. Nelson, J. Kim, S.-W. Yu, H. Choi, *Sci. Rob.* **2019**, *4*, eaav4317.

[58] C. Xin, L. Yang, J. Li, Y. Hu, D. Qian, S. Fan, K. Hu, Z. Cai, H. Wu, D. Wang, D. Wu, J. Chu, *Adv. Mater.* **2019**, *31*, 1808226.

[59] X. Yan, Q. Zhou, M. Vincent, Y. Deng, J. Yu, J. Xu, T. Xu, T. Tang, L. Bian, Y.-X. J. Wang, K. Kostarelos, L. Zhang, *Sci. Rob.* **2017**, *2*, eaaq1155.

[60] X. Wang, X.-H. Qin, C. Hu, A. Terzopoulou, X.-Z. Chen, T.-Y. Huang, K. Maniura-Weber, S. Pané, B. J. Nelson, *Adv. Funct. Mater.* **2018**, *28*, 1804107.

[61] A. Servant, F. Qiu, M. Mazza, K. Kostarelos, B. J. Nelson, *Adv. Mater.* **2015**, *27*, 2981.

[62] D. Gong, J. Cai, N. Celi, L. Feng, Y. Jiang, D. Zhang, *J. Magn. Magn. Mater.* **2018**, *468*, 148.

[63] K. Kim, X. Liu, Y. Zhang, Y. Sun, *J. Micromech. Microeng.* **2008**, *18*, 055013.

[64] Z. Zhang, X. Wang, J. Liu, C. Dai, Y. Sun, *Annu. Rev. Control Rob. Auton. Syst.* **2019**, *2*, 181.

[65] M. P. Kummer, J. J. Abbott, B. E. Kratochvil, R. Borer, A. Sengul, B. J. Nelson, *IEEE Trans. Rob.* **2010**, *26*, 1006.

[66] H. Xie, M. Sun, X. Fan, Z. Lin, W. Chen, L. Wang, L. Dong, Q. He, *Sci. Rob.* **2019**, *4*, eaav8006.

[67] J. Li, T. Li, T. Xu, M. Kiristi, W. Liu, Z. Wu, J. Wang, *Nano Lett.* **2015**, *15*, 4814.

[68] S. Palagi, A. G. Mark, S. Y. Reigh, K. Melde, T. Qiu, H. Zeng, C. Parmeggiani, D. Martella, A. Sanchez-Castillo, N. Kapernaum, F. Giesselmann, D. S. Wiersma, E. Lauga, P. Fischer, *Nat. Mater.* **2016**, *15*, 647.

[69] S. Fournier-Bidoz, A. C. Arsenault, I. Manners, G. A. Ozin, *Chem. Commun.* **2005**, 441.

[70] W. Wang, L. A. Castro, M. Hoyos, T. E. Mallouk, *ACS Nano* **2012**, *6*, 6122.

[71] J. S. Randhawa, T. G. Leong, N. Bassik, B. R. Benson, M. T. Jochmans, D. H. Gracias, *J. Am. Chem. Soc.* **2008**, *130*, 17238.

[72] T. G. Leong, C. L. Randall, B. R. Benson, N. Bassik, G. M. Stern, D. H. Gracias, *Proc. Natl. Acad. Sci. USA* **2009**, *106*, 703.

[73] S. Fusco, M. S. Sakar, S. Kennedy, C. Peters, S. Pane, D. Mooney, B. J. Nelson, in *2014 IEEE Int. Conf. on Robotics and Automation (ICRA)*, IEEE, Piscataway, NJ **2014**, pp. 3777–3782.

[74] E. Diller, M. Sitti, *Adv. Funct. Mater.* **2014**, *24*, 4377.

[75] J. Zhang, O. Onaizah, K. Middleton, L. You, E. Diller, *IEEE Rob. Autom. Lett.* **2017**, *2*, 835.

[76] I. S. M. Khalil, F. van den Brink, O. S. Sukas, S. Misra, in *2013 IEEE Int. Conf. on Robotics and Automation*, IEEE, Piscataway, NJ **2013**, pp. 5527–5532.

[77] A. E. El-Etriby, A. Klingner, A. F. Tabak, I. S. M. Khalil, in *2018 Int. Conf. on Manipulation, Automation and Robotics at Small Scales (MARSS)*, IEEE, Piscataway, NJ **2018**, pp. 1–4.

[78] P. J. Burke, in *Encyclopedia of Nanoscience and Nanotechnology*, (Ed: H. S. Nalwa), American Scientific Publishers, Stevenson Ranch, CA Eds, **2004**, pp. 1–19.

[79] K. C. Neuman, S. M. Block, *Rev. Sci. Instrum.* **2004**, *75*, 2787.

[80] H. Becker, L. E. Locascio, *Talanta* **2002**, *56*, 267.

[81] J. Shi, D. Ahmed, X. Mao, S.-C. S. Lin, A. Lawit, T. J. Huang, *Lab Chip* **2009**, *9*, 2890.

[82] A. Masuda, T. Yamakawa, L. Zimin, in *2008 SICE Annual Conf.*, IEEE, Piscataway, NJ **2008**, pp. 1747–1750.

[83] K.-F. Böhringer, V. Bhatt, B. R. Donald, K. Goldberg, *Algorithmica* **2000**, *26*, 389.

[84] H. Lee, A. M. Purdon, R. M. Westervelt, *Appl. Phys. Lett.* **2004**, *85*, 1063.

[85] S. Floyd, C. Pawashe, M. Sitti, *IEEE Trans. Rob.* **2009**, *25*, 1332.

[86] C. Pawashe, S. Floyd, E. Diller, M. Sitti, *IEEE Trans. Rob.* **2012**, *28*, 467.

[87] K. E. Peyer, L. Zhang, B. J. Nelson, *Appl. Phys. Lett.* **2011**, *99*, 174101.

[88] T. Petit, L. Zhang, K. E. Peyer, B. E. Kratochvil, B. J. Nelson, *Nano Lett.* **2012**, *12*, 156.

[89] M. A. Seif, A. Hassan, A. H. El-Shaer, A. Alfar, S. Misra, I. S. M. Khalil, in *2017 IEEE Int. Conf. on Advanced Intelligent Mechatronics (AIM)*, IEEE, Piscataway, NJ **2017**, pp. 1095–1102.

[90] Z. Ye, E. Diller, M. Sitti, *J. Appl. Phys.* **2012**, *112*, 064912.

[91] A. G. El-Gazzar, L. E. Al-Khouly, A. Klingner, S. Misra, I. S. M. Khalil, in *2015 IEEE/RSJ Int. Conf. on Intelligent Robots and Systems (IROS)*, IEEE, Piscataway, NJ **2015**, pp. 778–783.

[92] H.-W. Tung, K. E. Peyer, D. F. Sargent, B. J. Nelson, *Appl. Phys. Lett.* **2013**, *103*, 114101.

[93] I. S. M. Khalil, A. Klingner, Y. Hamed, Y. S. Hassan, S. Misra, *IEEE Trans. Rob.* **2020**.

[94] I. S. M. Khalil, A. F. Tabak, Y. Hamed, M. E. Mitwally, M. Tawakol, A. Klingner, M. Sitti, *Adv. Sci.* **2018**, *5*, 1700461.

[95] C. Hu, S. Pané, B. J. Nelson, *Annu. Rev. Control Rob. Auton. Syst.* **2018**, *1*, 53.

[96] D. R. Frutiger, K. Vollmers, B. E. Kratochvil, B. J. Nelson, *Int. J. Rob. Res.* **2009**.

[97] C. Pawashe, S. Floyd, M. Sitti, *Int. J. Rob. Res.* **2009**.

[98] I. A. Ivan, G. Hwang, J. Agnus, M. Rakotondrabe, N. Chaillet, S. Régnier, in *2011 IEEE Int. Conf. on Robotics and Automation*, IEEE, Piscataway, NJ **2011**, pp. 102–108.

[99] H.-W. Tung, M. Maffioli, D. R. Frutiger, K. M. Sivaraman, S. Pané, B. J. Nelson, *IEEE Trans. Rob.* **2014**, *30*, 26.

[100] E. Diller, C. Pawashe, S. Floyd, M. Sitti, *Int. J. Rob. Res.* **2011**.

[101] S. Floyd, E. Diller, C. Pawashe, M. Sitti, *Int. J. Rob. Res.* **2011**.

[102] E. Diller, J. Giltinan, M. Sitti, *Int. J. Rob. Res.* **2013**.

[103] E. Diller, M. Sitti, *Found. Trends Robt.* **2013**, *2*, 143.

[104] H. Ceylan, J. Giltinan, K. Kozielski, M. Sitti, *Lab Chip* **2017**, *17*, 1705.

[105] B. Hemes, D. Canelon, J. Dancs, N. Papanikolopoulos, in *2011 IEEE Int. Conf. on Robotics and Automation*, IEEE, Piscataway, NJ **2011**, pp. 5063–5069.

[106] G.-L. Jiang, Y.-H. Guu, C.-N. Lu, P.-K. Li, H.-M. Shen, L.-S. Lee, J. A. Yeh, M. T.-K. Hou, *J. Micromech. Microeng.* **2010**, *20*, 085042.

[107] L. Zhang, T. Petit, Y. Lu, B. E. Kratochvil, K. E. Peyer, R. Pei, J. Lou, B. J. Nelson, *ACS Nano* **2010**, *4*, 6228.

[108] J. Burdick, R. Laocharoensuk, P. M. Wheat, J. D. Posner, J. Wang, *J. Am. Chem. Soc.* **2008**, *130*, 8164.

[109] S. Sundararajan, P. E. Lammert, A. W. Zudans, V. H. Crespi, A. Sen, *Nano Lett.* **2008**, *8*, 1271.

[110] L. O. Mair, S. Chowdhury, G. A. Paredes-Juarez, M. Guix, C. Bi, B. Johnson, B. W. English, S. Jafari, J. Baker-McKee, J. Watson-Daniels, O. Hale, P. Stepanov, D. Sun, Z. Baker, C. Ropp, S. B. Raval, D. R. Arifin, J. W. M. Bulte, I. N. Weinberg, B. A. Evans, D. J. Cappelleri, *Micromachines* **2019**, *10*, 230.

[111] C. E. Sing, L. Schmid, M. F. Schneider, T. Franke, A. Alexander-Katz, *Proc. Natl. Acad. Sci. USA* **2010**, *107*, 535.

[112] H. Morimoto, T. Ukai, Y. Nagaoka, N. Grobert, T. Maekawa, *Phys. Rev. E: Stat., Nonlinear, Soft Matter Phys.* **2008**, *78*, 021403.

[113] P. Tierno, R. Golestanian, I. Pagonabarraga, F. Sagués, *Phys. Rev. Lett.* **2008**, *101*, 218304.

[114] R. S. Pieters, H.-W. Tung, D. F. Sargent, B. J. Nelson, *IFAC Proc. Vol.* **2014**, *47*, 7480.

[115] D. Sargent, H.-W. Tung, R. Pieters, B. Nelson, *Acta Crystallogr., Sect. A: Found. Adv.* **2014**, *70*, C1753.

[116] H.-W. Tung, D. F. Sargent, B. J. Nelson, *J. Appl. Crystallogr.* **2014**, *47*, 692.

[117] S. Charreyron, R. S. Pieters, H.-W. Tung, M. Gonzenbach, B. J. Nelson, in *2015 IEEE/RSJ Int. Conf. on Intelligent Robots and Systems (IROS)*, IEEE, Piscataway, NJ **2015**, pp. 177–182.

**ADVANCED
SCIENCE NEWS**

www.advancedsciencenews.com

**ADVANCED
FUNCTIONAL
MATERIALS**

www.afm-journal.de

[118] W. Jing, N. Pagano, D. J. Cappelleri, in *2013 IEEE Int. Conf. on Robotics and Automation*, IEEE, Piscataway, NJ **2013**, pp. 5514–5519.

[119] W. Jing, N. Pagano, D. J. Cappelleri, *J. Micro-Bio Rob.* **2013**, *8*, 1.

[120] M. T. Hou, H.-M. Shen, G.-L. Jiang, C.-N. Lu, I.-J. Hsu, J. A. Yeh, *Appl. Phys. Lett.* **2010**, *96*, 024102.

[121] C. Bi, M. Guix, B. V. Johnson, W. Jing, D. J. Cappelleri, *Micromachines* **2018**, *9*, 68.

[122] J. Xie, C. Bi, D. J. Cappelleri, N. Chakraborty, *American Society of Mechanical Engineers Digital Collection*, ASME, New York **2019**.

[123] C. Bi, E. E. Niedert, G. Adam, E. Lambert, L. Solorio, C. J. Goergen, D. J. Cappelleri, in *2019 Int. Conf. on Manipulation, Automation and Robotics at Small Scales (MARSS)*, IEEE, Piscataway, NJ **2019**, pp. 1–6.

[124] H.-W. Huang, M. S. Sakar, K. Riederer, N. Shamsudhin, A. Petruska, S. Pané, B. J. Nelson, in *2016 IEEE Int. Conf. on Robotics and Automation (ICRA)*, IEEE, Piscataway, NJ **2016**, pp. 1719–1724.

[125] W. Hu, G. Z. Lum, M. Mastrangeli, M. Sitti, *Nature* **2018**, *554*, 81.

[126] L. Sonntag, J. Simmchen, V. Magdanz, *Molecules* **2019**, *24*, 3410.

[127] M. Sun, X. Fan, X. Meng, J. Song, J. Chen, L. Sun, H. Xie, *Nanoscale* **2019**, *11*, 18382.

[128] K. Kamata, Z. Piao, S. Suzuki, T. Fujimori, W. Tajiri, K. Nagai, T. Iyoda, A. Yamada, T. Hayakawa, M. Ishiwara, S. Horaguchi, A. Belay, T. Tanaka, K. Takano, M. Hangyo, *Sci. Rep.* **2015**, *4*, 4919.

[129] X. Yan, Q. Zhou, M. Vincent, Y. Deng, J. Yu, J. Xu, T. Xu, T. Tang, L. Bian, Y.-X. J. Wang, K. Kostarelos, L. Zhang, *Sci. Rob.* **2017**, *2*, eaaq1155.

[130] X. Li, J. Cai, L. Sun, Y. Yue, D. Zhang, *RSC Adv.* **2016**, *6*, 76716.

[131] S. K. Srivastava, M. Medina-Sánchez, B. Koch, O. G. Schmidt, *Adv. Mater.* **2015**, *28*, 832.

[132] V. Magdanz, J. Gebauer, D. Mahdi, J. Simmchen, I. K. M. Khalil, in *Int. Conf. on Manipulation, Automation and Robotics at Small Scales (MARSS)*, IEEE, Piscataway, NJ **2019**.

[133] I. S. M. Khalil, V. Magdanz, J. Simmchen, A. Klingner, S. Misra, *Appl. Phys. Lett.* **2020**, *116*, 063702.

[134] V. Magdanz, S. Sanchez, O. G. Schmidt, *Adv. Mater.* **2013**, *25*, 6581.

[135] I. S. M. Khalil, V. Magdanz, S. Sanchez, O. G. Schmidt, S. Misra, *J. Micro-Bio Rob.* **2014**, *9*, 79.

[136] V. Magdanz, M. Medina-Sánchez, Y. Chen, M. Guix, O. G. Schmidt, *Adv. Funct. Mater.* **2015**, *25*, 2763.

[137] V. Magdanz, M. Guix, F. Hebenstreit, O. G. Schmidt, *Adv. Mater.* **2016**, *28*, 4084.

[138] H. Xu, M. Medina-Sánchez, V. Magdanz, L. Schwarz, F. Hebenstreit, O. G. Schmidt, *ACS Nano* **2018**, *12*, 327.

[139] C. Ridzewski, M. Li, B. Dong, V. Magdanz, *ACS Appl. Bio Mater.* **2020**, *3*, 1616.

[140] F. Striggow, M. Medina-Sánchez, G. K. Auernhammer, V. Magdanz, B. M. Friedrich, O. G. Schmidt, *Small* **2020**, *16*, 2000213.

[141] H. Xu, M. Medina-Sánchez, M. F. Maitz, C. Werner, O. G. Schmidt, *ACS Nano* **2020**, *14*, 2982.

[142] M. Medina-Sánchez, L. Schwarz, A. K. Meyer, F. Hebenstreit, O. G. Schmidt, *Nano Lett.* **2015**, *16*, 555.

[143] V. Magdanz, I. S. M. Khalil, J. Simmchen, G. P. Furtado, S. Mohanty, J. Gebauer, H. Xu, A. Klingner, A. Aziz, M. Medina-Sánchez, O. G. Schmidt, S. Misra, *Sci. Adv.* **2020**.

[144] R. M. Harshey, *Annu. Rev. Microbiol.* **2003**, *57*, 249.

[145] J. Bastos-Arrieta, A. Revilla-Guarinos, W. E. Uspal, J. Simmchen, *Front. Rob. AI* **2018**, *5*, 97.

[146] Y. Alapan, O. Yasa, B. Yigit, I. C. Yasa, P. Erkoc, M. Sitti, *Annu. Rev. Control Rob. Auton. Syst.* **2019**, *2*, 205.

[147] V. Du Nguyen, J.-W. Han, Y. J. Choi, S. Cho, S. Zheng, S. Y. Ko, J.-O. Park, S. Park, *Sens. Actuators, B* **2016**, *224*, 217.

[148] D. Li, H. Choi, S. Cho, S. Jeong, Z. Jin, C. Lee, S. Y. Ko, J. O. Park, S. Park, *Biotechnol. Bioeng.* **2015**, *112*, 1623.

[149] O. Schauer, B. Mostaghaci, R. Colin, D. Hürtgen, D. Kraus, M. Sitti, V. Sourjik, *Sci. Rep.* **2018**, *8*, 9801.

[150] D. Kim, A. Liu, E. Diller, M. Sitti, *Biomed. Microdevices* **2012**, *14*, 1009.

[151] O. Felfoul, M. Mohammadi, S. Taherkhani, D. de Lanauze, Y. Z. Xu, D. Loghin, S. Essa, S. Jancik, D. Houle, M. Lafleur, L. Gaboury, M. Tabrizian, N. Kaou, M. Atkin, T. Vuong, G. Batist, N. Beauchemin, D. Radzioch, S. Martel, *Nat. Nanotechnol.* **2016**, *11*, 941.

[152] Z. Lu, S. Martel, in *28th Annual Int. Conf. on Engineering in Medicine and Biology Society (EMBS'06)*, IEEE, Piscataway, NJ **2006**, pp. 3415–3418.

[153] S. Martel, M. Mohammadi, O. Felfoul, Z. Lu, P. Pouponneau, *Int. J. Rob. Res.* **2009**, *28*, 571.

[154] J. Zhuang, R. W. Carlsen, M. Sitti, *Sci. Rep.* **2015**, *5*, 11403.

[155] B.-W. Park, J. Zhuang, O. Yasa, M. Sitti, *ACS Nano* **2017**, *11*, 8910.

[156] Á. Barroso, S. Landwerth, M. Woerdemann, C. Alpmann, T. Buscher, M. Becker, A. Studer, C. Denz, *Biomed. Microdevices* **2015**, *17*, 26.

[157] M. M. Stanton, B.-W. Park, A. Miguel-López, X. Ma, M. Sitti, S. Sánchez, *Small* **2017**, *13*, 1603679.

[158] M. M. Stanton, J. Simmchen, X. Ma, A. Miguel-López, S. Sánchez, *Adv. Mater. Interfaces* **2016**, *3*, 1500505.

[159] R. W. Carlsen, M. R. Edwards, J. Zhuang, C. Pacoret, M. Sitti, *Lab Chip* **2014**, *14*, 3850.

[160] O. Yasa, P. Erkoc, Y. Alapan, M. Sitti, *Adv. Mater.* **2018**, *30*, 1804130.

[161] D. Faivre, D. Schüler, *Chem. Rev.* **2008**, *108*, 4875.

[162] C. T. Lefèvre, F. Abreu, U. Lins, D. A. Bazylinski, in *Metal Nanoparticles in Microbiology*, (Eds.: M. Rai, N. Duran, Springer, Berlin, Heidelberg **2011**, pp. 75–102.

[163] L. Yan, H. Da, S. Zhang, V. M. López, W. Wang, *Microbiol. Res.* **2017**, *203*, 19.

[164] C. T. Lefevre, D. A. Bazylinski, *Microbiol. Mol. Biol. Rev.* **2013**, *77*, 497.

[165] C. T. Lefèvre, M. Bennet, L. Landau, P. Vach, D. Pignol, D. A. Bazylinski, R. B. Frankel, S. Klumpp, D. Faivre, *Biophys. J.* **2014**, *107*, 527.

[166] T. Islam, C. Peng, I. Ali, *J. Basic Microbiol.* **2018**, *58*, 378.

[167] S. Seong, T. H. Park, *Biotechnol. Bioeng.* **2001**, *76*, 11.

[168] Y. Wang, W. Lin, J. Li, Y. Pan, *Front. Microbiol.* **2013**, *4*, 4.

[169] C. T. Lefèvre, T. Song, J.-P. Yonnet, L.-F. Wu, *Appl. Environ. Microbiol.* **2009**, *75*, 3835.

[170] I. S. M. Khalil, S. Misra, *IEEE Trans. Magn.* **2014**, *50*, 1.

[171] C. T. Lefèvre, M. L. Schmidt, N. Viloria, D. Trubitsyn, D. Schüler, D. A. Bazylinski, *Appl. Environ. Microbiol.* **2012**, *78*, 7238.

[172] D. A. Bazylinski, R. B. Frankel, H. W. Jannasch, *Nature* **1988**, *334*, 518.

[173] C. L. Monteil, G. Perrière, N. Menguy, N. Ginet, B. Alonso, N. Waisbord, S. Cruveiller, D. Pignol, C. T. Lefèvre, *Environ. Microbiol.* **2018**, *20*, 4415.

[174] T. J. Williams, C. T. Lefevre, W. Zhao, T. J. Beveridge, D. A. Bazylinski, *Int. J. Syst. Evol. Microbiol.* **2012**, *62*, 2443.

[175] S. Bellini, *Chin. J. Oceanol. Limnol.* **2009**, *27*, 3.

[176] R. Blakemore, *Science* **1975**, *190*, 377.

[177] R. B. Frankel, R. P. Blakemore, R. S. Wolfe, *Science* **1979**, *203*, 1355.

[178] R. Uebe, F. Ahrens, J. Stang, K. Jäger, L. H. Böttger, C. Schmidt, B. F. Matzanke, D. Schüler, *mBio* **2019**, *10*, e02795.

[179] S. Ullrich, M. Kube, S. Schubbe, R. Reinhardt, D. Schuler, *J. Bacteriol.* **2005**, *187*, 7176.

[180] R. Uebe, D. Schüler, *Nat. Rev. Microbiol.* **2016**, *14*, 621.

[181] A. Scheffel, M. Gruska, D. Faivre, A. Linaroudis, J. M. Plitzko, D. Schüler, *Nature* **2006**, *440*, 110.

[182] M. Toro-Nahuelpan, G. Giacomelli, O. Raschdorf, S. Borg, J. M. Plitzko, M. Bramkamp, D. Schüler, F.-D. Müller, *Nat. Microbiol.* **2019**, *4*, 1978.

[183] H. C. McCausland, A. Komeili, *PLoS Genet.* **2020**, *16*, e1008499.

**ADVANCED
SCIENCE NEWS**

www.advancedsciencenews.com

**ADVANCED
FUNCTIONAL
MATERIALS**

www.afm-journal.de

[184] F. Abreu, D. Acosta-Avalos, *Microorganisms*, IntechOpen, London **2018**.

[185] B. L. Taylor, I. B. Zhulin, M. S. Johnson, *Annu. Rev. Microbiol.* **1999**, *53*, 103.

[186] T. Schweinitzer, C. Josenhans, *Arch. Microbiol.* **2010**, *192*, 507.

[187] S. Klumpp, C. T. Lefèvre, M. Bennet, D. Faivre, *Phys. Rep.* **2019**, *789*, 1.

[188] A. M. Spormann, R. S. Wolfe, *FEMS Microbiol. Lett.* **1984**, *22*, 171.

[189] D. C. Guell, H. Brenner, R. B. Frankel, H. Hartman, *J. Theor. Biol.* **1988**, *135*, 525.

[190] M. Bennet, A. McCarthy, D. Fix, M. R. Edwards, F. Repp, P. Vach, J. W. C. Dunlop, M. Sitti, G. S. Buller, S. Klumpp, D. Faivre, *PLoS One* **2014**, *9*, e101150.

[191] A. Codutti, K. Bente, D. Faivre, S. Klumpp, *PLoS Comput. Biol.* **2019**, *15*, e1007548.

[192] K. Bente, S. Mohammadinejad, M. A. Charsooghi, F. Bachmann, A. Codutti, C. T. Lefèvre, S. Klumpp, D. Faivre, *eLife* **2020**, *9*, e47551.

[193] S. Rismani Yazdi, R. Nosrati, C. A. Stevens, D. Vogel, P. L. Davies, C. Escobedo, *Small* **2018**, *14*, 1702982.

[194] S. Rismani Yazdi, R. Nosrati, C. A. Stevens, D. Vogel, C. Escobedo, *Biomicrofluidics* **2018**, *12*, 011101.

[195] F. Popp, J. P. Armitage, D. Schüler, *Nat. Commun.* **2014**, *5*, 5398.

[196] M. Mahmoudi, A. Tachibana, A. B. Goldstone, Y. J. Woo, P. Chakraborty, K. R. Lee, C. S. Foote, S. Piecewicz, J. C. Barrozo, A. Wakeel, B. W. Rice, C. B. BellIII, P. C. Yang, *Sci. Rep.* **2016**, *6*, 26960.

[197] M. Boucher, F. Geffroy, S. Prévéral, L. Bellanger, E. Selingue, G. Adryanczyk-Perrier, M. Péan, C. T. Lefèvre, D. Pignol, N. Ginet, S. Mériaux, *Biomaterials* **2017**, *121*, 167.

[198] M. Kuhara, H. Takeyama, T. Tanaka, T. Matsunaga, *Anal. Chem.* **2004**, *76*, 6207.

[199] T. Yoshino, H. Hirabe, M. Takahashi, M. Kuhara, H. Takeyama, T. Matsunaga, *Biotechnol. Bioeng.* **2008**, *101*, 470.

[200] N. Ginet, R. Pardoux, G. Adryanczyk, D. Garcia, C. Brutesco, D. Pignol, *PLoS One* **2011**, *6*, e21442.

[201] I. Y. Iskusnykh, T. N. Popova, *Biomed. Khim.* **2010**, *56*, 530.

[202] R. Le Fèvre, M. Durand-Dubief, I. Chebbi, C. Mandawala, F. Lagroix, J.-P. Valet, A. Idbaih, C. Adam, J.-Y. Delattre, C. Schmitt, C. Maake, F. Guyot, E. Alphandéry, *Theranostics* **2017**, *7*, 4618.

[203] R. Liu, J. Liu, J. Tong, T. Tang, W.-C. Kong, X. Wang, Y. Li, J. Tang, *Prog. Nat. Sci. Mater. Int.* **2012**, *22*, 31.

[204] A. Plan Sangnier, S. Preveral, A. Curcio, A. K. A. Silva, C. T. Lefèvre, D. Pignol, Y. Lalatonne, C. Wilhelm, *J. Controlled Release* **2018**, *279*, 271.

[205] J. Xu, L. Liu, J. He, S. Ma, S. Li, Z. Wang, T. Xu, W. Jiang, Y. Wen, Y. Li, J. Tian, F. Li, *J. Nanobiotechnol.* **2019**, *17*, 17.

[206] E. Alphandéry, D. Abi Haidar, O. Seksek, F. Guyot, I. Chebbi, *Nanoscale* **2018**, *10*, 10918.

[207] Y. Pan, N. Li, J. Mu, R. Zhou, Y. Xu, D. Cui, Y. Wang, M. Zhao, *Appl. Microbiol. Biotechnol.* **2015**, *99*, 703.

[208] J. J. Jacob, K. Suthindhiran, *Biotechnol. Rep.* **2020**, *25*, e00422.

[209] C.-Y. Chen, C.-F. Chen, Y. Yi, L.-J. Chen, L.-F. Wu, T. Song, *Biomed. Microdevices* **2014**, *16*, 761.

[210] M. R. Benoit, D. Mayer, Y. Barak, I. Y. Chen, W. Hu, Z. Cheng, S. X. Wang, D. M. Spielman, S. S. Gambhir, A. Matin, *Clin. Cancer Res.* **2009**, *15*, 5170.

[211] J. E.l Fouladi, Z. Lu, Y. Savaria, S. Martel, in *2007 29th Annual Int. Conf. of the IEEE Engineering in Medicine and Biology Society*, IEEE, Piscataway, NJ **2007**, pp. 119–122.

[212] D. Gandia, L. Gandarias, I. Rodrigo, J. Robles-García, R. Das, E. Garaio, J. Á. García, M. Phan, H. Srikanth, I. Orue, J. Alonso, A. Muela, M. L. Fdez-Gubieda, *Small* **2019**, *15*, 1902626.

[213] T. Matsunaga, F. Tadokoro, N. Nakamura, *IEEE Trans. Magn.* **1990**, *26*, 1557.

[214] S. Martel, in *The First IEEE/RAS-EMBS Int. Conf. on Biomedical Robotics and Biomechatronics*, (BioRob 2006), IEEE, Piscataway, NJ, **2006**, pp. 829–834.

[215] M. M. Stanton, B.-W. Park, D. Vilela, K. Bente, D. Faivre, M. Sitti, S. Sánchez, *ACS Nano* **2017**, *11*, 9968.

[216] C. Chen, L. Chen, P. Wang, L.-F. Wu, T. Song, *J. Magn. Magn. Mater.* **2019**, *479*, 74.

[217] G. Harasko, H. Pfutzner, K. Futschik, *IEEE Trans. Magn.* **1995**, *31*, 938.

[218] A. S. Bahaj, I. W. Croudace, P. A. B. James, F. D. Moeschler, P. E. Warwick, *J. Magn. Magn. Mater.* **1998**, *184*, 241.

[219] A. S. Bahaj, D. C. Ellwood, J. H. P. Watson, *IEEE Trans. Magn.* **1991**, *27*, 5371.

[220] A. S. Bahaj, P. A. B. James, I. W. Croudace, *IEEE Trans. Magn.* **1994**, *30*, 4707.

[221] A. S. Bahaj, P. A. B. James, F. D. Moeschler, *J. Appl. Phys.* **1998**, *83*, 6444.

[222] J. A. Diaz-Alarcón, M. P. Alfonso-Pérez, I. Vergara-Gómez, M. Díaz-Lagos, S. A. Martínez-Ovalle, *J. Environ. Manage.* **2019**, *249*, 109381.

[223] B. A. Smit, E. Van Zyl, J. J. Joubert, W. Meyer, S. Prévéral, C. T. Lefèvre, S. N. Venter, *Lett. Appl. Microbiol.* **2018**, *66*, 362.

[224] N. Zeytuni, R. Uebe, M. Maes, G. Davidov, M. Baram, O. Raschdorf, A. Friedler, Y. Miller, D. Schüler, R. Zarivach, *PLoS One* **2014**, *9*, e97154.

[225] S. Martel, C. C. Tremblay, S. Ngakeng, G. Langlois, *Appl. Phys. Lett.* **2006**, *89*, 233904.

[226] S. Martel, J.-B. Mathieu, O. Felfoul, A. Chanu, E. Aboussouan, S. Tamaz, P. Pouponneau, L. Yahia, G. Beaudoin, G. Soulez, M. Mankiewicz, *Appl. Phys. Lett.* **2007**, *90*, 114105.

[227] A. Ghanbari, P. H. Chang, B. J. Nelson, H. Choi, *Smart Mater. Struct.* **2014**, *23*, 035013.

[228] I. S. M. Khalil, M. P. Pichel, L. Abelmann, S. Misra, *Int. J. Rob. Res.* **2013**, *32*, 637.

[229] I. S. M. Khalil, M. P. Pichel, B. A. Reefman, O. S. Sukas, L. Abelmann, S. Misra, in *2013 IEEE Int. Conf. on Robotics and Automation*, IEEE, Piscataway, NJ **2013**, pp. 5508–5513.

[230] Y. Zhang, N.-T. Nguyen, *Lab Chip* **2017**, *17*, 994.

[231] H. Wang, L. Chen, L. Sun, *Front. Mech. Eng.* **2017**, *12*, 510.

[232] S. Rismani Yazdi, P. Agrawal, E. Morales, C. A. Stevens, L. Oropeza, P. L. Davies, C. Escobedo, R. D. Oleschuk, *Anal. Chim. Acta* **2019**, *1085*, 107.

[233] C. J. Pierce, H. Wijesinghe, E. Osborne, E. Mumper, B. Lower, S. Lower, R. Sooryakumar, *AIP Adv.* **2020**, *10*, 015335.

[234] Q. Li, H. Chen, X. Feng, C. Yu, F. Feng, Y. Chai, P. Lu, T. Song, X. Wang, L. Yao, *Small* **2019**, *15*, 1900427.

[235] B. J. Nelson, I. K. Kaliakatsos, J. J. Abbott, *Annu. Rev. Biomed. Eng.* **2010**, *12*, 55.

[236] K. C. Leptos, K. Y. Wan, M. Polin, I. Tuval, A. I. Pesci, R. E. Goldstein, *Phys. Rev. Lett.* **2013**, *111*, 158101.

[237] G. Santomauro, A. V. Singh, B. Park, M. Mohammadrahimi, P. Erkoc, E. Goering, G. Schütz, M. Sitti, J. Bill, *Adv. Biosyst.* **2018**, *2*, 1800039.

[238] U. K. Cheang, D. Roy, J. H. Lee, M. J. Kim, *Appl. Phys. Lett.* **2010**, *97*, 213704.

[239] I. S. M. Khalil, S. Misra, *Microbiorobotics*, Elsevier, Amsterdam **2017**, pp. 61–79.

[240] H. A. Hassan, M. Pichel, T. Hageman, L. Abelmann, I. S. M. Khalil, in *2016 IEEE/RSJ Int. Conf. on Intelligent Robots and Systems (IROS)*, IEEE, Piscataway, NJ **2016**, pp. 5119–5124.

[241] J. Baumgartner, L. Bertinetti, M. Widdrat, A. M. Hirt, D. Faivre, *PLoS One* **2013**, *8*, e57070.

[242] D. M. S. Esquivel, H. G. P. Lins de Barros, *J. Exp. Biol.* **1986**, *121*, 153.

[243] Y. Pan, W. Lin, L. Tian, R. Zhu, N. Petersen, *Geomicrobiol. J.* **2009**, *26*, 313.

[244] R. Nadkarni, S. Barkley, C. Fradin, *PLoS One* **2013**, *8*, e82064.

[245] E. Wajnberg, L. H. S. de Souza, H. G. P. L. de Barros, D. M. S. Esquivel, *Biophys. J.* **1986**, *50*, 451.

[246] M. Blondeau, Y. Guyodo, F. Guyot, C. Gatel, N. Menguy, I. Chebbi, B. Haye, M. Durand-Dubief, E. Alphandery, R. Brayner, T. Coradin, *Sci. Rep.* **2018**, *8*, 7699.

[247] M. Naresh, K. Gopinadhan, S. Sekhar, P. Juneja, M. Sharma, A. Mittal, *IEEE Trans. Magn.* **2009**, *45*, 4861.

[248] C. Rosenblatt, F. F. T. de Araujo, R. B. Frankel, *J. Appl. Phys.* **1982**, *53*, 2727.

[249] C. Rosenblatt, F. F. T. de Araujo, R. B. Frankel, *Biophys. J.* **1982**, *40*, 83.

[250] S. Taherkhani, M. Mohammadi, J. Daoud, S. Martel, M. Tabrizian, *ACS Nano* **2014**, *8*, 5049.

[251] Q. Ma, C. Chen, S. Wei, C. Chen, L.-F. Wu, T. Song, *Biomicrofluidics* **2012**, *6*, 024107.

[252] S. K. Alsaiari, A. H. Ezzedine, A. M. Abdallah, R. Sougrat, N. M. Khashab, *OpenNano* **2016**, *1*, 36.

[253] I. Boldea, S. A. Nasar, *IEEE Trans. Energy Convers.* **1999**, *14*, 712.

[254] T. N. Do, H. Phan, T.-Q. Nguyen, Y. Visell, *Adv. Funct. Mater.* **2018**, *28*, 1800244.

[255] M. Ziegler, K. Ochs, M. Hansen, H. Kohlstedt, *Appl. Phys. A* **2014**, *114*, 565.

[256] R. Guo, L. Sheng, H. Gong, J. Liu, *Sci. China Technol. Sci.* **2018**, *61*, 516.

[257] R. C. Chiechi, E. A. Weiss, M. D. Dickey, G. M. Whitesides, *Angew. Chem., Int. Ed.* **2008**, *47*, 142.

[258] M. D. Dickey, R. C. Chiechi, R. J. Larsen, E. A. Weiss, D. A. Weitz, G. M. Whitesides, *Adv. Funct. Mater.* **2008**, *18*, 1097.

[259] G. J. Hayes, J.-H. So, A. Qusba, M. D. Dickey, G. Lazzi, *IEEE Trans. Antennas Propag.* **2012**, *60*, 2151.

[260] B.-H. Jo, L. M. Van Lerberghe, K. M. Motsegood, D. J. Beebe, *J. Microelectromech. Syst.* **2000**, *9*, 76.

[261] A. Mata, A. J. Fleischman, S. Roy, *Biomed. Microdevices* **2005**, *7*, 281.

[262] M. Amjadi, Y. J. Yoon, I. Park, *Nanotechnology* **2015**, *26*, 375501.

[263] K. O. Siegenthaler, A. Künkel, G. Skupin, M. Yamamoto, in *Synthetic Biodegradable Polymers*, Springer, Berlin **2011**, pp. 91–136.

[264] M. Yamamoto, U. Witt, G. Skupin, D. Beimborn, R.-J. Müller, *Biopolymers, Biology, Chemistry, Biotechnology, Applications*, (Ed: A. Steinbuchel), Polyesters III - Applications and Commercial Products, Wiley, New York **2005**, p. 4.

[265] J. O'Connor, J. Punch, N. Jeffers, J. Stafford, *Microfluid. Nanofluidics* **2015**, *19*, 385.

[266] D. P. Parekh, C. Ladd, L. Panich, K. Moussa, M. D. Dickey, *Lab Chip* **2016**, *16*, 1812.

[267] S. Dottermusch, D. Busko, M. Langenhorst, U. W. Paetzold, B. S. Richards, *Opt. Lett.* **2019**, *44*, 29.

[268] D. B. Fullager, G. D. Boreman, T. Hofmann, *Opt. Mater. Express* **2017**, *7*, 888.

[269] J. G. Rider, C. T. B. Foxon, *Philos. Mag. J. Theor. Exp. Appl. Phys.* **1967**, *16*, 1133.

[270] Y.-H. Lin, S.-W. Kang, T.-Y. Wu, *Appl. Therm. Eng.* **2009**, *29*, 573.

[271] B. Slusarek, K. Zakrzewski, *Electr. Rev.* **2012**, *88*, 123.

[272] L. A. Dobrzański, M. Drak, B. Ziębowicz, *J. Achiev. Mater. Manuf. Eng.* **2006**, *17*, 37.

[273] W. Fang, I. Panagiotopoulos, F. Ott, F. Boué, K. Ait-Atmane, J.-Y. Piquemal, G. Viau, F. Dalmas, *J. Nanoparticle Res.* **2014**, *16*, 2265.

[274] M. De Cuyper, P. Müller, H. Lueken, M. Hodenius, *J. Phys.: Condens. Matter* **2003**, *15*, S1425.

[275] N. Ebrahimi, P. Schimpf, A. Jafari, *Sens. Actuators Phys.* **2018**, *284*, 276.

[276] S. Odenbach, *Ferrofluids: Magnetically Controllable Fluids and Their Applications*, Vol. *594*, Springer, Berlin **2008**.

[277] H. Hay, *Organisation of Magnetic Microparticles in a Ferrofluid: A Computational Approach to a Self-assembly Process*, Uppsala Universitet, Uppsala **2012**.

[278] A. Marette, A. Poulin, N. Besse, S. Rosset, D. Briand, H. Shea, *Adv. Mater.* **2017**, *29*, 1700880.

[279] J. J. Rassweiler, R. Autorino, J. Klein, A. Mottrie, A. S. Goezen, J.-U. Stolzenburg, K. H. Rha, M. Schurr, J. Kaouk, V. Patel, *BJU Int.* **2017**, *120*, 822.

[280] B. Mosadegh, A. D. Mazzeo, R. F. Shepherd, S. A. Morin, U. Gupta, I. Z. Sani, D. Lai, S. Takayama, G. M. Whitesides, *Lab Chip* **2014**, *14*, 189.

[281] K.-Y. Shin, J.-Y. Hong, J. Jang, *Chem. Commun.* **2011**, *47*, 8527.

[282] J. Zhang, S. Yan, D. Yuan, G. Alici, N.-T. Nguyen, M. E. Warkiani, W. Li, *Lab Chip* **2016**, *16*, 10.

[283] D. Rus, M. T. Tolley, *Nature* **2015**, *521*, 467.

[284] R. M. McKenzie, M. E. Sayed, M. P. Nemitz, B. W. Flynn, A. A. Stokes, *Soft Rob.* **2019**, *6*, 195.

[285] M. P. Nemitz, P. Mihaylov, T. W. Barraclough, D. Ross, A. A. Stokes, *Soft Rob.* **2016**, *3*, 198.

[286] A. Jafari, N. Ebrahimi, US Patent App. 16/457,452, **2020**.

[287] B. Zhang, Y. Fan, P. Yang, T. Cao, H. Liao, *Soft Rob.* **2019**, *6*, 399.

[288] N. Ebrahimi, S. Nugroho, A. F. Taha, N. Gatsis, W. Gao, A. Jafari, in *2018 IEEE Int. Conf. on Robotics and Automation (ICRA)*, IEEE, Piscataway, NJ **2018**, pp. 2857–2864.

[289] L. Sliker, G. Ciuti, M. Rentschler, A. Menciassi, *Expert Rev. Med. Devices* **2015**, *12*.

[290] J. J. Abbott, E. Diller, A. J. Petruska, *Annu. Rev. Control Robot. Auton. Syst.* **2020**, *3*, 57.

[291] R. D. Brewer, K. E. Loewke, E. F. Duval, J. K. Salisbury, in *Proc. of the 2nd Biennial IEEE/RAS-EMBS Int. Conf. on Biomedical Robotics and Biomechatronics (BioRob 2008)*, IEEE, Piscataway, NJ **2008**, pp. 580–586.

[292] D. Rus, M. T. Tolley, *Nature* **2015**, *521*, 467.

[293] G. Ciuti, P. Valdastri, A. Menciassi, P. Dario, *Robotica* **2010**, *28*, 199.

[294] G. Ciuti, R. Donlin, P. Valdastri, A. Arezzo, A. Menciassi, M. Morino, P. Dario, *Endoscopy* **2010**, 42.

[295] A. Arezzo, A. Menciassi, P. Valdastri, G. Ciuti, G. Lucarini, M. Salerno, C. Di Natali, M. Verra, P. Dario, M. Morino, *Dig. Liver Dis.* **2013**, *46*, 45.

[296] A. W. Mahoney, J. J. Abbott, *Appl. Phys. Lett.* **2011**, *99*, 134103.

[297] A. W. Mahoney, J. J. Abbott, *IEEE Trans. Rob.* **2014**, *30*, 411.

[298] T. L. Bruns, K. E. Riojas, D. S. Ropella, M. S. Cavilla, A. J. Petruska, M. H. Freeman, R. F. Labadie, J. J. Abbott, R. J. Webster, *IEEE Rob. Autom. Lett.* **2020**, *5*, 2240.

[299] S. E. Wright, A. W. Mahoney, K. M. Popek, J. J. Abbott, in *IEEE Transactions on Robotics*, IEEE, Piscataway, NJ **2017**, pp. 1013–1024.

[300] A. W. Mahoney, J. J. Abbott, *Int. J. Rob. Res.* **2016**, *35*, 129.

[301] L. J. Sliker, G. Ciuti, *Expert Rev. Med. Devices* **2014**, *11*, 649.

[302] N. Shamsudhin, V. I. Zverev, H. Keller, S. Pane, P. W. Egolf, B. J. Nelson, A. M. Tishin, *Magnetically Guided Capsule Endoscopy*, Vol. *44*, Wiley, New York, NY **2017**, pp. e91–e111.

[303] G. Ciuti, R. Caliò, D. Camboni, L. Neri, F. Bianchi, A. Arezzo, A. Koulaouzidis, S. Schostek, D. Stoyanov, C. M. Oddo, B. Magnani, A. Menciassi, M. Morino, M. O. Schurr, P. Dario, *J. Micro-Bio Rob.* **2016**, *11*, 1.

[304] F. Carpi, S. Galbiati, A. Carpi, *Biomed. Pharmacother.* **2006**, *60*, 370.

[305] F. Carpi, S. Galbiati, A. Carpi, *IEEE Trans. Biomed. Eng.* **2007**, *54*, 2028.

[306] F. Carpi, C. Pappone, *Biomed. Pharmacother.* **2008**, *62*, 546.

[307] F. Carpi, C. Pappone, *IEEE Trans. Biomed. Eng.* **2009**, *56*, 1482.

[308] F. Carpi, C. Pappone, *Expert Med. Rev. Devices* **2009**, *6*, 487.

[309] F. Carpi, N. Kastelein, M. Talcott, C. Pappone, *IEEE Trans. Biomed. Eng.* **2011**, *58*, 231.

[310] J. Keller, C. Fibbe, F. Volke, J. Gerber, A. C. Mosse, M. Reimann-Zawadzki, E. Rabinovitz, P. Layer, P. Swain, *Gastroint. Endosc.* **2010**, *72*, 941.

[311] J. Keller, C. Fibbe, F. Volke, J. Gerber, A. C. Mosse, M. Reimann-Zawadzki, E. Rabinovitz, P. Layer, D. Schmitt, V. Andresen, U. Rosien, P. Swain, *Gastroint. Endosc.* **2011**, *73*, 22.

ADVANCED
SCIENCE NEWS
www.advancedsciencenews.com

ADVANCED
FUNCTIONAL
MATERIALS
www.afm-journal.de

[312] G. S. Lien, C. W. Liu, J. A. Jiang, C. L. Chuang, M. T. Teng, *IEEE Trans. Biomed. Eng.* **2012**, *59*, 2068.

[313] Z. Li, Z. Liao, M. McAlindon, *Handbook of Capsule Endoscopy*, Springer, Netherlands **2014**.

[314] I. Rahman, M. Pioche, C. S. Shim, S. P. Lee, I. K. Sung, J. C. Saurin, P. Patel, *Gastrointest. Endosc.* **2016**, *83*, 889.

[315] J. F. Rey, H. Ogata, N. Hosoe, K. Ohtsuka, N. Ogata, K. Ikeda, H. Aihara, I. Pangtay, T. Hibi, S. Kudo, H. Tajiri, *Endoscopy* **2010**, *42*, 541.

[316] J. F. Rey, H. Ogata, N. Hosoe, K. Ohtsuka, N. Ogata, K. Ikeda, H. Aihara, I. Pangtay, T. Hibi, S. E. Kudo, H. Tajiri, *Gastrointest. Endosc.* **2012**, *75*, 373.

[317] U. W. Denzer, T. Rösch, B. Hoytat, M. Abdel-Hamid, X. Hebuterne, G. Vanbiervielt, J. Filippi, H. Ogata, N. Hosoe, K. Ohtsuka, N. Ogata, K. Ikeda, H. Aihara, S. E. Kudo, H. Tajiri, A. Treszl, K. Wegscheider, M. Greff, J. F. Rey, *J. Clin. Gastroenterol.* **2015**, *49*, 101.

[318] X. Dong, M. Sitti, *Int. J. Rob. Res.* **2020**, *39*, 617.

[319] D. Loghin, C. Tremblay, M. Mohammadi, S. Martel, *Int. J. Rob. Res.* **2017**, *36*, 1195.

[320] L. Dong, B. J. Nelson, *IEEE Rob. Autom. Mag.* **2007**, *14*, 111.

[321] J. J. Abbott, Z. Nagy, F. Beyeler, B. J. Nelson, *IEEE Rob. Autom. Mag.* **2007**, *14*, 92.

[322] X. Jiang, J. Pan, Z. S. Li, Z. Liao, *VideoGIE* **2019**, *4*, 239.

[323] Z. Liao, X. Hou, E. Q. Lin-Hu, J. Q. Sheng, Z. Z. Ge, B. Jiang, X. H. Hou, J. Y. Liu, Z. Li, Q. Y. Huang, X. J. Zhao, N. Li, Y. J. Gao, Y. Zhang, J. Q. Zhou, X. Y. Wang, J. Liu, X. P. Xie, C. M. Yang, H. L. Liu, X. T. Sun, W. Bin Zou, Z. S. Li, *Clin. Gastroenterol. Hepatol.* **2016**, *14*, 1266.

[324] C. S. Cheng, T. J. Sun, H. de Zhang, *BMC Gastroenterol.* **2019**, *19*, 184.

[325] P. Valdastri, G. Ciuti, A. Verbeni, A. Menciassi, P. Dario, A. Arezzo, M. Morino, *Surg. Endosc. Interv. Tech.* **2012**, *26*, 1238.

[326] L. J. Sliker, G. Ciuti, M. E. Rentschler, A. Menciassi, *Tribol. Int.* **2016**, 102.

[327] J. Li, E. S. Barjuei, G. Ciuti, Y. Hao, P. Zhang, A. Menciassi, Q. Huang, P. Dario, *J. Magn. Magn. Mater.* **2018**, 452.

[328] M. Salerno, G. Ciuti, G. Lucarini, R. Rizzo, P. Valdastri, A. Menciassi, A. Landi, P. Dario, *Meas. Sci. Technol.* **2012**, *23*, 015701.

[329] A. Taddese, P. Slawinski, M. Pirotta, E. De Momi, K. L. Obstein, P. Valdastri, *Int. J. Rob. Res.* **2018**, *37*, 890.

[330] F. Bianchi, A. Masaracchia, E. Shojaei Barjuei, A. Menciassi, A. Arezzo, A. Koulaouzidis, D. Stoyanov, P. Dario, G. Ciuti, *Expert Rev. Med. Devices* **2019**, *16*, 381.

[331] G. Ciuti, M. Salerno, G. Lucarini, P. Valdastri, A. Arezzo, A. Menciassi, M. Morino, P. Dario, *IEEE Trans. Rob.* **2012**, *28*, 534.

[332] P. R. Slawinski, N. Simaan, A. Z. Taddese, K. L. Obstein, P. Valdastri, *IEEE Trans. Rob.* **2019**, *35*, 1123.

[333] L. Barducci, G. Pittiglio, J. C. Norton, K. L. Obstein, P. Valdastri, *IEEE Rob. Autom. Lett.* **2019**, *4*, 3633.

[334] P. R. Slawinski, A. Z. Taddese, K. B. Musto, S. Sarker, P. Valdastri, K. L. Obstein, *Gastroenterology* **2018**, *154*, 1577.

[335] J. C. Norton, P. R. Slawinski, H. S. Lay, J. W. Martin, B. F. Cox, G. Cummins, M. P. Y. Desmulliez, R. E. Clutton, K. L. Obstein, S. Cochran, P. Valdastri, *Sci. Rob.* **2019**, 4.

[336] L. J. Sliker, G. Ciuti, M. E. Rentschler, A. Menciassi, *Tribol. Int.* **2016**, *102*, 472.

[337] F. Bianchi, G. Ciuti, A. Koulaouzidis, A. Arezzo, D. Stoyanov, S. Schostek, C. M. Oddo, A. Menciassi, P. Dario, *An Innovative Robotic Platform for Magnetically Driven Painless Colonoscopy*, Vol. 5, AME Publishing Company, Hong Kong **2017**.

[338] M. Salerno, G. Ciuti, G. Lucarini, R. Rizzo, P. Valdastri, A. Menciassi, A. Landi, P. Dario, *Meas. Sci. Technol.* **2011**, *23*, 015701.

[339] P. Brandao, O. Zisimopoulos, E. Mazomenos, G. Ciuti, J. Bernal, M. Visentini-Scarzanella, A. Menciassi, P. Dario, A. Koulaouzidis,

[340] A. Arezzo, D. J. Hawkes, D. Stoyanov, *J. Med. Rob. Res.* **2018**, *03*, 1840002.

[340] D.i. K. Iakovidis, G. DImas, A. Karargyris, F. Bianchi, G. Ciuti, A. Koulaouzidis, *IEEE J. Biomed. Health Inform.* **2019**, *23*, 2211.

[341] M. Visentini-Scarzanella, H. Kawasaki, R. Furukawa, M. Bonino, S. Arolfo, G. Lo Secco, A. Arezzo, A. Menciassi, P. Dario, G. Ciuti, *Endosc. Int. Open* **2018**, *06*, E602.

[342] G. Dimas, F. Bianchi, D. K. Iakovidis, A. Karargyris, G. Ciuti, A. Koulaouzidis, *Meas. Sci. Technol.* **2020**.

[343] G. Lucarini, M. Mura, G. Ciuti, R. Rizzo, A. Menciassi, *J. Med. Biol. Eng.* **2015**, *35*, 428.

[344] G. Lucarini, G. Ciuti, M. Mura, R. Rizzo, A. Menciassi, *Int. J. Adv. Rob. Syst.* **2015**, *12*, 25.

[345] S. Nouda, K. Ota, K. Higuchi, *Dig. Endosc.* **2018**, *30*, 117.

[346] D. Son, H. Gilbert, M. Sitti, *Soft Rob.* **2020**, *7*, 10.

[347] K. T. Nguyen, M. C. Hoang, E. Choi, B. Kang, J. O. Park, C. S. Kim, *Int. J. Control Autom. Syst.* **2020**, *18*, 65.

[348] P. M. Price, W. E. Mahmoud, A. A. Al-Ghamdi, L. M. Bronstein, *Front. Chem.* **2018**, *6*, 619.

[349] E. T. Nicknejad, S. M. Ghoreishi, N. Habibi, *AAPS PharmSciTech* **2015**, *16*, 1480.

[350] D. Honarmand, S. M. Ghoreishi, N. Habibi, E. T. Nicknejad, *J. Appl. Polym. Sci.* **2016**, *133*, 43556.

[351] M. Giannaccini, M. Giannini, M. P. Calatayud, G. F. Goya, A. Cuschieri, L. Dente, V. Raffa, *Int. J. Mol. Sci.* **2014**, *15*, 1590.

[352] U. K. Cheang, M. J. Kim, *J. Nanopart. Res.* **2015**, *17*, 145.

[353] V. Hamdipoor, M. R. Afzal, T.-A. Le, J. Yoon, *Micromachines* **2018**, *9*, 14.

[354] J. Hwang, J. Kim, H. Choi, *Intell. Serv. Rob.* **2020**, *13*, 1.

[355] E. P. Furlani, *Permanent Magnet and Electromechanical Devices: Materials, Analysis, and Applications*, Academic Press, San Diego, CA **2001**.

[356] V. Iacovacci, G. Lucarini, C. Innocenti, N. Comisso, P. Dario, L. Ricotti, A. Menciassi, *Biomed. Microdevices* **2015**, *17*, 112.

[357] K. Tsuchida, H. M. García-García, W. J. van der Giessen, E. P. McFadden, M. van der Ent, G. Sianos, H. Meulenbrug, A. T. L. Ong, P. W. Serruys, *Catheter. Cardiovasc. Interv.* **2006**, *67*, 356.

[358] S. Jeon, A. K. Hoshiar, K. Kim, S. Lee, E. Kim, S. Lee, J. Kim, B. J. Nelson, H.-J. Cha, B.-J. Yi, H. Choi, *Soft Robot* **2018**, *6*, 54.

[359] C. Chautems, A. Tonazzini, Q. Boehler, S. H. Jeong, D. Floreano, B. J. Nelson, *Adv. Intell. Syst.* **2019**, *2*, 1900086.

[360] V. Lalande, F. P. Gosselin, S. Martel, in *2010 Annual Int. Conf. of the IEEE Engineering in Medicine and Biology*, IEEE, Piscataway, NJ **2010**, pp. 1874–1877.

[361] F. P. Gosselin, V. Lalande, S. Martel, *Med. Phys.* **2011**, *38*, 4994.

[362] V. Lalande, F. P. Gosselin, M. Vonthron, B. Conan, C. Tremblay, G. Beaudoin, G. Soulez, S. Martel, *Med. Phys.* **2015**, *42*, 969.

[363] A. Azizi, C. C. Tremblay, K. Gagné, S. Martel, *Sci. Robot.* **2019**, *4*, eaax7342.

[364] A. D. Losey, P. Lillaney, A. J. Martin, D. L. Cooke, M. W. Wilson, B. R. H. Thorne, R. S. Sincic, R. L. Arenson, M. Saeed, S. W. Hetts, *Radiology* **2014**, *271*, 862.

[365] Y. Kim, G. A. Parada, S. Liu, X. Zhao, *Sci. Rob.* **2019**, *4*, eaax7329.

[366] O. Vermesh, A. Aalipour, T. J. Ge, Y. Saenz, Y. Guo, I. S. Alam, S. Park, C. N. Adelson, Y. Mitsutake, J. Vilches-Moure, E. Godoy, M. H. Bachmann, C. C. Ooi, J. K. Lyons, K. Mueller, H. Arami, A. Green, E. I. Solomon, S. X. Wang, S. S. Gambhir, *Nat. Biomed. Eng.* **2018**, *2*, 696.

[367] V. Iacovacci, L. Ricotti, E. Sinibaldi, G. Signore, F. Vistoli, A. Menciassi, *Adv. Sci.* **2018**, *5*, 1800807.

[368] V. Iacovacci, L. Ricotti, G. Signore, F. Vistoli, E. Sinibaldi, A. Menciassi, in *2019 Int. Conf. on Robotics and Automation (ICRA)*, IEEE, Piscataway, NJ **2019**, pp. 2495–2501.

[369] H. Gadêlha, P. Hernández-Herrera, F. Montoya, A. Darszon, G. Corkidi, *Sci. Adv.* **2020**, *6*, eaba5168.

[370] L. Xie, X. Pang, X. Yan, Q. Dai, H. Lin, J. Ye, Y. Cheng, Q. Zhao, X. Ma, X. Zhang, G. Liu, X. Chen, *ACS Nano* **2020**, *14*, 2880.

[371] V. Iacovacci, A. Blanc, H. Huang, L. Ricotti, R. Schibli, A. Menciassi, M. Behe, S. Pané, B. J. Nelson, *Small* **2019**, *15*, 1900709.

[372] J. Cypriano, J. Werckmann, G. Vargas, A. Lopes dos Santos, K. T. Silva, P. Leão, F. P. Almeida, D. A. Bazylinski, M. Farina, U. Lins, F. Abreu, *PLoS One* **2019**, *14*, e0215657.

[373] A. Curcio, A. Van de Walle, A. Serrano, S. Preveral, C. Péchoux, D. Pignol, N. Menguy, C. T. Lefevre, A. Espinosa, C. Wilhelm, *ACS Nano* **2020**, *14*, 1406.

[374] R. Fernandes, M. Zuniga, F. R. Sassine, M. Karakoy, D. H. Gracias, *Small* **2011**, *7*, 588.

[375] O. I. Sentürk, O. Schauer, F. Chen, V. Sourjik, S. V. Wegner, *Adv. Healthcare Mater.* **2020**, *9*, 1900956.

[376] R. Di Leonardo, L. Angelani, D. Dell'Arciprete, G. Ruocco, V. Iebba, S. Schippa, M. P. Conte, F. Mecarini, F. De Angelis, E. Di Fabrizio, *Proc. Natl. Acad. Sci. USA* **2010**, *107*, 9541.

[377] Y.-A. Chen, A. D. King, H.-C. Shih, C.-C. Peng, C.-Y. Wu, W.-H. Liao, Y.-C. Tung, *Lab Chip* **2011**, *11*, 3626.

[378] R. Alonso-Matilla, D. Saintillan, *EPL Europhys. Lett.* **2018**, *121*, 24002.

[379] F. Guzmán-Lastra, A. Kaiser, H. Löwen, *Nat. Commun.* **2016**, *7*, 13519.

[380] F. R. Koessel, S. Jabbari-Farouji, *EPL Europhys. Lett.* **2019**, *125*, 28001.

[381] F. Meng, D. Matsunaga, R. Golestanian, *Phys. Rev. Lett.* **2018**, 120.

[382] B. Vincenti, G. Ramos, M. L. Cordero, C. Douarche, R. Soto, E. Clement, *Nat. Commun.* **2019**, *10*, 5082.

[383] F. Bianchi, A. Masaracchia, E. S. Barjuei, A. Menciassi, A. Arezzo, A. Koulaouzidis, D. Stoyanov, P. Dario, G. Ciuti, *Expert Rev. Med. Devices* **2019**, *16*, 381.

Nafiseh Ebrahimi is a Ph.D. student at the Advanced Robotic Manipulators ARM lab, Department of Mechanical Engineering at the University of Texas at San Antonio UTSA, since 2016. She received her Master's degree in mechanical engineering from Iran University of Science and Technology IUST in 2010 and Bachelor's in Mechanical Engineering from Isfahan University of Technology IUT in 2007 both in Iran. She then spent four years in SBR, an international engineering consultants company and then moved to the US for her Ph.D. studies. Her research interests include soft robotics, rehabilitation robotics, compliant mechanisms, and mechatronics.

David J. Cappelleri is an associate professor in the School of Mechanical Engineering at Purdue University. His research interests include mobile microrobotics for biomedical and manufacturing applications, surgical robotics, automated manipulation and assembly, and unmanned aerial and ground robot design for industrial and agricultural applications. He received his B.S. degree from Villanova University, M.S. degree from The Pennsylvania State University, and Ph.D. degree from the University of Pennsylvania in Mechanical Engineering.

Amir Jafari received the Ph.D. degree in robotics from the Italian Institute of Technology (IIT), Italy, in 2011. He is currently an assistant professor with the Department of Mechanical Engineering, at the University of Texas at San Antonio. From 2011 to 2012, he was a postdoctoral researcher with the IIT and from 2012 to 2013, he was a postdoctoral researcher with Swiss Federal Institute of Technology ETH in Zurich, Switzerland. From 2014 to 2016, he was with the Agency of Science, Technology and Research, Singapore, before he joined UTSA in 2016.